UNIVERSITY OF CALIFORNIA
RIVERSIDE

The Study of the Properties of Collagen Hydrogel and 3T3 Fibroblast Cells' Behavior Within Collagen Hydrogel by Multiphoton Microscopy (MPM)

A Dissertation submitted in partial satisfaction
of the requirements for the degree of

Doctor of Philosophy

in

Biochemistry and Molecular Biology

by

Xuye Lang

August 2016

Dissertation Committee:

Dr. Julia G. Lyubovitsky, Chairperson
Dr. Russ Hille
Dr. Gregor Blaha

The Dissertation of Xuye Lang is approved:

_____

_____

_____

Committee Chairperson

University of California, Riverside

Acknowledgements

I would like to express my deepest appreciate to Dr. Julia G. Lyubovitsky for her patient guidance, continual encouragements and persistent help. I would also like to thank Dr. Russ Hille and Dr. Gregor Blaha as my thesis committee members and their useful suggestions. I would like to thanks my parents and all my families for their continual support and love.

I would like to thanks all the professors, colleagues and friends at UC riverside for shearing the experiment instruments with me and giving me the valuable advice. Thanks Dr. Jiayu Liao for the permission of the using the flexStation fluorescence plate reader. Thanks Dr. Victor Rodgers for the permission of using UV-Vis spectrophotometer. Thanks He Qu and Cassandra C. Turgman for showing the operation of FlexStation. Thanks Dr. Hong Xu for the permission of using incubator. Thanks Dr. Krassimir N. Bozhilov and Stephen McDaniel for the training of the Transmission Electron Microscopy (TEM). Thanks Dr. Dan Borchardt for the training of Temperature-controlling UV-Vis spectrophotometer and Circular Dichroism (CD). Thanks Dr. David Carter for the training of SP5 Confocal Microscopy. Thanks Matthew Spousta, Jackie Gigante, Anh Vu, Mark Van Zee and Austin Berdick for their help of sample preparation and data processing.

I would like also acknowledge the journal (Analytical Methods) for giving the permission to use the published materials (figures and text) in my thesis chapter.

http://pubs.rsc.org/is/content/articlelanding/2015/ay/c4ay02242d#!divAbstract and

http://pubs.rsc.org/is/content/articlelanding/2016/ay/c5ay02520f#!divAbstract

ABSTRACT OF THE DISSERTATION

The Study of the Properties of Collagen Hydrogel and 3T3 Fibroblast Cells' Behavior Within Collagen Hydrogel by Multiphoton Microscopy (MPM)

by

Xuye Lang

Doctor of Philosophy, Graduate Program in Biochemistry and Molecular Biology
University of California, Riverside, August 2016
Dr. Julia G. Lyubovitsky, Chairperson

The goal of tissue engineering is to create the functional engineered tissue to replace or repair the damaged one in human body. The complex multi-phase collagen hydrogel systems are more and more popular in the tissue engineering field where they are used as scaffolds because of biodegradability and biocompatibility. The properties of collagen hydrogel are very important because they can lead to different cellular behavior. My study employed the non-invasive technologies to probe the properties of collagen-based materials (optical, microstructural and mechanical properties) and fibroblast cells' behavior within collagen hydrogels.

We identified that the ion types and ionic strength, initial pH and self-assembly temperature all affect the microstructure of collagen hydrogels, which was detected with the Second Harmonic Generation (SHG) images. Besides that, initial collagen concentration can affect the mechanical properties of collagen hydrogels, which was determined with rheology (storage modulus of 4 g/l collagen hydrogels is five times higher compared to 2 g/l collagen hydrogels).

Collagen hydrogel needs to be crosslinked with cross-linkers to improve its mechanical strength since it is generally too soft to support cellular behavior, such as, cell proliferation and migration. According to our experience, the 3D collagen hydrogel collapsed into film after 2 days cell culture. Zero-length cross-linker (EDC) and non-zero-length cross-linker (Genipin) were employed to crosslink collagen hydrogel. Genipin can introduce very strong fluorescence into the collagen hydrogels and weaken their SHG signal. Genipin crosslinked collagen hydrogel has higher cross-linking degree (~85%) compared to EDC cross-linked collagen hydrogel (~10%). The storage modulus of genipin cross-linked collagen hydrogel is more than two times of EDC cross-linked collagen hydrogel.

Different "aged" genipin solution can result in different properties of collagen hydrogel. For the optical properties, older genipin solution can increase the fluorescence signal in the green channel (470 nm – 550 nm) and weaken fluorescence signal in the red channel (570 nm – 610 nm). For the microstructural properties, older genipin can result in a thinner collagen fiber within a hydrogel. For the mechanical properties, the storage modulus of genipin cross-linked collagen hydrogel dropped down along with the age increasing of genipin solutions. The embryonic BALB/3T3 (clone A31) fibroblasts cultured on collagen hydrogels cross-linked with stored genipin reagent are disproportionately more round compared to cells cultured on unmodified collagen hydrogels and collagen hydrogels stabilized with fresh genipin solutions. The best correlation of cellular extension is with morphological properties of synthesized hydrogels and no correlation is identified with mechanical properties of materials.

Table of Contents

List of Figures

List of Tables

Chapter 1: Thesis overview

Introduction

In the tissue engineering field, the main procedure is to prepare the engineered tissue by seeding the sub-cultured cells into a 3D scaffold, then use the engineered tissue to repair or replace the damaged one in our body. The 3D scaffold plays a very important role in the tissue engineering field because it can affect the cells behavior within it, such as: cell proliferation, survival rate, migration rate, gene expression and so on. To date, a lot of polymer materials have been used as scaffolds in the tissue engineering field, such as, Poly Lactic-*co*-Glycolic Acid (PLGA), Polyglycolic Acid (PGA), gelatin and so on. Now collagen-based biomaterial is more and more popular, as a scaffold in the tissue engineering field[4], to support cell behavior because of the properties of biocompatibility[5], biodegradability[6] and low cytotoxicity.[7]

Collagen is the main component of the extracellular matrix (ECM) in human connective tissue.[1] So far, 28 kinds of collagen have been identified and described by researchers [2]. Collagen accounts for 20-30 % of the total protein found in the human body[3] and 90% of collagen is collagen type I. Collagen type I molecules have a triple helix structure which contains two α_1 and one α_2 peptide chains.[8] The length of collagen type I molecule is about 300 nm and diameter of collagen type I molecule is about 1.5 nm. Collagen molecules undergo assembly process to form the fibrils (nanostructure) and fibers (microstructure) sequentially. (Figure 1.1)

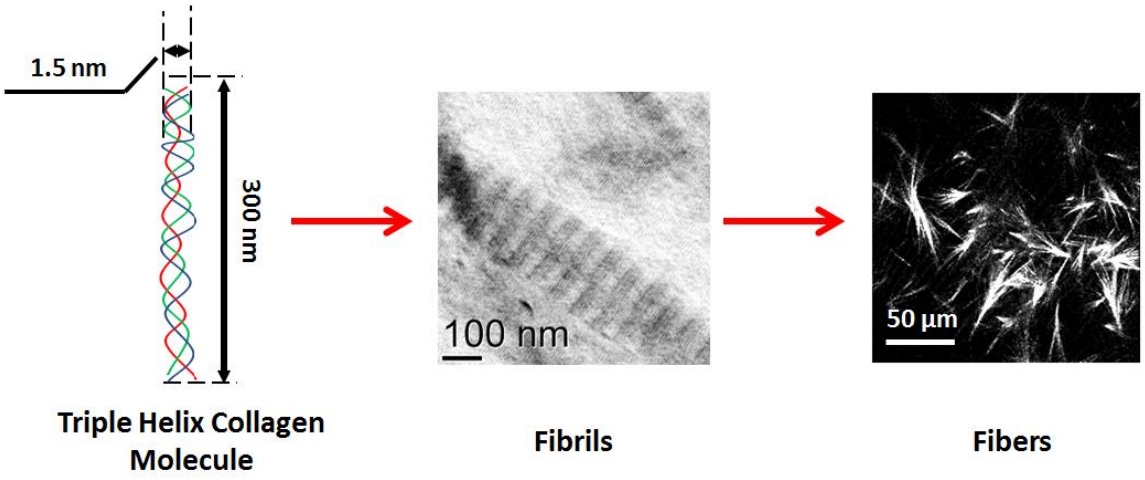

Figure 1.1 The collagen fibers formation process.

Besides the advantages, collagen hydrogel material also has shortcomings, it is too soft (the storage modulus, G', is less than 10 Pa) to support the cell behavior within it. Specifically, uncross-linked 3D collagen hydrogel material will often collapse to 2D collagen film material in the very beginning of cell culturing (2 or 3 days), especially at low solid collagen content (2 g/l). In tissue engineering field, the chemical cross-linkers are normally employed to crosslink collagen hydrogel in order to improve the mechanical properties.[10] The chemical cross-linkers can be divided into two groups, (1) zero-length crosslinking agents and (2) non-zero-length crosslinking agents.[7] On the one hand, zero-length cross-linkers crosslink two amino acid residues by an ester condensation reaction without leaving any part of the cross-linker molecules remaining after the crosslinking process. On the other hand, the whole non-zero-length cross-linker molecule or part of the non-zero-length crosslinking molecule becomes part of the materials after the cross-linking process. The most obvious disadvantage of the traditional chemical cross-linkers, for example, glutaraldehyde, is cytotoxicity.[11] New alternative cross-linkers, for example *genipin*, are finding wider use as a kind of a natural cross-linker in tissue engineering due

to the properties of low-cytotoxicity[12] and anti-inflammatory[13] activity It has been reported by Nishi et al.[14] that genipin is 5000-10000 times less cytotoxicity than glutaraldehyde.

For any kind of 3D scaffold in the tissue engineering field, the properties need to be studied first because the properties of the scaffold can result in different cell behavior at different levels (molecular level and morphology level). At the molecular level, Mui et al.[15] reported that stiffer materials can result in the higher level expression of N-cadherin, which is related to cell proliferation, Zhu et al.[16] also reported that the higher elasticity of the material can induce the high level expression of collagen type I. At the morphology level, Herley et al.[17] and Pizzo et al.[18] further detailed that the microstructure of the material can affect the cell migration rate and cells' shape. For my research, I focused on the microstructural, mechanical and optical properties of collagen hydrogel material.

The 3D collagen hydrogel materials can be formed by incubating collagen molecules at different conditions and/or crosslinked by cross-linkers.[9] The collagen hydrogel is a very complicated and sensitive system. It contains two phases, a liquid phase and a solid phase. Liquid phase (solutions) account for ~90% of the hydrogel system, the solid phase (collagen fibers) account for another 10% of the hydrogel system. There are a lot of elements that can affect the microstructure of collagen hydrogel, such as: collagen concentration, self-assembly temperature, self-assembly time, ionic conditions and pH. So far, most research has focused on the effect of ionic conditions or pH on the nanostructures formed by collagen molecules and the stability of collagen molecules in the solution. This kind knowledge can help us to understand how the collagen molecule

behave in solution, but it is not adequate for us to understand how the 3D collagen performs and functions as it exists within various tissues and organs. There is currently very little research on collagen at the microstructural level as it occurs in tissues and hydrogels. My work looked at experimentally modeling how the 3D collagen performs in different tissues and tissue structures. My research aims to fill this gap to help us understand the performance and function of collagen hydrogels with a future goal to potentially apply that knowledge to the construction of more functional engineered tissues.

The cross-linking process of collagen hydrogel by a specific cross-linker can improve the mechanical properties of the material. At the same time, other properties (microstructural, optical, etc.) are also altered after the cross-linking process. The properties of crosslinked collagen hydrogel also need to be further studied. In my study, I studied the properties of EDC (1-ethyl-3-(3-dimethylaminopropyl) carbodiimide hydrochloride), EDC/NHS (*N*-hydroxysuccinimide) and genipin crosslinked collagen hydrogels.

All of the prior investigations (Mui's, Zhu's, Herley's and Pizzo's research) suggest that the cells' responses to materials with different properties need to be studied. The knowledge obtained can help us to understand the mechanism of the interaction between cells and materials. In my study, I investigated the 3T3 fibroblast cells response to different "aged" genpin crosslinked collagen hydrogel.

Specifically I investigated the *in situ* non-invasive methods needed to characterize the properties of collagen-based materials at the microstructural level. The Second Harmonic Generation (SHG) contrast and Two Photon excited Fluorescence (TPF) can serve as

label-free spectroscopic probes that can be used to directly, non-invasively and *in situ* image the microstructure of collagen hydrogels.[19] The SHG signal is from the interaction between the collagen hydrogel fibers and near-infrared (NIR) pulsed, femtosecond laser produced by scanning non-liner microscopy. The photons are combined when they are interacting with the collagen fibers. The photons form a new photon with exactly twice the energy as the original photon. (Figure 1.2) Because NIR scattering is less compared with UV and visible excitation wavelengths, it is possible to generate and image the contrast deep inside the 3D collagen hydrogels. The advantage of SHG contrast is that it does not bleach, therefore, it had been employed to successfully image structural proteins with high resolution and contrast in biomedical assessment of tissue structure.[20] The TPF signal is generated from the energy released from real excited state, which is excited by the absorption of two photons.

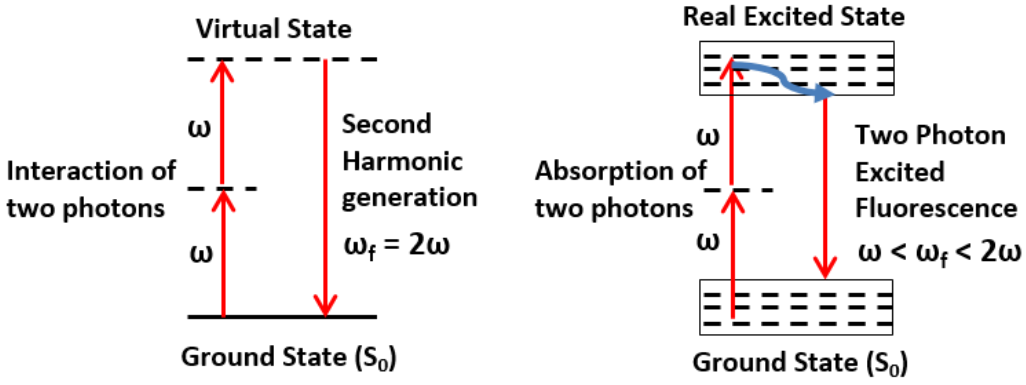

Figure 1.2 Generation process of Second Harmonic Generation (SHG) and Two Photon excited Fluorescence (TPF) signal.

References

1. S. S. Sakamuria, A. Takawale. R. Basu, P. W. Fedakc, D. Freedd, C. Sergie, G. Y. Ouditb, Z. Kassiri, Differential impact of mechanical unloading on structural and nonstructural components of the extracellular matrix in advanced human heart failure. *Transl. Res.* **2016,** *172*, 30-44.

2. V. R. Sherman, W. Yang., M. A. Meyersa, The materials science of collagen. *J Mech. Behav. Biomed. Mater.* **2015,** *52*, 22-50.

3. R. D. Harkenss, Biological functions of collagen. *Biol. Rev.* **1961,** *36*, 399-454.

4. Y. Hwang, J. G. Lyubovitsky., Collagen hydrogel characterization: multi-scale and multi-modality approach. *Anal. Methods* **2011,** *3*, 529-536.

5. X. Lang, J. G. Lyubovitsky, Structural dependency of collagen fibers on ion types revealed by in situ second harmonic generation (SHG) imaging method, Anal. Methods. *Anal. Methods* **2015,** *7*, 1637-1650.

6. X. Lang, J. G. Lyubovitsky., Noninvasive imaging of embryonic stem cell cultures by multiphoton microscopy reveals the significance of collagen hydrogel preparation parameters. *Anal. Methods* **2016,** *8*, 280-294.

7. Y. Hwang, J. G. Lyubovitsky, Effects of zero-length and non-zero-length cross-linking reagents on the optical spectral properties and structures of collagen hydrogels. *ACS Appl. Mater. Interfaces* **2012,** *4*, 261-267.

8. D. A. D. Parry, The molecular fibrillar structure of collagen and its relationship to the mechanical properties of connective tissue. *Biophys. Chem.* **1988,** *29*, 195-209.

9. Y. Hwang, J. G. Lyubovitsky, The structural analysis of three-dimensional fibrous collagen hydrogel by Raman Microspectrectroscopy. *Biopolymers* **2012,** *99*, 319-328.

10. Y. Hwang, J. Larsen, T. B. Krasieva, J. G. Lyubovitsky, Effect of Genipin Crosslinking on the Optical Spectral Properties and Structures of Collagen Hydrogels. *ACS Appl. Mater. Interfaces* **2011,** *3*, 2579-2583.

11. H. G. Sundararaghavan, G. A. Monterio, N. A. Lapin, Y. J. Chabal, J. R. Miksan, D. I. Shreiber, Genipin-induced changes in collagen gels: Correlation of mechanical properties to fluorescence. *J. Biomed. Mater. Res. Part B Appl. Biomater.* **2008,** *87*, 308-320.

12. Y. Kwon, E. Lim., H. Kim,Y. Hwang, K. Lee, K. Min, Genipin, a Cross-linking Agent, Promotes Odontogenic Differentiation of Human Dental Pulp Cells. *J Endod.* **2015,** *41*, 501-507.

13. H. Koo, K. Lim., H. Jung, E. Park, Anti-inflammatory evaluation of gardenia extract, geniposide and genipin. *J Ethnopharmacol* **2006,** *103*, 496-500.

14. C. Nishi, N. Nakajima, Y. Ikada, In vitro evaluation of cytotoxicity of diepoxy compounds used for biomaterial modification. *J Biomed. mater. Res.* **1995,** *29*, 829-834.

15. K. L. Mui, Y. H. Bae, L. Gao, S. Liu, T. Xu, G. L. Radice, C. S. Chen, R. K. Assoian, N-cadherin induction by ECM stiffness and FAK overrides the spreading requirement for proliferation of vascular smooth muscle cells. *Cell Rep.* **2015,** *10*, 1477-1486.

16. C. Zhu, J. Li, C. Liu, P. Zhou, H. Yang, B. Li, Effect of scaffold elasticity on the gene expression of annulus fibrosus-derived stem cells. *Data Brief* **2015,** *5*, 1007-1014.

17. B. A. C. Harley, H. Kim., M. H. Zaman, L. V. Yannas, D. A. Lauffenburger, L. J. Gibson, Microarchitecture of three-dimensional scaffolds influences Cell Migration Behavior via Junction Interactions. *Biophys. J.* **2008,** *2008* (95), 4013-4022.

18. A. M. Pizzo, K. Kokini, L. C. Vaughn, B. Z. Waisner, S. L. Voytik-Harbin, Extracellular matrix (ECM) microstructural composition regulates local cell-ECM biomechanics and fundamental fibroblast behavior: a multidimensional perspective. *J Mammary Gland Biol Neoplasia* **2010,** *9*, 361-374.

19. C. B. Raub, V. Suresh, T. B. Krasieva, J. G. Lyubovitsky, J. D. Mih, A. J. Putnam, B. J. Tromberg, S. C. George, Noninvasive Assessment of Collagen Gel Microstructure and Mechanics Using Multiphoton Microscopy. *Biophys. J.* **2007,** *92*, 2212-2222.

20. J.G. Lyubovitsky, T. B. Krasieva, X. Xu, B. Andersen, B. J. Tromberg, In situ multiphoton optical tomography of hair follicles in mice. *J Biomed. Opt.* **2007,** *12*, 044003.

Chapter 2: Structural dependency of collagen fibers on ion types revealed by *in situ* second harmonic generation (SHG) imaging method

Abstract

Ionic species in aqueous solutions alter protein solubility and aggregation behavior through a variety of complex interactions. Employing second harmonic generation (SHG) imaging in a backscattering configuration *in situ* we discovered that added phosphate modulates the aggregated collagen fibers' lengths within 3D hydrogels. For example, the about 1 μm in length collagen fibers formed in 30 mM phosphate-only buffer, 37 °C, 2 g l^{-1} collagen solid content extended to about 45 μm and increased in width in high (>/ = 60 mM) phosphate. Adding sodium sulfate in a 30 mM phosphate buffer to polymerize collagen into a hydrogel at 37 °C had similar effects. On the other hand, adding sodium chloride did not lengthen collagen fibers. The fiber lengths and widths decreased in very high concentrations of all salts. To establish the timescales of the involved polymerization processes, we used traditional turbidity measurements of gelation. Based on the solubility experiments we concluded that over 85% of collagen had precipitated under all experimental conditions. The non-invasive *in situ* SHG imaging in this study is valuable because it reduces the possibility of artifacts associated with changes to the fragile collagen hydrogels taking place in the conventional electron and optical imaging experiments.

Introduction

The exact mechanism of how salt ions and other charged species interact with proteins is not fully understood. These interactions, however, are known to modulate proteins'

solubility and aggregation processes. There are many works to date that focused on the effects of ions on the water environment and described how it may affect protein stability in solutions and formation of nanostructures. Few studies explored the impact of the interactions on the fiber structures self-assembled at the microscopic scale. *In situ* non-invasive methods are needed to characterize the structures formed to understand the contributions of ions to the formation of the higher order assemblies that form microstructures within the biologically derived protein 3D scaffolds.

Collagen protein is a major component of the extracellular matrix (ECM) within the mammalian connective tissues. It accounts for approximately 20–30% of all protein in a human body.[1] Due to collagen ability to form fibers that contribute to stability within the polymeric networks, it remains a popular biomaterial choice for tissue engineering[2] and preparation of 3D scaffolds. Collagen protein undergoes a complex hierarchical organization at multiple length scales that range from triple-stranded helical collagen molecules to nano- (fibrils), micro- (fibers and fiber bundles) and macro- (gel) scales. Second harmonic generation (SHG) contrast serves as a valuable label-free spectroscopic probe that can be used to directly detect aggregated collagen structures (fibers) within scaffolds non-invasively and *in situ*. The SHG contrast results from an interaction between fibrillar collagen and near-infrared (NIR) pulsed, femtosecond laser light of scanning non-liner microscopy.[3] SHG is produced when photons interacting with fibrillar collagen are combined to form new photons with exactly twice the energy. The interaction between laser pulses and collagen's noncentrosymmetric, triple helix structure in addition to collagen packing within the materials leads to scattering from the tertiary

(fibrils)[4] and quaternary (fibers)[5] level of collagen organization thus producing SHG[6] contrast. Because NIR wavelengths are utilized,[7] it is possible to generate and image this contrast deep inside opaque 3D samples such as collagen hydrogels. A significant advantage of SHG contrast is no bleaching and it had been employed to successfully image structural proteins with high resolution and contrast in biomedical assessment of tissue structure.[8]

We have examined with SHG contrast the contributions of different ions to collagen aggregation that forms microscopic fiber structures within three-dimensional (3D) hydrogels. To our knowledge, these studies represent first attempts to systematically study directly, non-invasively and *in situ* the effect of various ions on collagen fibers and hydrogel microstructure assembled with different salts. To gain insights into the structural changes associated with adding salts to proteins, we carried out such studies throughout a wide range of salt concentrations. We further combined our optical imaging experiments with traditional turbidity measurements of gelation to establish the timescales of the involved processes and solubility to assess the amount of collagen remaining in solution after completion of *fibrogenesis*.

Materials and methods

Collagen hydrogel preparation: High concentration rat-tail type I collagen stock was obtained from BD Biosciences (354249), used as received and stored in 4 °C. The polymerization process of collagen was started by mixing 2× *fibrogenesis* initiation buffer with 0.02 N acetic acid, collagen stock and adjusting the final pH of samples with 1 M NaOH to the pH = 7.4. The mixing process was done gently on ice. The samples

were then incubated under experimental temperature (room temperature (RT), 27 °C or 37 °C). We used Henderson–Hasselbalch equation (pH = pK_a + log([base]/[acid])) to calculate the concentrations of mono- and dibasic phosphate for the pH = 7.4. At pH 7.4, the $[HPO_4]^{2-}$ ion is in 2 to almost 4 fold excess compared to $[H_2PO_4]^-$ ion. After the pH adjustment, all the buffers were filtered with 0.22 μm, 33 mm syringe filter (Millipore, Millex-GV, SLGV033RS). For NaCl and Na_2SO_4 assisted collagen hydrogel assembly the salts were dissolved in 60 mM phosphate buffer (2× fibrogenesis initiation buffer). The 2× fibrogenesis initiation buffers were prepared by mixing buffer A and buffer B in the appropriated ratios. The composition of buffer A was 36 mM K_2HPO_4, 23 mM KH_2PO_4 and 1.8 M NaCl or 0.9 M Na_2SO_4. Buffer B contained only K_2HPO_4 and KH_2PO_4 at the same concentration as buffer A and was used to dilute the concentration of salt of buffer A to the appropriate 2× concentration values as needed. The composition of the ionic species in the final mix was the following: (1) phosphate assembled collagen hydrogels – only phosphate buffer giving 5, 10, 20, 30, 40, 50, 60, 80, 100, 120, 140, 160, 180, 200, 300 and 500 mM concentrations; (2) NaCl assisted collagen hydrogel assembly – the final concentrations of NaCl employed to polymerize collagen hydrogels were 0, 150, 300, 600, 900 mM; (3) Na_2SO_4 assisted collagen hydrogel assembly – the final concentrations of Na_2SO_4 employed to polymerize collagen hydrogels were 0, 5, 10, 20, 50, 75, 100, 150, 300 mM. The measurement experiments on hydrogels prepared under these different conditions were repeated at least three times and/or on different days to verify reproducibility.

Solubility measurement: For the solubility measurements, fibrogenesis was carried out for 24 hours at the specified polymerization conditions and 2 g l^{-1} collagen solid content. Upon completion of fibrogenesis, the samples were centrifuged at 12 000*g* for 5 minutes to separate precipitated collagen from soluble collagen molecules in the supernatant. We recorded the volume of the supernatant and measured the absorbance values at 218 nm. The absorbance values were converted to concentrations through dividing absorbance by an extinction coefficient value[9] of 9.43 ml mg^{-1} $cm^{-1}$and 1 cm pathlength of the cuvette. The average values and standard deviations from the mean were calculated with Microsoft Excel.

Turbidity assays: The kinetics of collagen self-polymerization process was followed by detecting changes in turbidity at 450 nm. The samples were prepared as described in collagen hydrogel preparation section. After preparation, the samples were transferred into pre-chilled on ice cuvettes (NSG Precision Cells Inc., 9 PS). We used temperature controlled UV-Vis-NIR spectrophotometer (Varian 500 Scan) to measure turbidity at the specified experimental temperatures (room temperature (RT), 27 °C or 37 °C). The turbidity was measured every 30 seconds until optical density (OD) value was stable for at least 20 minutes. From the kinetics curves, we determined delay times ($Time_{lag}$) which were the times needed to start the polymerization process, total times ($Time_{total}$), which were the times needed to complete the polymerization process, half times ($Time_{1/2}$), which were the times needed to get the half of maximum optical density (OD) values, and maximum OD values. The average values and standard deviations from the mean were calculated with Microsoft Excel.

Second harmonic generation (SHG) imaging experiments: The samples were prepared according to the procedure described in collagen hydrogel preparation section. A silicone gasket was manually secured to the glass slide to prepare a chamber. The diameter of the chamber was 17 mm and the depth of the chamber was 2.2 mm. We placed the silicone chamber on ice. The liquid sample was introduced into the chamber and cover-slipped with no. 1 thickness cover glass. We incubated the sample under experimental temperature (room temperature (RT), 27 °C or 37 °C). The upright multiphoton laser scanning microscope used to image collagen hydrogels in this work was the Thorlabs Multiphoton Microscope. It is based on an upright Nikon microscope equipped with a standard illumination system for the transmitted light. It was equipped with a femtosecond titanium:sapphire laser excitation source that provided femtosecond pulses at a repetition rate of about 80 MHz, with the center frequency tunable from 690 to 1040 nm. The long working distance immersion objectives (Zeiss, 63× water, N.A. 1.0; Zeiss, 10× water, N.A. 0.3; Olympus, 20× water, NA 1.0) were used to acquire images. The laser excitation used was linearly polarized at 810 nm. The two-photon signals from the samples were epi-collected and discriminated by the short pass 650 nm dichroic beamsplitter. Further spectral filtering with a dichroic (480 nm) and a 405 ± 5 nm bandpass filter was used to separate the SHG signal. Each image presented is 2048 × 2048 pixels corresponding to about 200 μm × 200 μm field of view for 63× images and about 1 mm × 1 mm for 10× images. We generally collected about forty 2D images with a step size of 10 μm through the depth of 3D collagen hydrogels. Twenty to fifty representative fibers and pores were commonly selected from the collected images and

measured using Image J (free open source Java image processing software developed at the National Institutes of Health (http://rsb.info.nih.gov/ij/)). The average values and standard deviations from the mean were then calculated with Microsoft Excel. To obtain the second harmonic generation (SHG) signal averaged intensities as a function of penetration depth we used eight-chambered cover glass (MP Biomedicals, 09LX155411A) to prepare the samples and Olympus, 20× water, NA 1.0 objective (XLUMPLFLN) to image them. In these experiments the imaging parameters were kept the same. The laser power before the entrance into the microscope was 250 mW as measured with 818P Series Power Detector and 842-PE Optical Power/Energy Meter (Newport). The *home written* Matlab code was used to evaluate SHG signal averaged intensities by calculating the average pixel values in the acquired images.

Results

To understand how salts influence polymerization of collagen into the aggregated 'fiber-like' structures as well as formation of hydrogels, we changed concentrations and kinds of salts in the polymerization mix.

37 °C phosphate assembled collagen hydrogels

Polymerization and kinetics: As the phosphate-buffer-induced-assembly proceeds from an optically transparent collagen solution into a scattering, semitranslucent hydrogel, there is an increase in the optical density (OD), which we detect at the wavelength of 450 nm. At this wavelength, there is no measurable absorption from collagen and an increase in the OD values indicates formation of structures within hydrogels that scatter 450 nm light. At pH 7.4, 5 mM through 20 mM phosphate concentrations, instead of inducing

hydrogel formation, precipitate collagen protein into small particles. These particles are detectable by eye. Because precipitated particles are randomly moving in and out of the excitation beam we could not detect an increase in turbidity in these samples. Figure 2.1 and Table 2.1 summarize the effect of 30 mM–200 mM phosphate on the polymerization of collagen into hydrogels. As seen in Figure 2.1, in agreement with somewhat similar prior experiments carried out on dilute solutions,[10] increasing phosphate concentration (from 30 mM up to about 140 mM in our experiment) slows down collagen polymerization. However, there is no significant change in how long it takes to assemble collagen into hydrogels when phosphate is added at concentrations of 100 mM to 140 mM. Upon increasing the phosphate concentration beyond about 140 mM, polymerization of collagen speeds up and becomes noticeably faster when the concentration of phosphate reaches 200 mM. Based on the solubility measurements,[9, 11] (Figure 2.S1) over 85% of collagen precipitates under all phosphate concentrations used in this work.

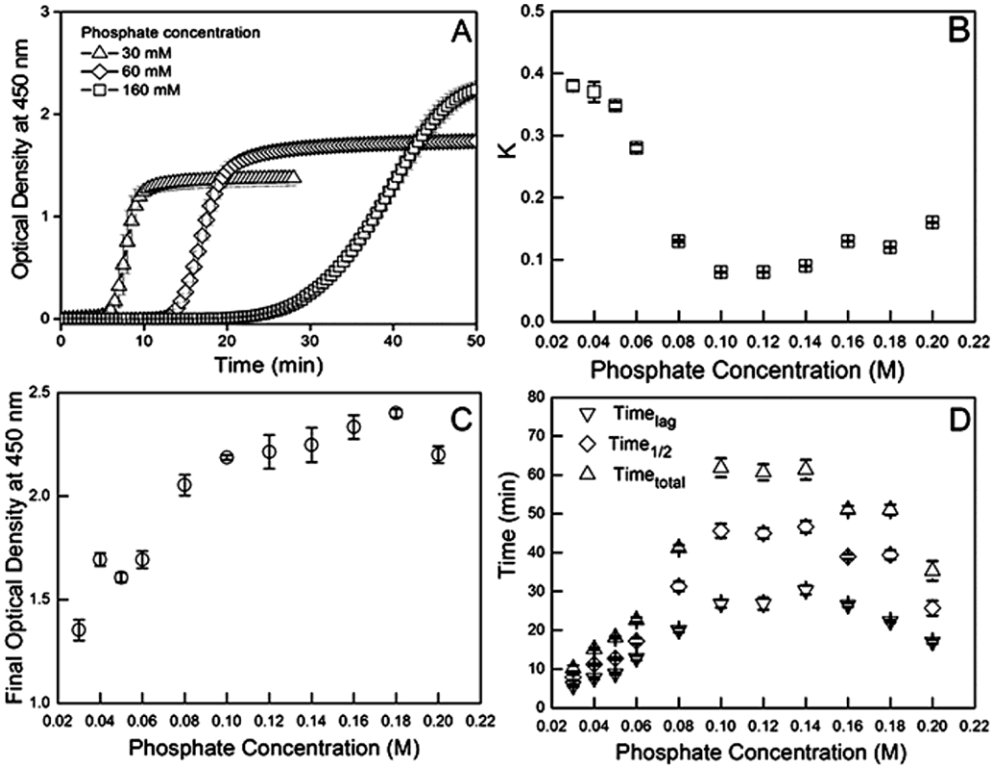

Figure 2.1 The effect of different concentrations of phosphate on turbidity and kinetic parameters during collagen self-assembly into a 2 g l^{-1}hydrogel at pH 7.4, 37 °C. (A) Typical turbidity–time curves and corresponding standard deviations of the mean during collagen self-assembly. (B) The rate constants (*K*, in units of min^{-1}) of collagen self-assembly evaluated by fitting the slopes of turbidity curves like those shown in (A). (C) The observed final optical densities as a function of final phosphate concentration and corresponding standard deviations from the mean. (D) The times to the beginning ($Time_{lag}$), middle ($Time_{1/2}$) and completion ($Time_{total}$) of collagen self-assembly and corresponding standard deviations from the mean.

Table 2.1 Summary of the effect of 30 mM–200 mM phosphate on the polymerization of collagen into a hydrogel at 37 °C, 2 g l^{-1} solid content, pH 7.4 and corresponding standard deviations from the mean

Phosphate concentration (mM)	Delay time (min)	Half time (min)	Total time (min)	OD value (min)	Rate (min^{-1})
30	5.7 ± 0.29	7.87 ± 0.65	10.2 ± 0.76	1.4 ± 0.05	0.38 ± 0.016
40	7.7 ± 0.29	11.2 ± 0.27	15.2 ± 0.29	1.7 ± 0.03	0.37 ± 0.006
50	8.8 ± 0.29	12.7 ± 0.27	18.2 ± 0.29	1.6 ± 0.02	0.35 ± 0.006
60	12.8 ± 0.60	17.2 ± 0.72	22.7 ± 0.57	1.7 ± 0.04	0.28 ± 0.002
80	20.0 ± 0.50	31.3 ± 1.20	41.2 ± 0.76	2.1 ± 0.05	0.13 ± 0.001
100	26.8 ± 1.04	45.6 ± 1.77	61.8 ± 2.47	2.2 ± 0.01	0.08 ± 0.001
120	26.8 ± 1.53	44.9 ± 1.37	60.7 ± 2.08	2.2 ± 0.08	0.08 ± 0.001
140	30.3 ± 1.15	46.6 ± 1.51	61.3 ± 2.52	2.2 ± 0.08	0.09 ± 0.001
160	26.5 ± 0.50	38.9 ± 0.66	51.0 ± 1.00	2.3 ± 0.06	0.13 ± 0.001
180	22.3 ± 0.29	39.4 ± 1.15	51.0 ± 1.32	2.4 ± 0.02	0.12 ± 0.001
200	17.0 ± 0.50	25.7 ± 1.91	35.3 ± 2.51	2.2 ± 0.04	0.16 ± 0.001

Second harmonic generation (SHG) imaging: The second harmonic generation images show that the microstructure formed within collagen hydrogels depends strongly on the concentrations of phosphate present (Figure 2.2 and Figure 2.S2). For example, when concentration of phosphate is 30 mM, the fibers formed are very small (about 1 μm, Figure 2.2). When concentration of phosphate reaches 60 mM, few fibers extend in length (up to 15 μm, Figure 2.2). Upon further increasing the concentration of phosphate in a buffer solution, we observe a progressive shift in the fiber length and width towards larger values. For example in 160 mM phosphate, the fiber length and width are about 40 μm and 18 μm respectively (Figure 2.2). Upon further increasing the phosphate concentration we observe reduction in fiber widths and lengths. For example in 200 mM phosphate, the fiber length and width are about 17 μm and 1 μm respectively.

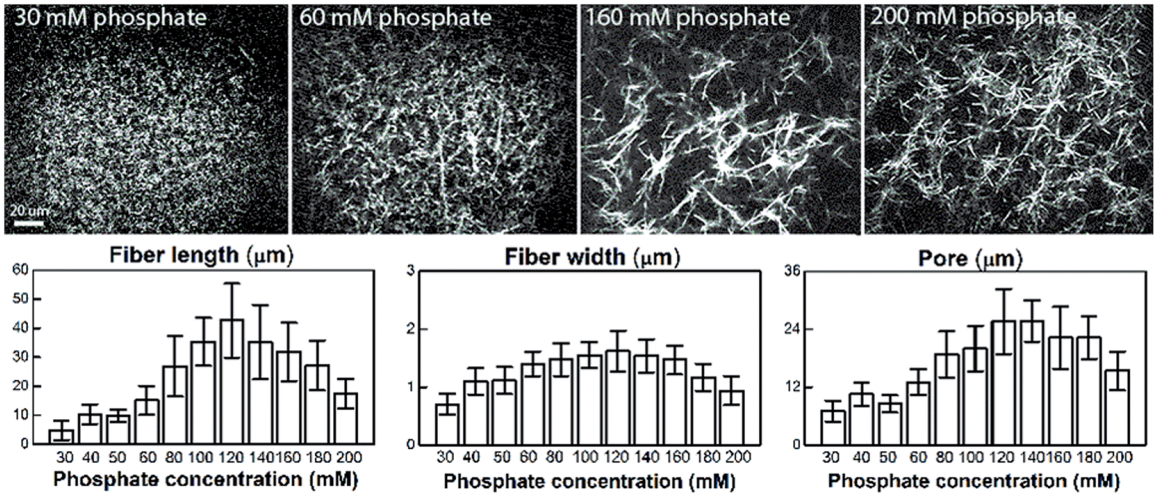

Figure 2.2 (Top row) backscattered second harmonic generation (SHG) images from collagen hydrogels assembled at pH 7.4, 37 °C and different phosphate concentrations; (bottom row) quantification of collagen hydrogel parameters: fiber lengths, widths and effective pore sizes and corresponding standard deviations from the mean.

Sodium chloride assisted collagen hydrogel assembly

Polymerization and kinetics: Figure 2.3 summarizes the contribution of 0–0.9 M sodium chloride to the polymerization of collagen into hydrogels. Overall, the self-assembly rate does not appear to be affected by NaCl concentration and remains relatively constant for all conditions. As seen in Figure 2.3A, when temperature is 37 °C, 4 g l^{-1} collagen hydrogels' self-assembly rate (*K*, in units of min^{-1}) is somewhat faster compared to that observed for 2 g l^{-1} collagen hydrogels for most concentrations of sodium chloride. At the same time, for 4 g l^{-1} collagen samples' final OD values (Figure 2.3B) are also higher than for 2 g l^{-1} collagen hydrogels. The total time ($Time_{total}$ – Figure 2.3C) for 4 g l^{-1} samples' polymerizations are shorter compared to 2 g l^{-1} samples. Polymerization kinetics of 27 °C and room temperature (RT) assembled samples show trends similar to 37 °C assembly condition. When NaCl concentration is set at the physiological value of 0.15 M, we obtain the maximum OD value for every combination of temperature and collagen concentration. Based on the solubility measurements, the amount of precipitated collagen is nearly 90% at 37 °C and is essentially the same at different sodium chloride concentrations.

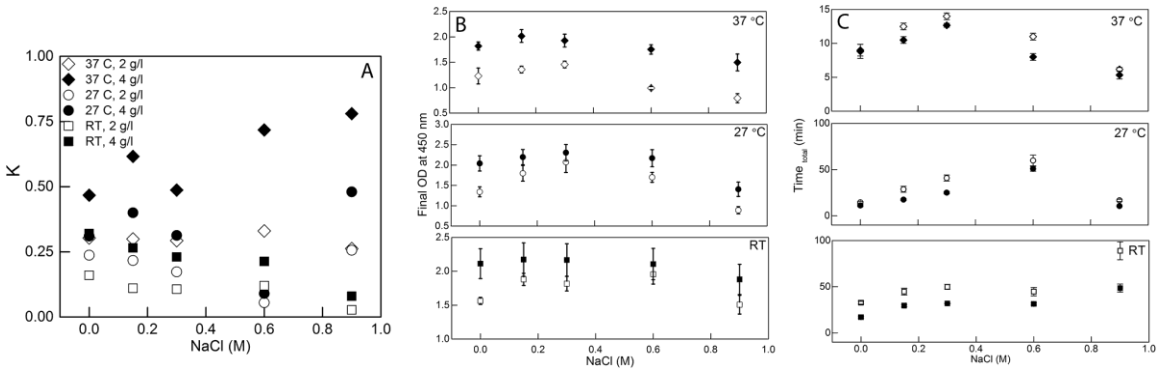

Figure 2.3 The effect of initial collagen concentrations, incubation temperatures and concentrations of sodium chloride on the kinetic parameters during collagen self-assembly into the fibers at pH 7.4, 30 mM phosphate. (A) The rate constants (*K*, in units of min^{-1}) of collagen self-assembly evaluated by fitting the slopes of turbidity curves. (B) The observed final optical densities as a function of final sodium chloride concentration and corresponding standard deviations from the mean. (C) The times ($Time_{total}$) to the completion of collagen self-assembly and corresponding standard deviations from the mean.

Second harmonic generation (SHG) imaging: When incubation temperature is RT, for sodium chloride concentration of 0.9 M, collagen fibers formed are very small within both 2 g l^{-1} (Figure 2.4, top row) and 4 g l^{-1} (Fig. S3) hydrogels. When sodium chloride concentration is 0 M, collagen fibers formed are larger compared to when sodium chloride concentration is 0.9 M. However, for both, 2 g l^{-1} and 4 g l^{-1} collagen hydrogels, fibers formed with 0 M sodium chloride concentration are smaller compared to fibers induced with 0.3 to 0.6 M sodium chloride. For sodium chloride concentration of 0 M, the fibers formed are slightly longer in 2 g l^{-1} collagen hydrogels (up to about 45 μm) compared to 4 g l^{-1} collagen hydrogels (about 20 μm). When sodium chloride concentration is 0.3 M, the resulting effective pores within collagen hydrogels are clear (Figure 2.4) but for sodium chloride concentration of 0.6 M (not shown), the effective pores are filled with smaller fibers. For sodium chloride concentration of 0.3 M, the fiber lengths are about 50 μm within both 2 g l^{-1} and 4 g l^{-1} collagen hydrogels. On average, 0.3 M sodium chloride induced fibers within 2 g l^{-1} collagen hydrogels are slightly

thinner compared to fibers within 4 g l^{-1} samples (about 3 μm *versus* 5 μm). An average diameter of the effective pores is about 60 μm within both 2 g l^{-1} and 4 g l^{-1} hydrogels prepared with 0.3 M sodium chloride.

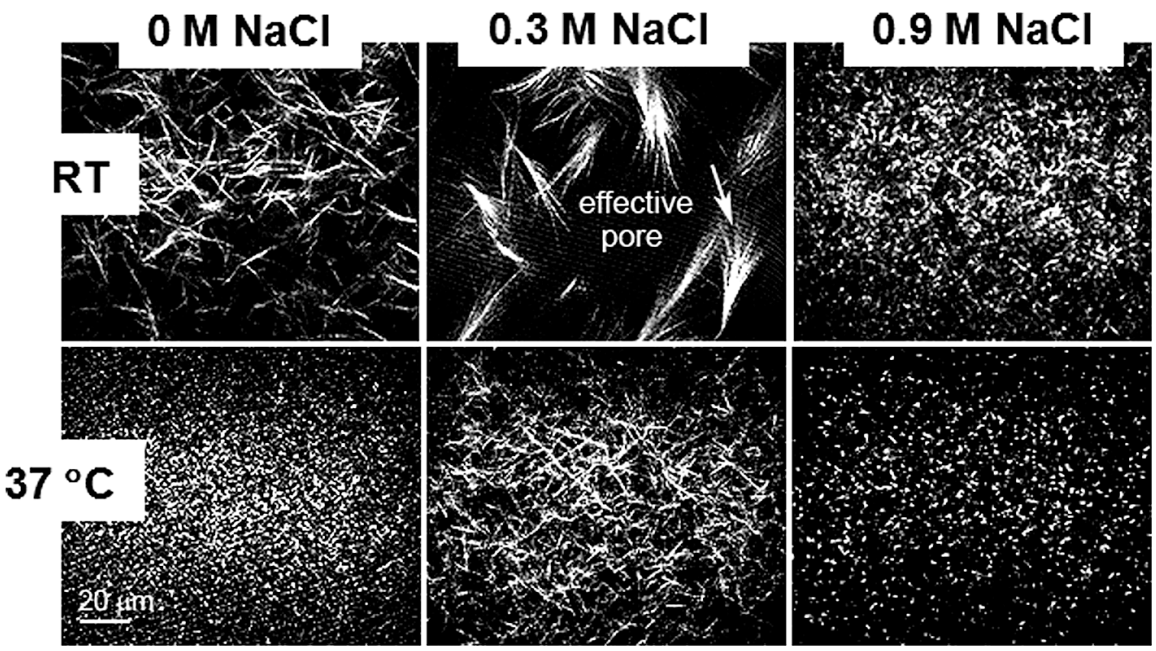

Figure 2.4 Backscattered second harmonic generation (SHG) images from 2 g l^{-1} collagen hydrogels assembled at pH 7.4, 30 mM phosphate and different sodium chloride concentrations as indicated. (Top row): room temperature (RT) assembly; (bottom row): 37 °C assembly. The effective pore is indicated with text and the fiber is indicated with an arrow.

The trend of how different sodium chloride concentrations affect the microstructure formation at 27 °C assembly temperature (Fig. S4) is similar to RT (Figure 2.4). When temperature is 27 °C, an average diameter of the effective pores formed at 0.3 M sodium chloride concentration (Fig. S4) is almost three times smaller compared to that observed at RT (about 22 μm *versus* about 60 μm). When temperature is 37 °C (Figure 2.4, bottom row), the fibers formed are smaller than at RT and at 27 °C. Nevertheless, the trend of how different sodium chloride concentrations affect the microstructure formation is similar to RT and 27 °C.

In summary, for all assembly temperatures, when sodium chloride concentrations are at the two extremes of 0 M and 0.9 M, the fibers formed are smaller compared to those formed at other sodium chloride concentrations under the same temperature and collagen solid content. For 0.9 M sodium chloride samples, the hydrogel's effective pore sizes are smaller than at other sodium chloride concentrations and some are too small to be reliably measured (Table 2.2). For samples polymerized at RT and 27 °C, for 0.3 M sodium chloride induced hydrogels, the effective pore structure is clear. On the contrary, there are many small fibers in the pore structure of 0.6 M sodium chloride samples at these incubation temperatures. In 0.3 M sodium chloride induced hydrogels, the fibers seem to be compacted better than in 0.6 M sodium chloride induced hydrogels. However, there are more connections between fibers in 0.6 M sodium chloride samples than in 0.3 M sodium chloride samples. When temperature is room temperature and sodium chloride concentration is 0.3 M, hydrogels have a good balance of fiber length, fiber width, effective pore structure and connections between fibers.

Table 2.2 Summary of the collagen hydrogel microstructural parameters upon sodium chloride assisted assembly at pH 7.4, 30 mM phosphate, different temperatures and collagen solid content (2 g l^{-1} or 4 g l^{-1}) and corresponding standard deviations from the mean

Condition temperature, Solid content	[NaCl] = 0 M Fibre Length Fiber Width Pore Diameter (μm)	[NaCl] = 0.3 M Fiber Length Fiber Width Pore Diameter (μm)	[NaCl] = 0.6 M Fiber Length Fiber Width Pore Diameter (μm)	[NaCl] = 0.9 M Fiber Length Fiber Width Pore Diameter (μm)
RT, 2 g l^{-1}	34.3 ± 10.2	52.0 ± 12.1	42.4 ± 9.3	2.6 ± 1.2
	1.7 ± 0.3	2.5 ± 0.8	2.5 ± 0.9	0.2 ± 0.1
	18.7 ± 8.7	60 ± 13	22.3 ± 4.7	3.9 ± 1.3
RT, 4 g l^{-1}	20.4 ± 4.7	50.0 ± 7.4	35.7 ± 5.4	2.7 ± 1.0
	1.3 ± 0.4	5.2 ± 1.4	1.9 ± 0.4	0.6 ± 0.2
	10.0 ± 2.6	60 ± 11.5	17 ± 4.0	4.5 ± 0.9
27 °C, 2 g l^{-1}	16.8 ± 4.4	43.0 ± 12.1	46.6 ± 10.1	2.5 ± 1.7
	0.7 ± 0.3	3.1 ± 0.8	2.4 ± 0.8	0.6 ± 0.6
	9.2 ± 3.3	21.7 ± 7.4	22.7 ± 7.1	8.5 ± 2.8
27 °C, 4 g l^{-1}	23.2 ± 5.0	38.9 ± 9.6	20.6 ± 7.0	—
	1.1 ± 0.4	2.1 ± 0.5	1.6 ± 0.4	—
	13.5 ± 3.3	16.4 ± 3.9	16.7 ± 5.1	—
37 °C, 2 g l^{-1}	3.2 ± 1.3	11.0 ± 3.1	9.6 ± 3.8	3.0 ± 1.3
	0.6 ± 0.2	1.1 ± 0.4	0.6 ± 0.2	0.9 ± 0.3
	5.2 ± 1.4	14.9 ± 4.2	10.2 ± 2.7	—
37 °C, 4 g l^{-1}	1.8 ± 1.1	9.0 ± 2.4	3.8 ± 1.5	—
	0.2 ± 0.1	1.0 ± 0.4	0.9 ± 0.3	—
	2.6 ± 0.5	3.1 ± 0.7	4.8 ± 1.2	—

The relative scattering intensities and attenuation lengths (the depth into the hydrogel at which maximum SHG signal at the surface of the gel drops to 1/*e* of its value) of the prepared hydrogels are estimated from second harmonic generation (SHG) images. They are shown in Figure 2.5 (2 g l^{-1} hydrogels; A, B: 37 °C assembly; C, D: RT assembly). The maximum of the SHG intensities, which is related to the amount of scattering, shows similar trend to the optical density (OD) values obtained in turbidity measurements (Figure 2.3B). As determined in this work, 37 °C, 2 g l^{-1} hydrogels have 2 mm and greater attenuation lengths. These attenuation lengths do not appear to be significantly affected by difference in the amount of scattering between samples formed at different sodium chloride concentrations. RT 2 g l^{-1} hydrogels, 0 M sodium chloride samples are too heterogeneous to obtain practical decay data or the attenuation lengths. The attenuation length shows both fast (about 100 μm) and slow (about 2 mm) decaying

components for RT 2 g l^{-1} hydrogels induced with 0.3 M sodium chloride. They are about 500 μm and 1500 μm for RT 2 g l^{-1} hydrogels induced with 0.6 M sodium chloride and RT 2 g l^{-1} hydrogels induced with 0.9 M sodium chloride respectively. Multi-exponential decaying components recovered for the values of attenuation length in RT hydrogels indicate heterogeneity[12] in these samples.

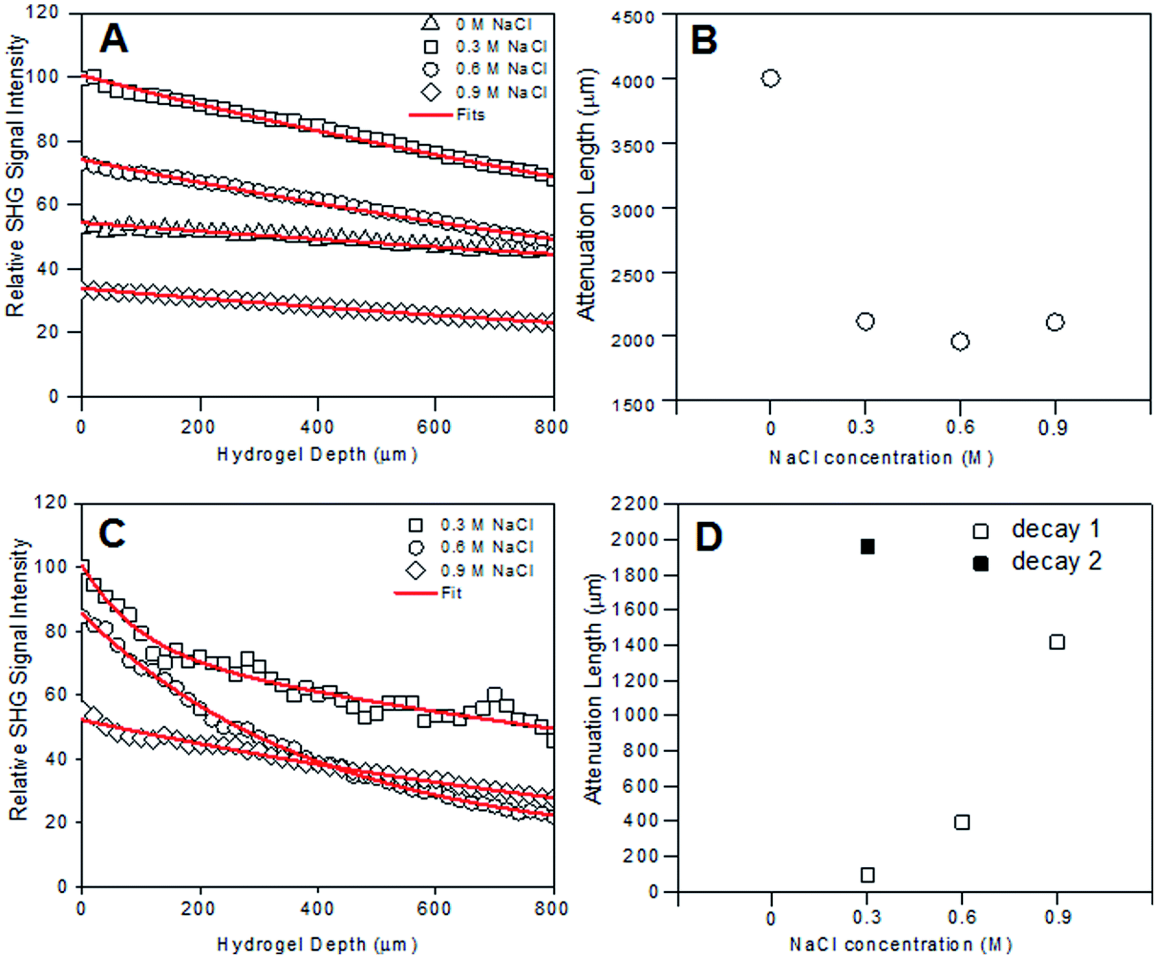

Figure 2.5 Backscattered second harmonic generation (SHG) signal averaged intensities plotted as a function of penetration depth (A), (C) and attenuation lengths (B), (D) in 2 g l^{-1} hydrogels assembled with 30 mM phosphate and different sodium chloride concentrations; (A) and (B) 37 °C assembly; (C) and (D) room temperature (RT) assembly. Lines are fits to the exponential decays.

Sodium sulfate assisted collagen hydrogel assembly

Polymerization and kinetics: Upon incubation at 37 °C, the samples formed stable hydrogels at all Na_2SO_4 concentrations. The polymerization trends with sodium sulfate are similar to polymerization with phosphate (Table 2.1). For example, the total time to polymerize collagen into hydrogels first increases upon increasing salt concentration (from about 17 min to about 50 min in the sodium sulfate concentration range of 5 mM to 75 mM). The total time subsequently decreases to about 26 min when salt concentration is further increased to 150 mM. Under the room temperature, collagen hydrogels assembled with different concentrations of Na_2SO_4 show three distinct regimes for the assembly. When Na_2SO_4 concentration is from 5 to about 50 mM, the measured delay times increase. When Na_2SO_4 concentration is from about 75 mM to 100 mM, the samples needed 7 to 10 days to polymerize. When Na_2SO_4 concentration is from 150 mM to 300 mM, the total time needed to polymerize hydrogels decreases along with increasing Na_2SO_4 content. The hydrogels formed under the room temperature are not homogenous by visual inspection.

Second harmonic generation (SHG) imaging: For 2 g l^{-1} hydrogels polymerized at room temperature (RT), on average, fibers become longer and thinner if we change final Na_2SO_4 concentration from 5 mM (Figure 2.6, top row, left image and Table 2.3) to 20 mM (Table 2.3). However, 5 mM to 20 mM Na_2SO_4 induced hydrogles are not stable and samples imaged consist of fiber clusters dispersed in a somewhat liquid phase. When Na_2SO_4 concentration is from 75 mM to 100 mM, the samples take 7–10 days to partially polymerize. Therefore, we could not obtain images of the final products for this regime.

When Na_2SO_4 concentration is from 150 to 300 mM, the total time needed to polymerize hydrogels decreases along with increasing Na_2SO_4 concentrations. The resulting fibers for 150 mM Na_2SO_4 are on the average longer and significantly thinner (Figure 2.6, top row, right image and Table 2.3) then in the first regime (5 mM to about 50 mM Na_2SO_4). The 4 g l^{-1} hydrogels polymerized at RT show similar trends (Table 2.3). In all three regimes, the RT polymerized hydrogels are not homogenous.

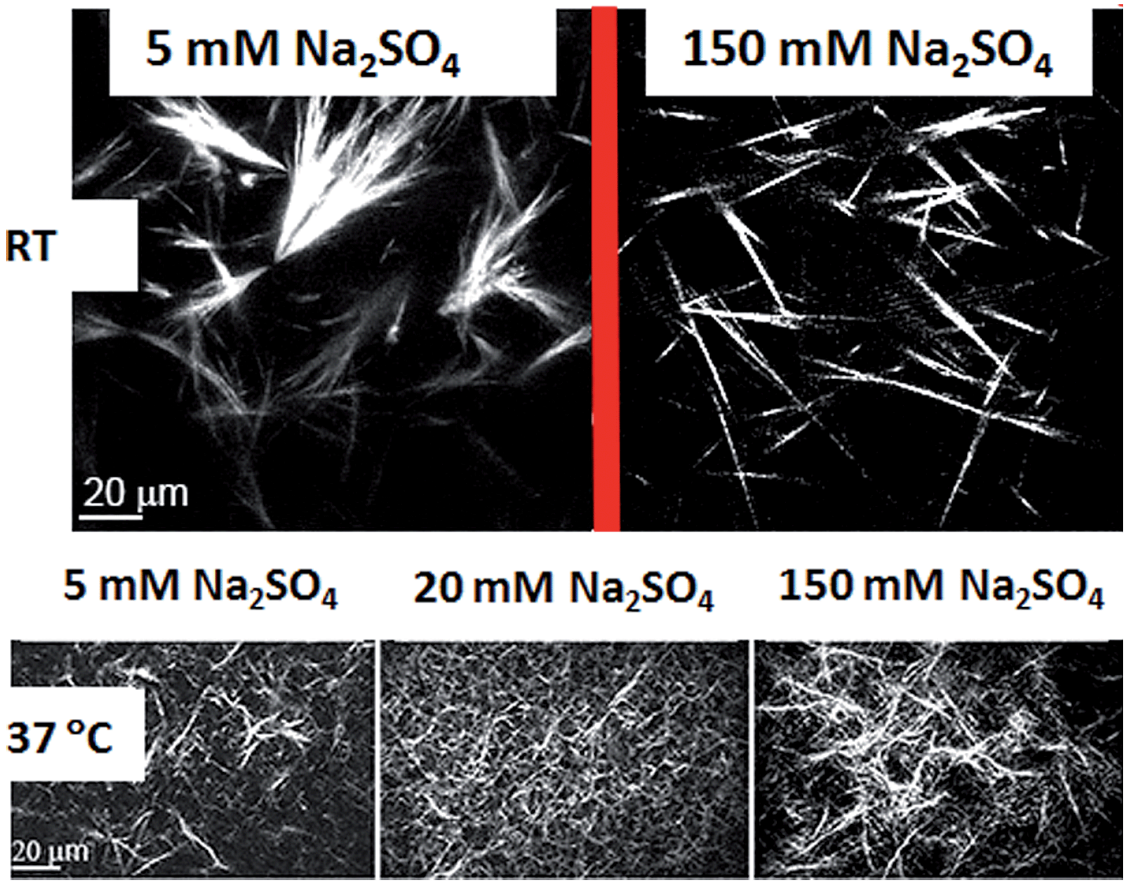

Figure 2.6 Backscattered second harmonic generation (SHG) images from 2 g l^{-1} collagen hydrogels assembled at pH 7.4, 30 mM phosphate and different sodium sulfate concentrations as indicated. (Top row): room temperature (RT) assembly. Red line indicates that fibers imaged correspond to different assembly regimes influenced by sodium sulfate concentration; (bottom row): 37 °C assembly.

Table 2.3 Summary of the collagen hydrogel microstructural parameters upon sodium sulfate assisted assembly at pH 7.4, 30 mM phosphate, different temperatures and different collagen solid content (2 g l^{-1} or 4 g l^{-1}) and corresponding standard deviations from the mean

Condition temperature, solid content	$[Na_2SO_4]$ = 5 mM fiber length, fiber width, pore size (μm)	$[Na_2SO_4]$ = 10 mM fiber length, fiber width, pore size (μm)	$[Na_2SO_4]$ = 20 mM fiber length, fiber width, pore size (μm)	$[Na_2SO_4]$ = 150 mM fiber length, fiber width, pore size (μm)
RT, 2 g l^{-1}	36.2 ± 12.3, 5.3 ± 1.9, 64.9 ± 16.7	50.2 ± 11.3, 6.4 ± 2.1, 36.7 ± 11.8	49.3 ± 16.0, 3.5 ± 1.2, 39.2 ± 14.2	52.8 ± 23.9, 1.2 ± 0.22, 49.9 ± 14.5
RT, 4 g l^{-1}	39.3 ± 15.3, 5.1 ± 1.4, 43.4 ± 11.6	37.1 ± 9.6, 4.8 ± 1.1, 53.1 ± 16.3	47.5 ± 11.6, 3.3 ± 0.7, 47.1 ± 11.5	71.9 ± 17.9, 1.5 ± 0.3, 35.1 ± 8.8
37 °C, 2 g l^{-1}	22.0 ± 8.2, 1.6 ± 0.3, 16.6 ± 4.4	24.6 ± 5.9, 1.7 ± 0.3, 14.1 ± 2.9	24.2 ± 6.0, 1.54 ± 0.2, 8.8 ± 2.8	25.6 ± 5.7, 1.56 ± 0.3, 19 ± 3.7
37 °C, 4 g l^{-1}	13.8 ± 5.9, 1.1 ± 0.3, 7.8 ± 2.4	19.1 ± 6.1, 1.3 ± 0.4, 16.5 ± 4.7	22.5 ± 5.2, 1.4 ± 0.2, 11.8 ± 4.1	19.2 ± 4.6, 1.6 ± 0.2, 22.8 ± 5.9

When polymerization temperature is 37 °C (Figure 2.6, bottom row), the hydrogels' microstructure is further altered. At this temperature, the microstructure of 2 g l^{-1} collagen hydrogels prepared with 5 mM Na_2SO_4 consists of some elongated fibers dispersed within material that does not produce strong second harmonic generation (SHG) signals. The somewhat smaller, however better defined SHG generating structures are observed within 4 g l^{-1} hydrogels (not shown) prepared under the same concentration of Na_2SO_4. A dense network of elongated fibers is seen in the SHG images of 2 g l^{-1} hydrogels prepared with 20 mM Na_2SO_4. On average, within 4 g l^{-1} hydrogels (not shown), fibers prepared at this Na_2SO_4 concentration appear slightly shorter and more densely packed. When Na_2SO_4 is 150 mM, similar to the phosphate-modulated polymerization, we observe substantially larger effective pores within both 2 g l^{-1} (Figure 2.6, bottom row, right image) and 4 g l^{-1} hydrogels (not shown) compared to lower concentration of sulfate.

Discussion

Mixing an initiation buffer solution which contains dissolved ions with stock collagen protein solution and adjusting pH of the mix to 7.4 initiates self-assembly of collagen

within forming hydrogels. Upon completion of the collagen polymerization process within these colloidal systems, fiber is a salted out fraction or a floc consisting of collagen protein.

Ions' ability to salt out or salt in proteins in solutions is ordered into the Hofmeister series.[13] The series can be applied to understand interactions among ions, water and macromolecules such as proteins in bulk solutions as well as at the interface.[14] The classical anion series are arranged as $SO_4^{2-} > HPO_4^{2-} > CH_3COO^- > OH^- > F^- > Cl^- > Br^- \approx NO_3^- > I^- > ClO_4^- > SCN^-$. The strongly hydrated anions, which have stabilizing effect and decrease solubility of proteins (salt out), are to the left of Cl^-. The weakly hydrated anions to the right of Cl^- are protein denaturants, which increase protein solubility (salt in) upon interaction. The divalent anions HPO_4^{2-} and SO_4^{2-} employed in this study are early in the Hofmeister series. Compared to monovalent Cl^- anion, which is later in the series, they carry a greater capacity to decrease the solubility of collagen molecules and to promote aggregation.

In spite of many works of the past decade, the specific salting out effects of different ions with respect to the protein structure are poorly understood and lack systematic explanation.[14] However, there is consensus that a type and a concentration of added salts are the driving forces behind aggregation behavior.[14] The two processes potentially explaining this behavior that can take place simultaneously are: (i) the attenuation of electrostatic repulsion through the specific association of ions with proteins' charged groups and (ii) the ions altering the tension at the protein-aqueous interfaces. Association of anions with positively charged protein residues reduces the effective surface charges

on the protein macromolecules. Larger (softer) anions are more efficient at screening the electrostatic repulsion between protein molecules and promoting salting-out behavior. Additionally, the surface tension of water increases along with an increase in the amount of salt[15] added thus stabilizing flocs[16] – collagen protein molecules and/or fibrils aggregated into the "fiber-like" structures observed in the second harmonic generation (SHG) images. Thus increased surface water tension and attenuated electrostatic repulsion due an increased amount of salt in the final polymerization mix can potentially lead to an increased size of the aggregated collagen flocs (fibers).

Under low phosphate concentrations (less than 20 mM), stable collagen hydrogels did not form and samples were essentially liquid. Along with inability to form stable gels, similar to previous studies, we observed an increase in collagen solubility in this range of phosphate concentrations. Kuznetsova *et al.*[17] referred to phosphate ions being strong fibrillogenesis inhibitors in the range of 10 to 25 mM and leading to an increase in collagen solubility. Subsequent studies by Mertz *et al.*[18] attribute this increase in solubility to the preferential interaction of the dibasic form of phosphate with collagen fibrils. The same study determined from infrared measurements that under physiological conditions there are one to two sulfate and dibasic phosphate binding sites per collagen molecule inside fibrils and none for the monovalent phosphate. The researchers proposed that bound divalent anions formed salt bridges between positively charged amino acid residues within the collagen fibrils. However, the study further suggested that this binding is insignificant to the formation, stability and structure of collagen fibrils and that the fibrils are stabilized by preferential exclusion of non-bound anions from interstitial

water within fibrils. NaCl was proposed to affect binding of dibasic phosphate and partitioning of monobasic phosphate in collagen fibrils.

When we increased the phosphate concentration to about 30 mM–60 mM, we formed stable hydrogels. Similarly to prior work on collagen assembly in diluted protein solutions (0.1 g l^{-1}),[10b] we observed a decrease in collagen polymerization rate when phosphate concentration was increased beyond 30 mM. The fibers in 30 mM–60 mM phosphate concentration range remained small. We believe that aggregation into the larger fiber structures is unfavorable in this phosphate concentration range due to only a modest disruption of the hydration shell of water around protein packed into the fiber structures. When phosphate concentration was high (80–160 mM), the phosphate in addition to maintaining the pH and binding to collagen molecules, must be significantly compressing the hydration shell within collagen fibers. The interactions of protein groups with salt can potentially make it easier for the fibrils to stick to each other to form a larger 'fiber' floc. This possibly explains why fibers are larger under this phosphate concentration compared to 30–60 mM phosphate-induced samples. Yet, increasing phosphate concentration further (200 or 300 mM) induced again smaller 'fiber-like' features within hydrogels. Very high phosphate concentrations (500 mM) resulted in the formation of fine precipitate along with slight increase in solubility. Proteins are often denatured by high concentrations of inorganic salts.[19] The ions formed due to dissolution of inorganic salts are possibly binding to ionic groups of proteins and disrupting interactions that stabilize collagen 'fiber-like' structures. These interactions lead to the formation of fine precipitate. Similar insight can be applied to the sodium sulfate and

sodium chloride assisted collagen materials assembly at 37 °C. In those samples, there was enough phosphate to maintain the pH and to stabilize collagen fibers. Similarly, high concentration of 0.9 M NaCl appeared to encourage collagen solubility and led to the formation of smaller 'fiber' flocs.

In general in self-assembling systems, lowering or raising temperature affects formation of colloidal flocs in different and not obvious ways. This further raises a need to conduct measurements on such systems directly, non-invasively and *in situ.* The optical methods presented in this study are perfectly suited for such task. In a sodium-chloride-assisted collagen materials assembly at lower temperature (27 °C and/or room temperature) we observed formation of longer and thicker "fiber-like" structures compared to 37 °C assembled gels. Lowering temperature is potentially improving an exothermic adsorption step thus leading to the formation of larger "fiber-like" aggregates seen at 27 °C and room temperature. Interestingly, when a divalent anion such as sulfate is used, in the 5 mM–20 mM concentration range of sulfate, large and long fibers are formed at room temperature. However, for these sulfate concentrations, a stable polymeric network within gels is not established perhaps due to insufficient overlap between the formed fibers. It is only more challenging to obtain a stable hydrogel in 75 mM to 100 mM sulfate since they did not seem to polymerize within even a few days. When sodium sulfate concentration was from 150 to 300 mM, the total time needed to polymerize hydrogels decreased along with increasing salt concentrations. The fibers were significantly thinner and somewhat longer then when sulfate was 5 mM–20 mM. Further experiments are carried out to understand these complex phenomena resulting from

combined effects of polymerization temperature,[5, 12] pH,[20] collagen solid content[14] and ionic species on the self-assembly of collagen at the fiber structural level.

The studies presented in this work are timely. Recently, Li *et al.*[21] also studied collagen molecular interactions with a focus on fibrils formed in various salts dissolved directly in the collagen solutions adjusted to the appropriate pH with 0.1 M NaOH. Based on the low resolution transmission electron microscopy (TEM) images the authors concluded that at pH 7.4, low concentrations of salts that have monovalent ions lead to the formation of small filaments without banding patterns. When the ionic strength was increased to 200 mM, the collagen fibrils were more ordered and some large fibrils with the banding patterns were observed. When salts with multivalent ions were used, collagen monomers aggregated to form ordered fibril bundles that showed clearer banding patterns. Polarized light microscopy images of dispersed on glass slides collagen fibrils formed in NaCl and KCl salts (100 mM, pH 7.4) and about 80 μm in diameter fibril bundles detected in Na_2SO_4 and Na_2HPO_4 samples (ionic strength 250 mM, pH 7.4) were also obtained.

In a somewhat related study, Jiang *et al.*[22] evaluated the effects of pH and electrolytes on the assembly of collagen into microribbons (about 3 nm anisotropic ribbon-like structures) deposited onto freshly cleaved mica supports. The deposition was controlled by employing hydrodynamic flow and the structures formed were examined with atomic force microscopy (AFM). The influence of $MgCl_2$, NaCl and KCl electrolytes on the assembly was studied at the neutral pH of 7.5. Interestingly, low NaCl concentration (50 mM) and high NaCl concentration (200 mM) resulted in single layer of collagen fibrils

on the mica surface. However, when NaCl concentration was 100 mM, the protrusions of the first layer merged into incomplete second fibrillar layer.

Gobeaux *et al.*[23] also recently studied polymerization of collagen from concentrated solutions (40–300 mg ml^{-1}) at different pHs and ionic strengths. Two methods were used to adjust ionic strength. One method was to increase the concentration of phosphate buffer from 10 to 500 mM. Alternative method was to add NaCl in a 200 mM phosphate buffer. The gels formed in low ionic strength (24 mM) consisted of a dense network of 15–20 nm wide and 200–250 nm long nanofibrils observed in low resolution transmission electron microcopy (TEM) images. The fibrils increased in size and formed bundles as the ionic strength increased up to 261 mM along with an increase in gels' strength and opacity. Similarly, Harris *et al.*[24] concluded that at pH 7.0 and 8.0, in presence of 150 mM NaCl, the characteristic 67 nm D-banded collagen fibrils organized into fiber bundles predominated. At 529 mM and 1300 mM ionic strengths, Gobeaux *et al.*[23] study found that the polymerized collagen systems were biphasic. Specifically, at 529 mM ionic strength, large fibrillar bundles were surrounded by nanofibrils (about 40 nm in width and about 600 nm in length). On the other hand, at 1300 mM ionic strength the nanofibrils were surrounded by larger fibrils. The authors reported similar structures when monovalent salt was used to adjust the ionic strength.

Non-destructive *in situ* SHG imaging-based methods furnish new structural information regarding gross microscopic morphology of the synthesized collagen hydrogels. In our studies, collagen hydrogels were several millimeters in thickness. The structural information presented in this work is not attainable from transmission electron

microscopy (TEM) methods used by prior investigations. TEM imaging is generally destructive to biological samples and requires transmission of the electron beams through ultra-thin specimens. Unlike prior studies, using SHG imaging, we assessed the parameters relevant to the structure of collagen fibers *in situ* without disturbing materials. For example, unlike the study by Li *et al.*[24] we did not need to smear samples on the glass substrates to form thin sections in order to pass the transmitted light to form optical images.

To quantify relative differences in the hydrogels' microstructural parameters, we used a straight forward method of measuring the resulting fibers and effective pore sizes. While we reproducibly attain the measured numbers, the data analysis can greatly benefit from implementing automated methods. Some recent automatated approaches to analyze the 2D SHG images include works of Bayan *et al.*[25]and Matteini *et al.*[26] which employed Fourier transform and entropy analysis methods to obtain information regarding orientation of collagen fibers in gels and cornea respectively. While these methods can work well for the thin and/or linear fibers, these approaches tend to be more global type of comparisons. It is not clear how to take into account the width of the fibers for larger/spreading fibers that we observed at the lower temperature. Texture analyses have also been employed to analyze the SHG images of the collagen structure within extracellular matrix of normal ovarian stroma and high grade ovarian serous cancer.[27] Another method recently developed and used to analyze collagen structure in 3D employs operators from mathematical morphology to obtain fiber orientations and radius distributions.[28]

The attenuation lengths parameters presented in this manuscript help to establish design criteria to construct hydrogels for applications in which imaging directly through such materials is anticipated. Our measurements indicate that 37 °C hydrogels we prepared are homogeneous and have great transparency using the imaging conditions we employ. When these gels were used topically on the mice skin, they did not impact imaging of the underlying either epidermal or deep dermal structures.

Endogenous fields and currents occur naturally due to presence of ions in the wounds in order to guide cell migration.[29] It is conceivable therefore to envision the data and methods developed to be useful in examining the wound healing process where newly synthesized collagen aggregation process could be under ionic regulation. Manufacturing medical devices for bone tissue repair requires interactions of ionic regions of inorganic molecules of hydroxyapatite with collagen at the surfaces of fibrils/fibers[30] during its crystallization onto them and will potentially benefit from this research as well. The studies presented are also scientifically important and relevant to the field of tissue engineering as well, especially in the context of using ions as therapeutic agents.[31]

Conclusion

The second harmonic generation (SHG) imaging in situ allowed us to determine that increasing concentrations of phosphate increase the lengths of 37 °C, pH 7.4 polymerized collagen fibers. When increasing concentrations of sodium sulfate are added to 30 mM phosphate buffer used to polymerize collagen into hydrogels, fiber lengths similarly increase. On the other hand, adding sodium chloride at physiological and higher concentrations does not significantly lengthen the fibers within 37 °C, pH 7.4

polymerized hydrogels. Lowering temperature leads to a multilateral response, which depends on the type of ion employed. The fiber lengths and widths decrease in very high concentrations of all salts at all temperatures. Traditional turbidity measurements provided timescales for the gelation processes examined and solubility data showed that 85% of collagen was precipitated under all experimental conditions. Ions are an important element to take into account when gelation of collagen and other biologically derived protein scaffolds takes place. The methods and knowledge presented in this work can be applied to understand these practically important and complex assembly processes.

Acknowledgements

This work was supported in part with UC Riverside startup research funds (J.G.L.), UC Riverside Biochemistry Department Graduate Research Fellowship (X.L.), NSF CAREER Award CBET-0847070 (J.G.L) and NSF BRIGE Award EEC-0927297 (J.G.L).

References

1. R. D. Harkenss, Biological Functions of collagen. *Biol. Rev.* **1961,** *36*, 399-455.
2. C. H. Lee, A. S., Y. Lee Biomedical applications of collagen. *Int. J. Pharm.* **2001,** *221*, 1-22.

3. W. R. Zipfel, R. M. Williams, W. W. Webb, Nonlinear magic: multiphoton microscopy in the biosciences. *Nat. Biotechnol.* **2002,** *21*, 1367-1377.

4. R. M. Williams, W. R. Zipfel, W. W. Webb, Interpreting second-harmonic generation images of collagen I fibrils. *Biophys. J.* **2005,** *88*, 1388-1397.

5. C. B. Raub, V. Suresh, T. B. Krasieva, J. G. Lyubovitsky, J. D. Mih, A. J. Putnam, B. J. Tromberg, S. C. George, Noninvasive assessment of collagen gel microstructure and mechanics using multiphoton microscopy. *Biophys. J.* **2007,** *92*, 2212-2222.

6. S. Roth, I. Freund, Second harmonic generation in collagen. *J. Chem. Phys.* **1979,** *70*, 1637-1644.

7. W. R. Zipfel, R. M. Williams, R. Christie, A. Y. Nikitin, B. T. Hyman, W. W. Webb, Live tissue intrinsic emission microscopy using multiphoton-excited native fluorescence and second harmonic generation. *Proc. Natl. Acad. Sci. U. S. A.* **2003,** *100*, 6.

8. F. Legare, C. Pfeffer., B. R. Olsen, The role of backscattering in SHG tissue imaging. *Biophys. J.* **2007,** *93*, 1312-1320.

9. G. C. Na, L. J. Butz, D. G. Bailey, R. J. Carroll, In vitro collagen fibril assembly in glycerol solution: evidence for a helical cooperative mechanism involving microfibrils. *Biochemistry* **1986,** *25*, 958-966.

10. (a) H. B. Bensusan, B. L. Hoyt., The effect of various parameters on the rate of formation of fibers from collagen solutions1. *J. Am. Chem. Soc.* **1958,** *58*, 719-724; (b) B. R. Williams, R. A. Gelman, D. C. Poppke, K. A. Piez, Collagen fibril formation. *J. Biol. Chem.* **1978,** *253*, 6578-6585.

11. (a) J. Hirshburg, B. Choi, S. Nelson, A. T. Yeh, Correlation between collagen solubility and skin optical clearing using sugars. *Lasers Surg. Med.* **2007,** *39*, 140-144; (b) J. Hirshburg, B. Choi, S. Nelson, A. T. Yeh, Collagen solubility correlates with skin optical clearing. *J. Biomed. Opt.* **2006,** *11*, 040501.

12. Y. Hwang, J. G. Lyubovitsky, Collagen hydrogel characterization: multi-scale and multi-modality approach. *Anal. Methods* **2011,** *3*, 529-536.

13. F.Hofmeister, Zur lehre von der wirkung der salze. *Arch. Exp. Pathol. Pharmakol.* **1888,** *24*, 247-259.

14. P. L. Nostro, B. W. Ninham., Hofmeister phenomena: an update on ion specificity in biology. *Chem. Rev.* **2012,** *112*, 2286-2322.

15. N. L. Jarvis, M. A. Scheiman, Surface potentials of aqueous electrolyte solutions. *J. Phys. Chem.* **1968,** *72*, 74-78.

16. P. C.Hiemenz, *Principles of colloid and surface chemistry, ed. M. Dekke, 2nd edn* **1986**.

17. N. Kuznetsova, S. L. Chi, S. Leikin, Sugars and polyols inhibit fibrillogenesis of type I collagen by disrupting hydrogen-bonded water bridges between the helices. *Biochemistry* **1998,** *37*, 11888-11895.

18. E. L. Mertz, S. Leikin, Interactions of inorganic phosphate and sulfate anions with collagen. *Biochemistry* **2004,** *43*, 14901-14912.

19. I. Palmer, P. T. W., *Curr. Protoc. Protein Sci.* **2004,** *38*, 6.3.1–6.3.18.

20. (a) S. Bancelin, C. Aime, T. Coradin, M. C. Schanne-Klein,, In situ three-dimensional monitoring of collagen fibrillogenesis using SHG microscopy. *Opt. Express* **2012,** *3*, 1446-1454; (b) C. B. Raub, J. Unruh, V. Suresh, T. Krasieva, T. Lindmo, E. Gratton, B. J. Tromberg, S. C. George, Image correlation spectroscopy of multiphoton images correlates with collagen mechanical properties. *Biophys. J.* **2008,** *94*, 13.

21. Y. Li, E. P. Douglas, Effects of various salts on structural polymorphism of reconstituted type I collagen fibrils. *Colloids Surf* **2013,** *112*, 42-50.

22. F. Z. Jiang, H. Horber, J. Howard, D. J. Müller, Assembly of collagen into microribbons: effects of pH and electrolytes. *J. Struct. Biol.* **2004,** *148*, 268-278.

23. F. Gobeaux, G. Mosser, A. Anglo, P. Panine, P. Davidson, M.-M. Giraud-Guille, E. Belamie, Fibrillogenesis in dense collagen solutions: a physicochemical study. *J. Mol. Biol.* **2008,** *376*, 1509-1522.

24. J. R. Harris, A. Reiber, Influence of saline and pH on collagen type I fibrillogenesis in vitro: fibril polymorphism and colloidal gold labelling. *Micron* **2007,** *38*, 513-521.

25. C. Bayan, J. M. Levitt, E. Miller, D. Kaplan, I. Georgakoudi, Fully automated, quantitative, noninvasive assessment of collagen fiber content and organization in thick collagen gels. *J. Appl. Phys.* **2009,** *105*, 102042.

26. P. Matteini, F. Ratto, F. Rossi, R. Cicchi, C. Stringari, D. Kapsokalyvas, F. S. Pavone, R. Pini, Photothermally-induced disordered patterns of corneal collagen revealed by SHG imaging. *Opt. Express* **2009,** *17*, 4868-4878.

27. B. L. Wen, M. A. Brewer, O. Nadiarnykh, J. Hocker, V. Singh, T. R. Mackie, P. J. Campagnola, Texture analysis applied to second harmonic generation image data for ovarian cancer classification. *J. Biomed. Opt.* **2014,** *19*, 096007.

28. H. Altendorf, E. Decenciere, D. Jeulin, P. De Sa Peixoto, A. Deniset-Besseau, E. Angelini, G. Mosser, M. C. Schanne-Klein, Imaging and 3D morphological analysis of collagen fibrils. *J. Microsc.* **2012,** *247*, 161-175.

29. (a) B. Reid, B. Song, C. D. McCaig, M. Zhao, Wound healing in rat cornea: the role of electric currents. *FASEB J.* **2005,** *19*, 379-386; (b) A. C. Vieira, B. Reid, L. Cao, M. J. Mannis, I. R. Schwab, M. Zhao, Ionic components of electric current at rat corneal wounds. *PLoS One* **2011,** *6*, e17411.

30. (a) S. Weinera, W. Traub, Organization of hydroxyapatite crystals within collagen fibrils. *FEBS Lett* **1986,** *206*, 262-266; (b) N. Roveri, G. Falini., M. C. Sidoti, A. Tampieri, E. Landi, M. Sandri, B. Parma, Biologically inspired growth of hydroxyapatite nanocrystals inside self-assembled collagen fibers. *Mater. Sci. Eng.* **2003,** *23*, 441-444; (c) D. A. Wahl, J. T. Czernuszka, Collagen-hydroxyapatite composites for hard tissue repair. *Eur. Cells Mater.* **2006,** *11*, 43-56.

31. (a) V. Mouriño, J. P. Cattalini, A. R. Boccaccini, Metallic ions as therapeutic agents in tissue engineering scaffolds: an overview of their biological applications and strategies for new developments. *J. R. Soc., Interface* **2012,** *9*, 401-419; (b) D. S. Adams, A new tool for tissue engineers: ions as regulators of morphogenesis during development and regeneration. *Tissue Eng., Part A* **2008,** *14*, 1461-1468.

Supplementary material

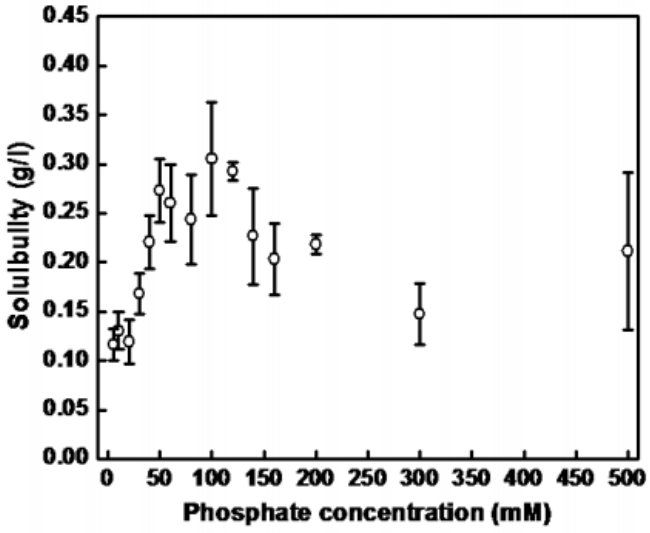

Figure 2.S1 The solubility of collagen in samples prepared under 37 °C and different concentrations of phosphate.

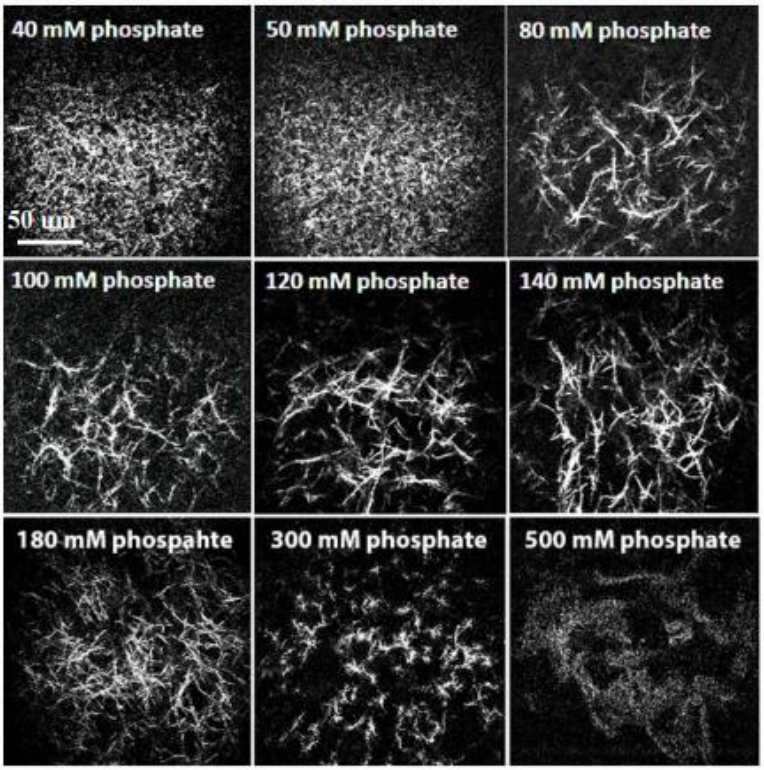

Figure 2.S2 Additional backscattered second harmonic generation (SHG) images from collagen materials assembled at pH 7.4, 37 °C and 40 mM, 50 mM, 80 mM, 100 mM, 120 mM, 140 mM, 180 mM, 300 mM and 500 mM phosphate concentrations.

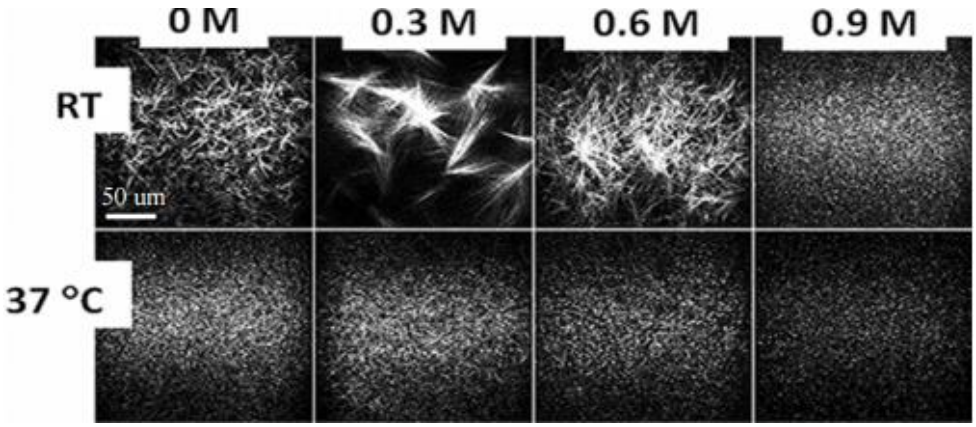

Figure 2.S3 Backscattered second harmonic generation (SHG) images from collagen materials assembled at pH 7.4, 4 g/l collagen solid content, room temperature as well as 37 °C and different sodium chloride concentrations.

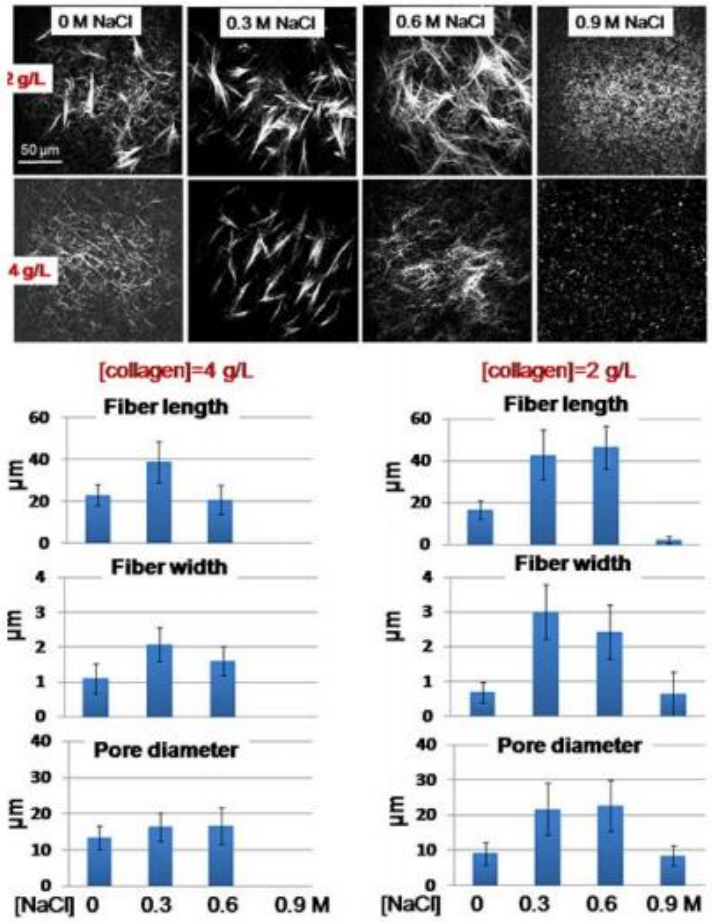

Figure 2.S4 Backscattered second harmonic generation (SHG) images from collagen materials assembled at pH 7.4, 27 °C, different sodium chloride concentrations and quantification of the collagen hydrogel parameters.

Chapter 3: The effect of pH on microstructure of collagen hydrogel

Abstract

Multiphoton Microscopy (MPM) is a noninvasive imaging technology that was used for the characterization of microstructure of collagen hydrogels by collecting Second Harmonic generation (SHG) signal and Two-Photon excited fluorescence (TPF) signal form collagen hydrogel which was prepared at different pH conditions. The fibers' length and the pore structure diameter were quantified by the image J. Higher pH (pH 8.2) results in 2-4 folds longer fibers compared with lower pH (pH5.5) at room temperature for four different ionic conditions. Fibers' length correlates well with the polymerization pH at room temperature (R^2 = 0.98 or 0.99) for most ionic conditions. When phosphate concentration is same, higher NaCl concentration (0.3M) can result in the 2 fold longer fibers compared with lower NaCl concentration (0.15M) at room temperature for all conditions. The 2 g/l pH 5.5 room temperature samples and 3 g/l pH 5.5 room temperature samples do not form hydrogels.

Introduction

Collagen, which is the main component of extracellular matrix[1] and accounts for 20-30% of protein in human body,[2] plays very important roles in connective tissue because collagen microstructure can determine the properties of the connective tissue. It has been reported by Parry et al. that different nano-structure (structure in molecule or fibril level) of collagen can result in different mechanical properties of connective tissue.[3] Patterson-Kane also identified that the more rigid property of tendon in axial direction than in lateral direction is due to the fibers of collagen (microstructure) being parallel to the

tendon axis.[4] So Far, collagen hydrogel materials are widely used in tissue engineering field as a scaffold for cell proliferation and differentiation. The microstructure of collagen hydrogel materials can result in different cellular behavior within collagen hydrogel materials. Then it is important and necessary to study the microstructure of collagen hydrogel materials. The structure of collagen can be affected by a lot of parameters, such as ionic conditions, temperature, pH and so on.[5] So far, Most of researches focus on the effect of pH on the nanostructure and/or stability of protein molecules in solution. On one hand, Yang and Schaefer has reported that protein stability is pH-dependence.[6] On another hand, Chan reported the effect of pH on the protein aggregation and deposition.[7] But few studies have been done about the effect of pH on the microstructure formation of collagen hydrogels. The mechanism is not well understood. *In situ* non-destructive methods are needed to characterize the microstructure properties of collagen hydrogel which was prepared at different pH. pH is not just an parameter to indicate $[H^+]$ in the solution. It is also a parameter to indicate the phosphate pH-dependent ionic forms and the side chain charge state of collagen molecules. In this chapter, we talk about the effect of pH on the microstructure of collagen hydrogel.

Multiphoton microscopy (MPM), a kind of nondestructive optical method, is used to real time and *in situ* to collect the Second Harmonic Generation (SHG) signal which is generated by the interaction of two photons on the fibers (microstructure) of collagen hydrogel with high resolution and contrast.[8] The light source is Near-Infrared (NIR) femtosecond pulsed laser which has the advantage of reduced scattering and deeper penetration than optical based techniques. SHG contrast can be used to directly detect

aggregated collagen structures within scaffolds. SHG signal is also label free and resists photobleaching.

Materials and methods

The preparation of 2X buffer: In this study, four kinds of 2X buffer were employed to prepare collagen hydrogel. They are 2X buffer A, 2X buffer B, 2X buffer C and 2X buffer D. The composition of 2X buffer A is 60 mM phospahte and 0.6 M NaCl. The composition of 2X buffer B is 60 mM phosphate and 0.3 M NaCl. The composition of 2X buffer C is 20 mM phosphate and 0.6 M NaCl. The composition of 2X buffer D is 20 m phosphate and 0.3 M NaCl. The pH of 2X buffers were adjusted to 7.4 by 1 M NaOH. All buffers are filtered with 0.22 μm, 33 mm syringe filter.

Collagen hydrogel preparation: The Type I collagen stock solution (9.07 g/l) was purchased from BD Biosciences (354249). It was stored at 4 °C. The collagen hydrogel was prepared by mixing the 2X buffer, 0.02 N acetic acid and collagen stock solution. The final concentration of collagen is 2 g/l, 3 g/l and 4g/l respectively. Then samples' pH was adjusted to 5.5, 7.5 or 8.2 before polymerization by 1 M NaOH or 1 N HCl. All the procedures are carried out on ice. The Henderson-Hasselbalch equation (pH = PKa + lg([base]/[acid])) is employed to calculate the concentration of mono- and dibasic of phosphate at different pH. The calculation procedure is shown in the result part.

Second Harmonic Generation (SHG) imaging experiment: The samples are prepared according to the description above. The SHG signal of 3D collagen hydrogel was collected by upright Thorlabs multiphoton laser scanning microscopy which is based on an upright Nikon microscopy. The femtosecond titanium:sapphire laser excitation source

provided femtosecond pulses at a repetition rate of about 80 MHz. The long working distance water immersion objectives (Zeiss, 63× water, N.A. 1.0; Zeiss, 10× water, N.A. 0.3; Olympus, 20× water, NA 1.0) were used to acquire images. The excitation wavelength is 810. 650 nm dichroic beamsplitter, 480 nm dichroic beamsplitter and 405 ± 5 nm bandpass filter are employed separate SHG signal. 63X image is 2048 × 2048 pixels size image which correspond to 200 μm × 200 μm field of view. 25 to 50 fibers' length and pore diameter are measured for each sample by image J.

Results

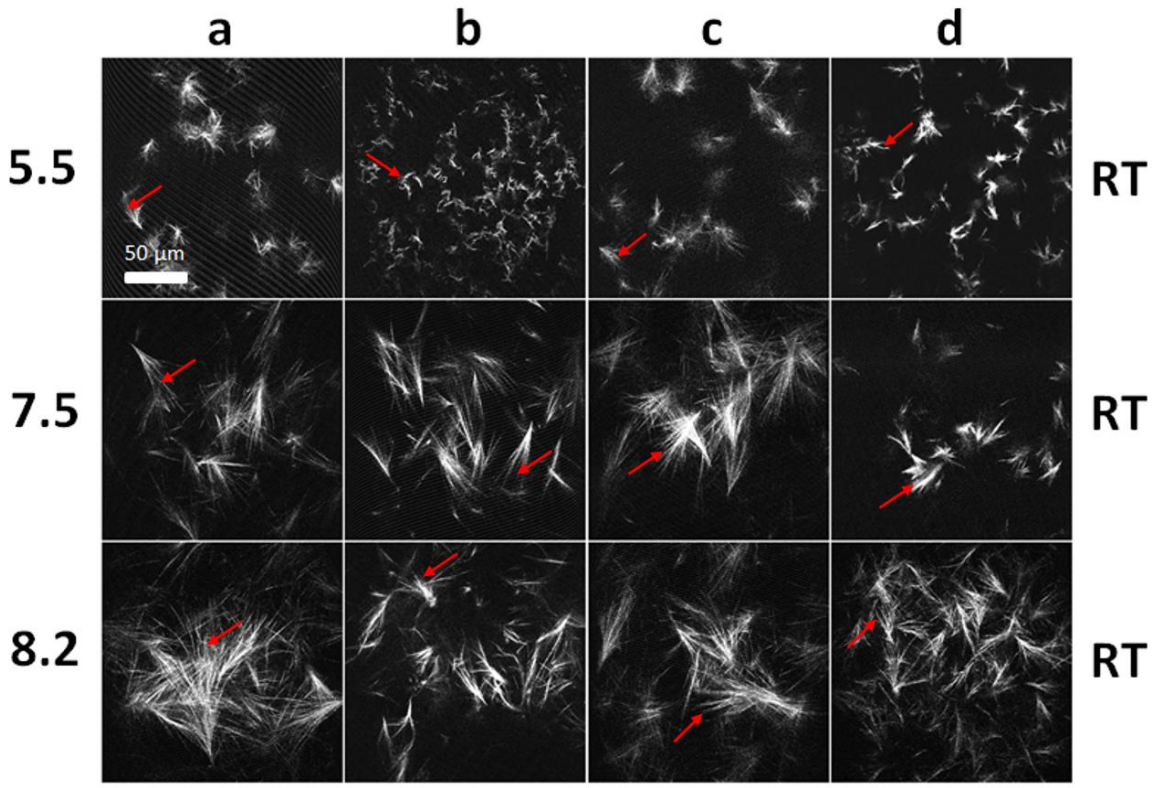

Figure 3.1 The effect of different pH on the microstructure of collagen hydrogel. Collagen concentration is 2 g/l. Polymerization temperature is room temperature. Top row is pH 5.5 samples. Middle row is pH 7.5 samples. Bottom row is pH 8.2 samples. The ionic condition a is 30 mM phosphate + 0.3 M NaCl. The ionic condition b is 30 mM phosphate + 0.15 M NaCl. The ionic condition c is 10 mM phosphate + 0.3 M NaCl. The ionic condition d is 10 mM phosphate + 0.15 M NaCl.

The effect of pH on the microstructure of collagen hydrogel

To study the effect of pH on the microstructure of collagen fibers, we prepare the samples at pH 5.5, pH 7.5, and pH 8.2 in different ionic conditions. When pH is 5.5, the average length of collagen fibers are 15.85 μm, 8.99 μm, 17.15 μm and 12.85 μm respectively for the four ionic conditions (A: 30 mM phosphate + 0.3 M NaCl; B: 30 mM phosphate + 0.15 M NaCl; C: 10 mM phosphate + 0.3 M NaCl; D: 10 mM phosphate + 0.15 M NaCl). The collagen fibers prepared at pH 5.5 are obviously much shorter than pH 7.5 and pH 8.2 samples' fibers for the same four ionic conditions. **(Figure 3.1)** The fibers expend wider at pH 7.5 and pH 8.2 compared with lower pH (pH 5.5) for the four ionic conditions. (**Figure 3.1** Arrow indicated). Different pH can result in different microstructure of collagen fibers, pH also can influence the samples state (hydrogel state or liquid state) at room temperature. When temperature is room temperature, the samples exist in the liquid state at pH 5.5, collagen hydrogel was formed at pH 7.5 and pH 8.2. **Figure 3.2** demonstrates the correlation between pH and fiber length. For most ionic conditions (A, B and C), the correlations between pH and the fiber length are very good (R^2 = 0.99 or 0.98). For the ionic condition D, there is no obvious correlation between pH and the fiber length.

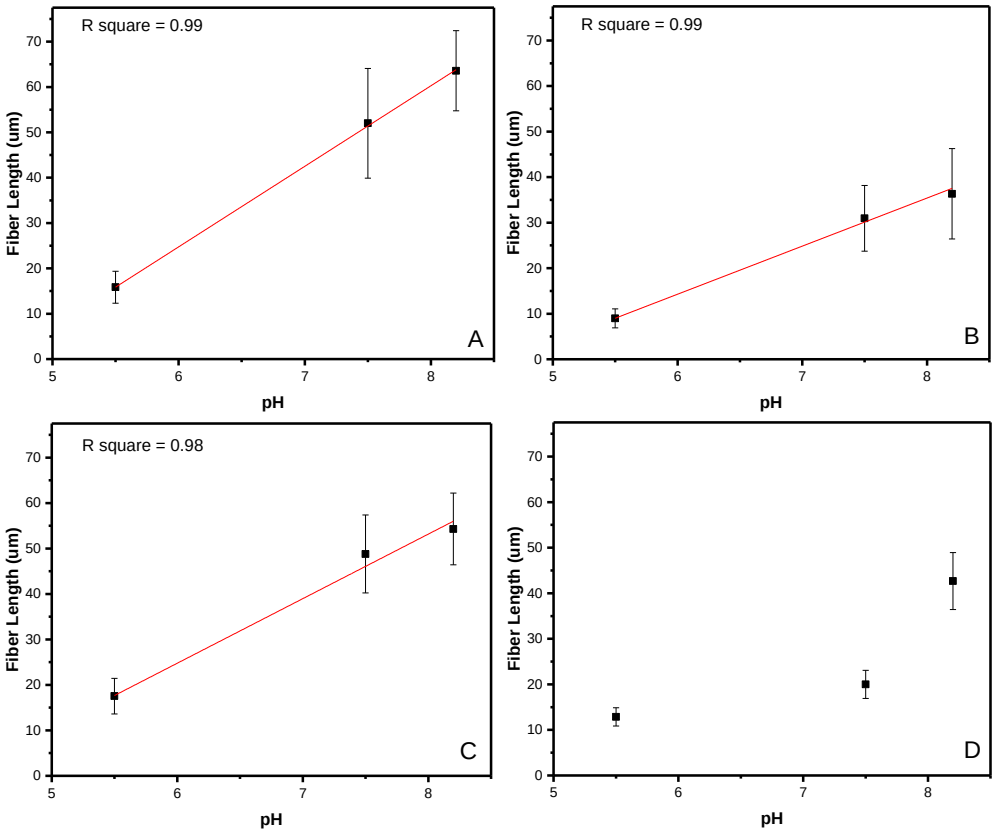

Figure 3.2 The correlation between pH and fiber length at different ionic conditions. (A: 30 mM Phosphate + 0.3 M NaCl; B: 30 mM Phosphate + 0.15 M NaCl; C: 10 mM Phosphate + 0.3 M NaCl; D: 10 mM Phosphate + 0.15 M NaCl). Collagen concentration is 2 g/l.

For the length of collagen fiber, it doesn't just depend on the pH, it also depends on the ionic conditions.[5] For our polymerization system, it is the phosphate and NaCl concentrations. When phosphate concentration is same, higher NaCl concentration (0.3 M) can result in longer fiber (~ 2 times) compared with lower NaCl concentration (0.15 M) at room temperature (**Table 3.1, Figure 3.2A, Figure 3.2B, Figure 3.2C and Figure 3.2D**). When NaCl concentration is same, there is no obvious fiber length difference for the high (30 mM) and low (10 mM) phosphate concentration samples at room

temperature for the equivalent pH (**Table 3.1, Figure 3.2A Figure 3.2C, Figure 3.2B and Figure 3.2C**).

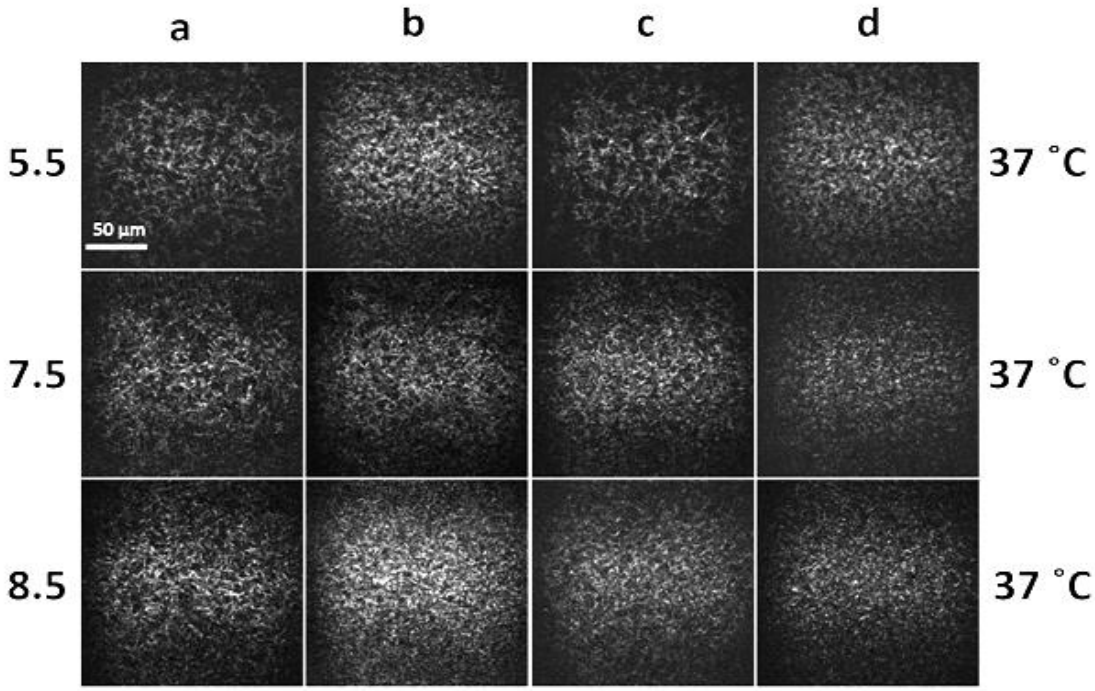

Figure 3.3 The effect of different pH on the microstructure of collagen hydrogel. Collagen concentration is 2 g/l. Polymerization temperature is 37 ˚C. Top row is pH 5.5 samples. Middle row is pH 7.5 samples. Bottom row is pH 8.2 samples. The ionic condition a is 30 mM phosphate + 0.3 M NaCl. The ionic condition b is 30 mM phosphate + 0.15 M NaCl. The ionic condition c is 10 mM phosphate + 0.3 M NaCl. The ionic condition d is 10 mM phosphate + 0.15 M NaCl.

Temperature also can result in the differences of microstructure and the state of collagen samples. When temperature is 37 °C, all samples exist in the hydrogel state for all pHs (5.5, 7.5 and 8.2) and all ionic conditions (a, b, c, d) (**Figure 3.3, Table 3.1**) and the 37 °C samples' fiber length are much shorter than room temperature samples' fiber length. When pH is 5.5, high NaCl concentration (0.3 M) result in longer collagen fibers (2-3 folds) compared with lower NaCl concentration (0.15 M) at 37 °C. (**Table 3.1**) When pH is 7.5 and 8.2 and temperature is 37 °C, the fibers' length and pore structure diameters are similar for the four ionic conditions samples.

Collagen concentration also can affect the microstructure of collagen fibers and the samples' state. To investigate the effect of collagen concentration on the microstructure of collagen fibers, we image the microstructure of collagen fibers which are prepared at different collagen concentration at pH 5.5. At pH 5.5, when collagen concentration is 2 g/l and 3 g/l, the samples existed in the liquid format at room temperature. (**Figure 3.4**) At room temperature, collagen hydrogel was formed when collagen concentration is 4 g/l. And the fiber density increased along with the increasing of the collagen concentration. (**Figure 3.4**) The fibers' microstructure is also altered by increasing collagen concentration at this low pH. As shown in the first column of fig.4 (indicate by the arrow), fibers just extend to one direction when collagen concentration is 4 g/l at room temperature, fibers extend to all directions when collagen concentration is 2 g/l and 3 g/l at room temperature.

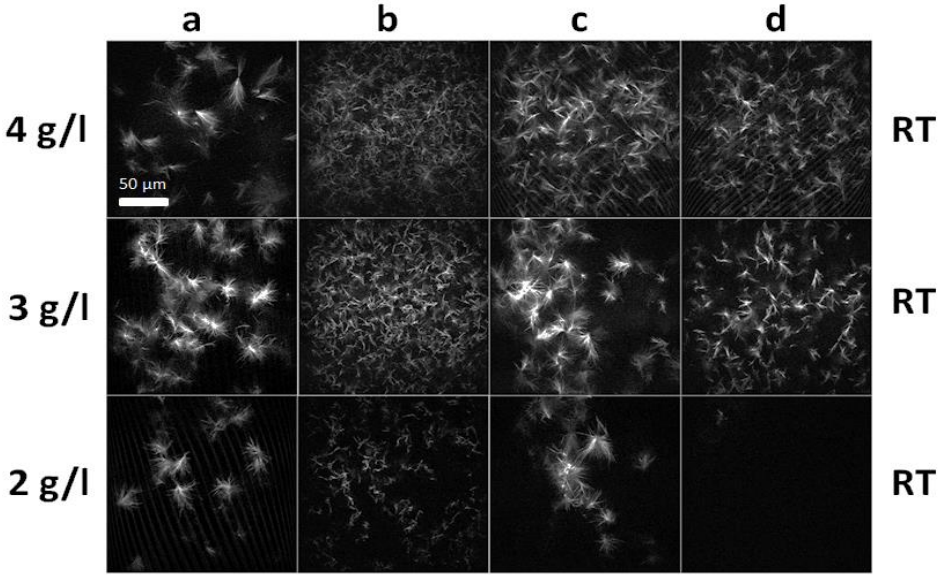

Figure 3.4 The effect of collagen concentration on the microstructure of collagen fiber at pH 5.5. Temperature is room temperature. Top row is 4 g/l collagen samples. Second row is 3 g/l collagen samples. Bottom row is 2g/l collagen samples (a: 30 mM Phosphate + 0.3 M NaCl; b: 30 mM Phosphate + 0.15 M NaCl; c: 10 mM Phosphate + 0.3 M NaCl; d: 10 mM Phosphate + 0.15 M NaCl)

Table 3.1 The summary of collagen microstructure parameters and the samples' state. (a: 30 mM Phosphate + 0.3 M NaCl; b: 30 mM Phosphate + 0.15 M NaCl; c: 10 mM Phosphate + 0.3 M NaCl; d: 10 mM Phosphate + 0.15 M NaCl) FL (Fiber Length), PD (Pore Diameter)

pH	Conc. of collagen (g/l)	Room Temperature				37 ˚C			
		A	B	C	D	A	B	C	D
5.5	2 g/l	Not hydrogel FL: 15.85 ± 3.51 PD: -------	Not hydrogel FL: 8.99 ± 2.08 PD: -------	Not hydrogel FL: 17.53 ± 3.90 PD: ------	Not hydrogel FL: 12.85 ± 2.00 PD: ------	Hydrogel FL: 5.64 ± 0.96 PD: 5.98 ± 0.98	Hydrogel FL: 2.65 ± 0.59 PD: 5.44 ± 1.01	Hydrogel FL: 7.06 ± 1.38 PD: 8.42 ± 1.60	Hydrogel FL: 1.94 ± 0.52 PD: 4.49 ± 0.66
	3 g/l	Not hydrogel FL: 18.97 ± 3.49 PD: 35.38 ± 6.21	Not hydrogel FL: 9.11 ± 1.64 PD: 8.47 ± 2.14	Not hydrogel FL: 20.07 ± 3.55 PD: 35.23 ± 6.74	Not hydrogel FL: 12.36 ± 2.49 PD: 20.56 ± 4.02				
	4 g/l	Hydrogel FL: 27.57 ± 5.01 PD: ------	Hydrogel FL: 11.24 ± 2.30 PD: 9.24 ± 1.95	Hydrogel FL: 14.44 ± 2.37 PD: 20.37 ± 5.16	Hydrogel FL: 13.67 ± 2.86 PD: 16.59 ± 3.27				
7.5	2 g/l	Hydrogel FL: 52.00 ± 12.1 PD: 40.17 ± 8.81	Hydrogel FL: 30.97 ± 7.21 PD: 41.06 ± 8.50	Hydrogel FL: 48.80 ± 8.57 PD: 34.81 ± 7.19	Hydrogel FL: 20.00 ± 3.09 PD: ------	Hydrogel FL: 5.61 ± 1.54 PD: 7.83 ± 1.06	Hydrogel FL: 5.38 ± 1.37 PD: 6.42 ± 1.03	Hydrogel FL: 6.40 ± 1.65 PD: 5.85 ± 0.91	Hydrogel FL: 4.37 ± 0.96 PD: 5.08 ± 0.65
8.2	2 g/l	Hydrogel FL: 63.59 ± 8.83 PD: 38.21 ± 6.27	Hydrogel FL: 36.34 ± 9.91 PD: 31.06 ± 6.18	Hydrogel FL: 54.30 ± 7.90 PD: 31.55 ± 5.51	Hydrogel FL: 42.67 ± 6.24 PD: 23.23 ± 4.45	Hydrogel FL: 3.80 ± 0.79 PD: 4.65 ± 0.69	Hydrogel FL: 3.81 ± 0.81 PD: 4.09 ± 0.56	Hydrogel FL: 5.04 ± 1.47 PD: 4.74 ± 1.11	Hydrogel FL: 4.18 ± 0.93 PD: 4.47 ± 0.79

Discussion

Henderson–Hasselbalch equation (pH = pKa + lg [Base]/[Acid]) was employed to calculate the ratio of $[H_2PO_4^-]/[HPO_4^{2-}]$ at pH 5.5, 7.5 and 8.2. Phosphate exists in four kinds of forms in solution (H_3PO_4, $H_2PO_4^-$, HPO_4^{2-} and PO_4^{3-}). Three chemical equilibrium equations (1)(2)(3) exist between four kinds of phosphate forms:

$$H_3PO_4 = H_2PO_4^- + H^+ \qquad (1)$$

$$H_2PO_4^- = HPO_4^{2-} + H^+ \qquad (2)$$

$$HPO_4^{2-} = PO_4^{3-} + H^+ \qquad (3)$$

For the equations (1)(2)(3), the pKa are 2.21, 7.21 and 12.67 respectively. When pH is 5.5, 7.5 or 8.2, the phosphate exists in the forms of $H_2PO_4^-$ or HPO_4^{2-}. Then equation (2) is employed to calculate the ratio of concentrations of $H_2PO_4^-$ and HPO_4^{2-} - two primary forms of phosphate ion existing at the pHs employed in self-assembly experiments. Based on the Henderson-Hasselbalch equation:

$$pH = PKa + \lg([HPO_4^{2-}]/[H_2PO_4^-])$$

$$\lg([HPO_4^{2-}]/[H_2PO_4^-]) = pH - pKa$$

When pH is 5.5, $\lg([HPO_4^{2-}]/[H_2PO_4^-]) = 5.5 - 7.21 = -1.71$, then $[HPO_4^{2-}]/[H_2PO_4^-]$ is 0.02;

When pH is 7.5, $\lg([HPO_4^{2-}]/[H_2PO_4^-]) = 7.5 - 7.21 = 0.29$, then $[HPO_4^{2-}]/[H_2PO_4^-]$ is 1.95;

When pH is 8.2, $\lg([HPO_4^{2-}]/[H_2PO_4^-]) = 8.2 - 7.21 = 0.99$, then $[HPO_4^{2-}]/[H_2PO_4^-]$ is 9.8.

The table below summarized the concentration ratio of $H_2PO_4^-$ or HPO_4^{2-} at different pHs employed in self-assembly experiments.

Table 3.2 The ratio of concentrations of $H_2PO_4^-$ and HPO_4^{2-} at different pH

pH	**$[H_2PO_4^-]/[HPO_4^{2-}]$**
5.5	**50:1**
7.5	**0.51:1**
8.2	**0.1:1**

When pH is 5.5, ~ 98% of phosphate is highly protonated and exists in the monobasic phosphate form, $H_2PO_4^-$ (**Table 3.2**). At the same time, the polar positively charged amino acid, such as lysine and arginine, exists in the positive charge state at pH 5.5 because the pH is lower than the pKas of those amino acids. At pH 5.5, collagen

molecules are surrounded by the monobasic phosphate ($H_2PO_4^-$) because of the electrostatics/hydrogen bond ($NH^+ \ldots O^-P$) between positive side chain of amino acid (NH^+) and negative charge of monobasic phosphate (O^-P).[9] The double bonded oxygen atom of phosphate bonded to collagen molecules has the potential to form the hydrogen bond with water molecules (21 kJ/mol). The hydration shell make collagen molecules stably exist in the solution. There is a need for more energy to overcome the hydration shell for the collagen molecules to form collagen fibers at pH 5.5 (**Figure 3.5**). When pH is 7.5 and 8.2, HPO_4^{2-} account for 66.1% and 90.7% respectively. At pH 7.5 or 8.2, the lysine and arginine also exist in the positive charge state. The dibasic phosphate (HPO_4^{2-}) can electrostatics/hydrogen bond bind to two different side chain of amino acid at the same time (**Figure 3.5**). This make it is easier for collagen molecules to form collagen fibers at higher dibasic phosphate concentration. This model provides an explanation why collagen fibers are longer at higher pH (pH 7.5 and pH 8.2) compared with lower pH (pH 5.5). (**Figure 3.1 and Table 3.1**) High temperature can alter the thermodynamic movement of collagen molecules. When temperature is 37 ˚C and pH is 5.5, the temperature is high enough to overcome the hydration shell of collagen molecules to form many small collagen nuclei leading to formation of many small fibers that stabilize a hydrogel state. (**Figure 3.3**)

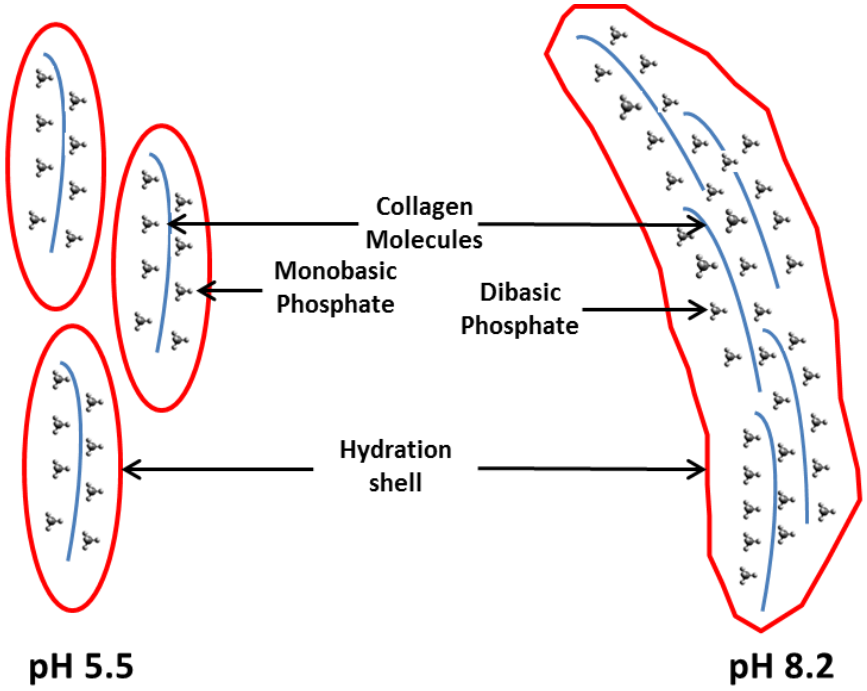

Figure 3.5 The model of the interaction between phosphate and collagen molecules at different pH

In the solution, the ion can bind water to form the hydration shell.[10] Then there are fewer "free" water molecules to accommodate other solutes. For our system, more free water molecules can be attracted by NaCl if we increase NaCl concentration. Then it decreases the water molecules amount in the hydration shell for the high NaCl concentration samples. Then the hydration shell of collagen molecules is weaker at high NaCl concentration (0.3 M) compared with lower NaCl concentration (0.15 M). This means it is easier for collagen molecules to form fibers at higher NaCl concentration (0.3 M) because of the weaker hydration shell. (**Figure 3.6**) This model can explain that higher NaCl concentration (0.3 M) samples' fiber length is longer compared with low NaCl concentration (0.15 M) samples' fiber length. When phosphate concentration is same, 0.3

M NaCl samples' the fiber length is about 2 times longer compared to 0.15 M NaCl samples' fiber length at room temperature. (**Figure 3.1 and Table 3.2**)

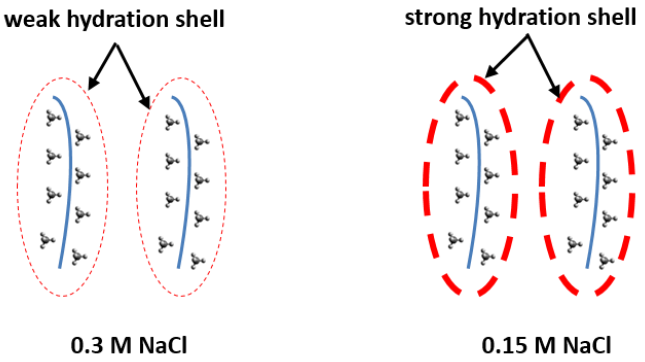

Figure 3.6 The modeling of the hydration shell at different NaCl concentration.

Conclusion

To investigate the effect of pH on microstructure of collagen fibers, *in situ* non-invasive technology (MPM) is employed to capture the microstructure of collagen hydrogel with Second Harmonic Generation (SHG) contrast imaging at different pHs. It shown that (1) higher pH (pH 8.2) results in 2-4 folds longer fibers compared with lower pH (5.5) at room temperature for four ionic conditions; (2) the higher NaCl concentration (0.3M) can result in the 2 folds longer fibers compared with lower NaCl concentration (0.15M) at room temperature for all conditions; (3) collagen concentration and polymerization temperature influence the sample' state (hydrogel or liquid). pH is a very significant element which needs to be considered for the collage-based or other protein-based scaffold preparation in tissue engineering field. The methods and results presented in this chapter can help us to understand (a) the effect of pH on microstructure of collagen hydrogel and (b) the collagen polymerization process.

Acknowledgement

This work was supported in part with UC Riverside startup research funds (J.G.L.), UC Riverside Biochemistry Department Graduate Research Fellowship (X.L.), NSF CAREER Award CBET-0847070 (J.G.L) and NSF BRIGE Award EEC-0927297 (J.G.L).

References

1. G. A. D. Lullo, S. M. Sweeney, J. Körkkö, L. Ala-Kokko, J. D. San Antonio, Mapping the Ligand-binding Sites and Disease-associated Mutations on the Most Abundant Protein in the Human, Type I Collagen. *J. Biol. Chem.* **2002,** *277*, 4223–4231.

2. R. D. Harkenss, Biological functions of collagen. *Biol. Rev.* **1961,** *36*, 399–455.

3. D. A. D. Parry, The molecular and fibrillar structure of collagen and its relationship to the mechanical properties of connective tissue. *Biophysical Chemistry* **1988,** *29*, 195-209.

4. J. C. Patterson-Kane, D. A. D. Parry, H. L. Birch, A. E. Goodship E. C. Firth, An age-related study of morphology and sross-link composition of collagen fibrils in the digital flexor tendons of young thoroughbred horses. *CONNECT TISSUE RES* **2009,** *36*, 253-260.

5. X. Lang, J. G. Lyubovitsky, Structural dependency of collagen fibers on ion types revealed by in situ second harmonic generation (SHG) imaging method. *Anal. Methods* **2015,** *7*, 1680-1690.

6. (a) M. Schaefer, M. Sommer, M. Karplus, pH-dependence of protein stability: absolute electrostatic free energy differences between conformations. *J. Phys. Chem. B* **1997,** *101*, 1663-1683; (b) A. Yang, B. Honig, On the pH dependence of protein stability. *J. Mol. Biol.* **1993,** *231*, 459-474.

7. R. Chan, V. Chen, The effects of electrolyte concentration and pH on protein aggregation and deposition: critical flux and constant flux membrane filtration. *J. Membr. Sci.* **2001,** *185*, 177–192.

8. X. Lang, M. Spousta, Y. J. Hwang, J. G. Lyubovitsky, Noninvasive imaging of embryonic stem cell cultures by multiphoton microscopy reveals the significance of collagen hydrogel preparation parameters. *Anal. Methods* **2015,** *8*, 280-294.

9. P. Carmona, M. L. Rodrigues, Hydrogen bonds between protein side chains and phosphates and their role in biological calcification. *Biophys. Chem.* **1987,** *28*, 161-167.

10. R. Mancinelli, A. Botti, F. Bruni, M. A. Ricci, Hydration of sodium, potassium and chloride ions in solution and the concept of structure maker/breaker. *J. Phys. Chem. B* **2007,** *111*, 13570-13577.

Chapter 4: The properties of crosslinked collagen hydrogel

Abstract

In situ multiphoton microscopy (MPM) imaging method combining two-photon fluorescence (TPF) and second harmonic generation (SHG) optical signals helped to discover the microstructure restructuring of collagen fibers within 3D hydrogels after chemical cross-linker modification. We prepared hydrogels at different solid contents (2 g l^{-1} or 4 g l^{-1}) and self-assembly temperatures (27 °C or 37 °C). In a separate experiment, we stabilized 2 g l^{-1} 37 °C hydrogels with the nontoxic cross-linkers carbodiimide (EDC), EDC/*N*-hydroxysuccinimide (NHS) or genipin. We used rheology measurements to assess the flow behavior of the materials we prepared. All cross-linkers reduced the viscous part *G″* of the modulus, implying that cross-linked materials are more rigid and non-flowing compared to non-cross-linked hydrogels. After genipin crosslinking, the SHG signal of collagen hydrogel decrease 5 fold, TPF signal increase 2 fold in the green channel and 5 fold in red channel. The crosslinked collagen hydrogel can resist the degradation by activated collagenase.

Introduction

The many potentialities of employing embryonic stem cells in regenerative medicine, and as models are described in the literature.[1] The majority of published research had focused on the roles that gene expressions, growth factors and cell communications play in the embryonic differentiation. Recently, there have been discussions that the nanoscale features of material surfaces can be used to control cellular behavior[2] and that the elasticity of the extracellular matrix can regulate mesenchymal stem cell differentiation.[3]

More detailed morphological *in situ* characterization of cell supporting scaffolds before cell culture is necessary for the development of successful applications.

Collagen hydrogels play an important role as scaffolds in tissue engineering and regenerative medicine. The 3D architecture of scaffolds composed of collagen type I includes micron-sized fibers that constitute the solid phase and effective pores, which are interconnected channels containing a fluid phase.[4] Optical properties and the overall architecture of collagen hydrogels are inevitably altered by changing the physicochemical self-assembly conditions[5] including temperature[6] and collagen biopolymer solid content as well as by adding cross-linkers. The above manipulations can further simultaneously change ligand type and/or ligand density sensed by the cells, mechanical strength of scaffolds and structures within. Previous research emphasized the mechanical properties of scaffolds in driving differences in cellular behaviors.[7] More recent studies uncovered the importance of microstructures defining these mechanical properties.[8] At present, the microstructure, which is one of the elements needed to rationally engineer functional tissues, organs and model systems, is also one of the least explored. Spectroscopic probes that can provide complementary information regarding microstructure in thick tissue,[9] biomaterial[5-6, 10] and wound examinations.[11] SHG contrast is used to directly detect aggregated collagen structures (fibers) within scaffolds. It resists photobleaching and is generated when NIR photons that interact with fibrillar collagen are combined to produce new photons at twice the energy. TPF detects fluorophores initially present or in this work induced as a result of modifying collagen with a chemical cross-linker genipin.

We chose 2 g l^{-1} and 4 g l^{-1} collagen concentrations because they covered the range commonly used in tissue engineering. These concentrations produce significantly different physical microenvironments resembling a provisional or immature extracellular matrix that occurs during development. 1.8 g l^{-1} was the lowest concentration at which, using the assembly conditions in this work, we could still form hydrogels,[6] compelling us to use concentrations above this critical value. The cellular behavior and collagen fiber structure could be clearly visualized in the low concentration 2 g l^{-1} gels. The 4 g l^{-1} gels could be readily made from the stock solution concentrations of eight to nine g l^{-1} we carry in the laboratory and served as a 'high' endpoint in establishing materials.

Our main goal was to provide further characterization of the synthesized materials *in situ* by employing the MPM imaging method. The properties characterized were (1) collagen fiber and effective pore structure within hydrogels prior to cell culture, (2) degradation pattern and degradation kinetics of hydrogels with collagenase, (3) optical properties of hydrogels stabilized with genipin, (4) storage and loss moduli of all materials. The prepared hydrogels are biodegradable, the chosen chemical cross-linkers are nontoxic and the *in situ* MPM method employed to characterize the models is nondestructive to biological samples. All seem highly valuable for biological applications.

Materials and methods

Crosslinking degree assay: We used the ninhydrin colorimetric method to determine the extent of modification of amino groups with cross-linking reagents within collagen hydrogels. The percentage of the remaining free amines after cross-linking was calculated

to establish the relative cross-linking degree. 100 µl of sample mix of the following final composition was added to a well of a 96 well plate: 30 mM phosphate buffer, [NaCl] = 0.3 M, [collagen] = 2 g l^{-1}, pH 7.4 and incubated under 37 °C for 24 hours. 100 µl of same-day-prepared 1 mM genipin or 0.1 M EDC or 0.1 M EDC/0.025 M NHS solution (in 30 mM phosphate buffer, [NaCl] = 0.3 M, pH = 7.4) was added on top of collagen hydrogels and incubated for another 24 hours under 37 °C. The control samples were incubated in 30 mM phosphate buffer, [NaCl] = 0.3 M, pH = 7.4 for the same duration of time. The cross-linking reagents were removed by adding double deionized H_2O (ddH_2O) and incubating for at least 30 min. This washing procedure was repeated at least three times. Subsequently, 10 µl of 2 g l^{-1} collagenase was added to the samples, adjusted to the volume of 650 µl with ddH_2O and incubated for 72 hours at 37 °C. 350 µl of 2% ninhydrin stock (in ethanol) was added to each sample and boiled for 2 min. A UV-vis-NIR spectrophotometer (Varian, Cary 500) was used to detect the absorbance of samples in the range of 300–900 nm. Different concentrations of glycine solution, 10 µl of 2 g l^{-1} collagenase solution and 350 µl of 2% ninhydrin stock solution (in ethanol) were used to construct the calibration curve and repeated at least three times. The cross-linking degree was then calculated as: crosslinking degree = (1 − (cross-linked $absorbance_{570}$/non-cross-linked $absorbance_{570}$)) × 100%. All samples were prepared in triplicate. For the cross-linked hydrogels the cross-linking degree was (a) genipin-cross-linked hydrogel: 87%; (b) EDC/NHS-cross-linked hydrogel: 60%; (c) EDC-cross-linked-hydrogel: 12%. The chemical modifications with the above reagents resulted in the

formation of covalent bonds between collagen molecules and were stable overtime (unpublished data).

Enzymatic degradation assay: The samples were prepared between no. 1 coverslips, separated with a 2.3 mm thick silicone gasket having an 18 mm round opening. All the preparations were done under sterile conditions on ice. 600 µl of the collagen hydrogel mix of the following final composition was used per sample: 30 mM phosphate buffer, [NaCl] = 0.3 M, [collagen] = 2 g l^{-1}, pH 7.4. To gel the samples we incubated them for 2 hours at the specified temperature. For the cross-linked hydrogels, 50 µl of cross-linker solutions prepared at 10× concentration in 30 mM phosphate buffer, [NaCl] = 0.3 M, pH = 7.4 were added on top of collagen hydrogels. The hydrogels were subsequently incubated with cross-linkers for 24 hours at 37 °C. To remove the cross-linkers, we incubated the hydrogels with 30 mM phosphate buffer, pH = 7.4, [NaCl] = 0.3 M for 20 minutes at room temperature. The cross-linker removal procedure was repeated at least three times. To digest the materials, we added 50 µl of collagenase (C0130, Sigma) activated with buffer as specified in the supplied instructions.

Rheology measurements: Rheological measurements were carried out with a computer interfaced Haake Rheo Stress 1 temperature controlled parallel plate rheometer. The sensor diameter was 35 mm and the measurements were carried out at the specified temperatures. Oscillation amplitude sweeps were performed in the controlled stress (CS) mode to establish the viscoelastic linear regions for the non-crosslinked hydrogels. The frequencies used were 0.5 Hz, 0.7 Hz and 1 Hz. The gap was re-calibrated prior to daily measurements. The samples for the synthesis of collagen hydrogels were prepared as

described previously.[7] Briefly, 550 μl of the self-assembly mix was loaded on the bottom plate of the rheometer preheated to the desired temperature. The gap was adjusted by lowering the top plate to create 0.2 mm distance between the two plates. The hydrogels were allowed to polymerize (20 min at 37 °C or 50 min at 27 °C) and the rheology data were collected. Oscillation frequency sweep (0.1–50 Hz) controlled deformation (CD) mode rheology data were obtained with a strain rate of 0.05. For measurements on the cross-linked hydrogels, the gap was 1 mm. 2 g l^{-1} 24 h 37 °C pre-polymerized collagen hydrogels were separately incubated with cross-linkers (1 mM genipin, 0.1 M EDC or 0.1 M EDC + 0.025 M NHS) for 24 hours at 37 °C. Upon transferring them to the bottom plate of the rheometer, we carried out oscillation frequency sweep (0.1–50 Hz) rheology measurements (strain rate 0.05) in a controlled deformation (CD) mode.

Spectral measurement: All UV-vis spectra were obtained with a UV-vis-NIR spectrophotometer (Varian, Cary 500). The multi-photon spectra were acquired with a 10×, 2.6 mm working distance, N-Achroplan, water immersion objective (Zeiss, 420947-9900-000, N.A. 0.3) in the epi-collected configuration.[18] The spectra were filtered from the laser excitation with a long pass 705 nm single-edge dichroic beamsplitter (Semrock, FF705-Di01-34 × 46) and additionally filtered through a 720 nm short pass filter (Semrock, FF01-720/SP-25) introduced at the original exit port of the modified Zeiss Axioexaminer.Z1. Spectra were obtained with an Acton SP2300 spectrograph equipped with a 68 mm × 68 mm, 300 grooves per mm ruled grating blazed at 500 nm and a Pixis 1024B CCD camera (Princeton Instruments, Trenton, New Jersey). The spectrograph and camera settings were PC-controlled through WinSpec/32 v.2.5 K software. The CCD

temperature was maintained at −75 °C in all the experiments to ensure low dark noise. The entrance slit of the spectrograph was set to a width of 1 mm. A typical spectral acquisition time was 16 s. The multiphoton spectra were corrected for a dark noise background and obtained under equivalent power and other settings for different samples and wavelengths.

Multiphoton microscopy (MPM) imaging: The inverted multiphoton laser-scanning microscope used in this work was the Zeiss LSM 510 NLO Meta microscopy system. It is based on an Axiovert 200M inverted microscope equipped with standard illumination systems for transmitted light and epi-fluorescence detection. It was also equipped with an NLO interface for a femtosecond titanium:sapphire laser excitation source (Chameleon-Ultra, Coherent, Incorporated, Santa Clara, CA) for multiphoton excitation. The chameleon laser provided femtosecond pulses at a repetition rate of 76 MHz, with the center frequency tunable from 690 to 1040 nm. A long working distance objective (Zeiss, 40× water, N.A. 0.8) was used to acquire images shown in this work. The signals from the samples were epi-collected and discriminated by a long pass 650 nm dichroic beamsplitter. The SHG images were collected with a 390–405 nm band-pass filter (λ_{ex} = 800 nm). The two-photon fluorescence (TPF) images were collected with the 390–465 nm + 530–590 nm band-pass filters and λ_{ex} = 770 nm. Unless noted, the images presented in this work are 12 bit, 512 × 512 pixels representing a 225 μm × 225 μm field of view. The multiphoton images were obtained from at least four gel replicates. Typically, two independent samples were imaged per day. Imaging was repeated at least one more time on another completely independent set consisting of two samples. Many fields of view

(10 and more) were acquired for each sample and the representative images are shown in the figures.

To confirm the validity and reproducibility of our imaging observations, randomly selected samples were additionally re-imaged on an upright Thorlabs Laser Scanning Multiphoton Microscope.[5] This upright Nikon microscope was used to obtain images used to follow degradation of collagen hydrogels with collagenase and to construct degradation kinetic data plots. It was equipped with a femtosecond titanium:sapphire laser excitation source (Mai-Tai HP, Spectra Physics, Santa Clara, CA) that provided femtosecond pulses at a repetition rate of 76 MHz, with the center frequency tunable from 690 to 1040 nm. Long working distance (2 mm to 2.6 mm imaging range) aberration corrected UV-vis/near IR imaging/excitation water immersion objectives (Zeiss, 63× water, N.A. 1.0; Zeiss 10× water, N.A. 0.4 and Olympus 20× water, N.A. 1.0) were used as needed. Spectral filtering with dichroics and bandpass filters was used to separate second harmonic generation (SHG) and two-photon excited fluorescence (TPF) signals as indicated in the text. Each image acquired was 2048 × 2048 pixels, which corresponded to a 700 μm × 700 μm field of view for an Olympus 20× water objective (Olympus, XLUMPLFLN, N.A. 1.0, 2.0 mm working distance). For the degradation experiments, the samples were placed on an in-house built temperature controlled stage adaptor made from anodized aluminum kept at 32 °C. We imaged the top 500 μm within the materials, throughout the duration of the degradation experiments. We imaged all the necessary controls for the same time durations and under the same conditions as the samples that were degraded with collagenase. To ensure reproducibility, all the

experiments were repeated on different days and at least two times. The in-house written Matlab code was used to evaluate SHG and TPF signals averaged intensities by calculating the average pixel values in the acquired images.

The SHG or TPF signal averaged intensities were plotted as a function of depth to obtain attenuation curves.[10c] Briefly, at different laser focus depths, there are different values of SHG and TPF signals. As the laser focus is moved deeper into the samples by adjusting the vertical position of the focusing objective, the SHG and TPF signal intensities first build up, reach the maxima and then decay due to both attenuation of excitation and decrease in the collection efficiency of the scattered signals. In all the degrading samples, we observed that the degradation with collagenase took place starting at the top of the materials where we applied it. Therefore, we found that SHG or TPF signal attenuation curves were moving as the signals were progressively attenuated due to the degradation of materials. The SHG or TPF signal attenuation curves remained stationary for the controls (no collagenase was applied) imaged for the same time durations and under the same conditions. To obtain the kinetic traces, we selected signal intensity values at the same imaging depths, which coincided with the top of the attenuation curve obtained at the zero time point. A Plan-Apochromat water immersion 63×, 2.1 mm working distance objective (Zeiss, 421480-9900-000, N.A. 1.0) was employed to obtain images used to evaluate the porosity of the degrading hydrogels. We first obtained SHG or TPF signal attenuation curves. We subsequently measured porosity at a section around the area of the possible maximum in SHG or TPF signal attenuation curves collected at zero degradation time. We followed the changes in the effective pore structure size at the selected depth

for the duration of the degradation experiment. These experiments were repeated at least three times and at least fifty effective pore structure sizes were measured.

To obtain the percentage of materials degraded after 24 hours of digestion, we imaged the height of materials from the side opposite to where collagenase was added and divided by an original 2 mm height of the materials.

The network structural parameters such as collagen fibers' length, width and pore dimensions were quantified with either LSM software or ImageJ (http://imagej.nih.gov/ij/) and the error bars are the standard deviations from the mean values. Between twenty and fifty independent measurements of each parameter were performed for each experimental system. For the cell-containing samples where the collagen fiber distribution was very heterogeneous, the measurements were grouped into separate categories (long and short fibers). We used a straightforward method of measuring the resulting fibers' lengths by tracing along the fibers, reproducibly attaining the measured numbers.

To determine how spherical (round) the cellular components are in our models we used images to determine their aspect ratios. The aspect ratio was estimated as a percent of sphericity by calculating the width to length ratio. Between fifteen and twenty independent measurements were performed to establish estimates. The aspect ratio of 100% indicates a perfectly round cell/cell cluster while small numbers indicate extended, slender objects. The errors were calculated as the standard deviations of the mean.

Results

Optical properties and microstructure of the synthesized collagen hydrogels

When we treat the opaque collagen hydrogels with clear solutions of fresh 1 mM genipin at pH 7.4 and room temperature, a noticeable blue-grey color[12] corresponding to ~590 nm absorbance (Figure 4.1B, left) and two-photon fluorescence (TPF) (Figure 4.1B, right) develops within 24 hours. The TPF spectra exhibit two peaks centered at ~490 nm and at ~615 nm. The ratio of the intensity of the 615 nm emission band to the intensity of the 490 nm emission band is five and does not change significantly at longer modification times (72 h). There is a very slight bathochromic (red) shift of fluorescence when the excitation wavelength is varied between 760 and 900 nm. Fluorescence from non-crosslinked gels is negligible compared to genipin cross-linked gels when excited with wavelengths we used. For example, in the two photon spectrum of a non-crosslinked gel excitation at 800 nm leads only to a second harmonic generation (SHG) signal at 400 nm that can be readily seen (Figure 4.S1).

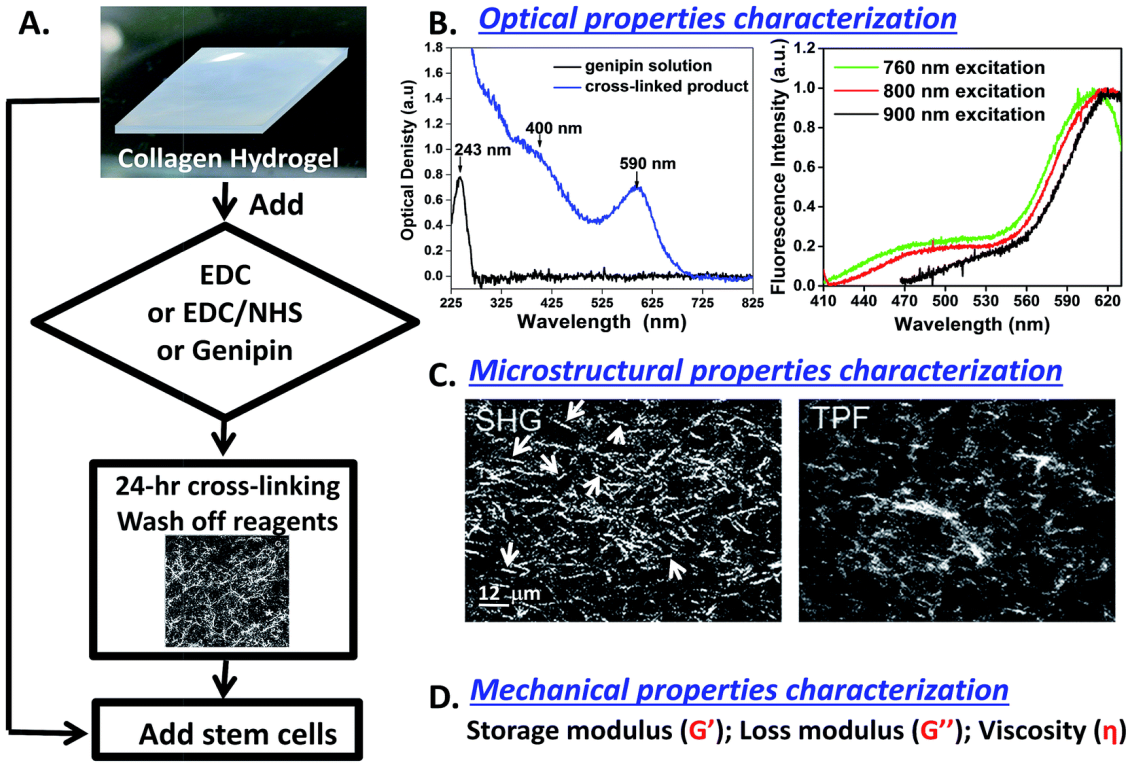

Figure 4.1 The experimental schematic. (A) Overview of the experimental strategy. (B) Typical one photon absorbance spectrum (left). The one photon absorbance spectrum of fresh genipin solution used to modify materials is shown for comparison. Typical two-photon fluorescence (TPF) spectra (right) of genipin modified collagen hydrogels. (C) Second harmonic generation (SHG) images ($\lambda_{ex}/\lambda_{em}$ = 810 nm/400–410 nm, white arrows point to the white fibers; effective pores are the black spaces between the white fibers) and two-photon fluorescence (TPF) images ($\lambda_{ex}/\lambda_{em}$ = 810 nm/470–550 nm + 570–610 nm) of a genipin-modified hydrogel. (D) The output mechanical properties such as storage modulus G', loss modulus G'' and viscosity η of the prepared materials were characterized as well.

Figure 4.2 shows that the genipin-modified hydrogels generate approximately five times less SHG signal compared to non-modified controls (24 hours of modification at 37 °C). On the other hand, as determined from the average TPF image intensities, TPF collected in the 470–550 nm spectral region (TPF #1) increases two fold and TPF collected in the 570–610 nm spectral region (TPF #2) increases nine fold compared to non-modified control hydrogels.

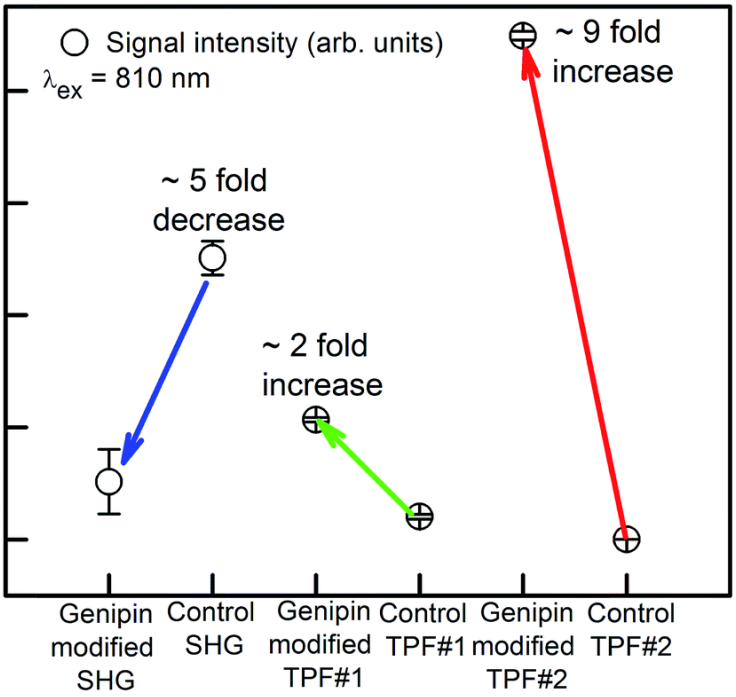

Figure 4.2 Quantifying genipin cross-linking reaction with collagen within hydrogels. The hydrogels were prepared under the conditions 0.3 M sodium chloride, pH 7.4, 30 mM phosphate, 37 °C polymerization temperature, 2 g l^{-1} collagen solid content. After 24 hour incubation, samples were modified for another 24 hours by 1 mM genipin solution adjusted to pH 7.4. The optical filter used to acquire SHG signals was 405 ± 5 nm. The spectral range of acquired TPF #1 was 470–550 nm. The spectral range of acquired TPF #2 was 570–610 nm.

In Table 4.1, we report sizes of collagen fibers and effective pores within hydrogels quantified from SHG and TPF images of synthesized hydrogels prior to stem cell culture. The 27 °C self-assembly temperature produces longer and thicker fibers separated by larger effective pores than those formed at 37 °C. As determined from SHG images, upon treating collagen hydrogels with the zero-length cross-linker EDC,[18] with or without addition of NHS, the microstructure within gels remains the same (the molecular changes, however, are detectable with Raman microspectroscopy[13]). Upon cross-linking with a genipin reagent,[10f] ~5 μm long SHG-generating fibers present within hydrogels prior to the cross-linking reaction 'wash out' leading to the less strong second harmonic generation (SHG) contrast. Newly induced TPF-generating fibers are less well structured

and are significantly longer (~19 μm, Table 4.1) than initially present SHG-generating fibers.

Table 4.1 Summary of the collagen hydrogel microstructural parameters and corresponding standard deviations from the mean. The hydrogels were prepared with 0.3 M sodium chloride, pH 7.4, 30 mM phosphate, 37 °C or 27 °C self-assembly temperatures and collagen solid content of 2 g l^{-1} or 4 g l^{-1}. Additionally, some hydrogels were separately cross-linked with carbodiimide (EDC), carbodiimide (EDC)/*N*-hydroxysuccinimide (NHS) or genipin

	Collagen hydrogel microstructural parameters
Collagen hydrogel preparation conditions	**Fiber length, fiber width, effective pore diameter; all in μm ± st. dev.**
37 °C, 2 g l^{-1}	4.8 ± 1.1, 0.95 ± 0.2, 5.2 ± 1
37 °C, 4 g l^{-1}	4.6 ± 0.8, 1.0 ± 0.1, 3.0 ± 0.5
27 °C, 2 g l^{-1}	43 ± 8.4, 7.1 ± 1.4, 50.2 ± 10.8
27 °C, 4 g l^{-1}	51.5 ± 7.2, 6.61 ± 1.7, 40 ± 11.5
37 °C, 2 g l^{-1}, EDC-crosslinked	6.13 ± 1, 1 ± 0.12, 5.6 ± 1.4
37 °C, 2 g l^{-1}, EDC/NHS-crosslinked	6.18 ± 0.9, 1.0 ± 0.1, 8.19 ± 1.2
37 °C, 2 g l^{-1} genipin-crosslinked – SHG contrast	2.9 ± 0.6, 0.7 ± 0.2, 5.1 ± 1.1
37 °C, 2 g l^{-1} genipin-crosslinked – TPF contrast	19.3 ± 3.9, 3.4 ± 1.4, 17.4 ± 4.5

Enzymatic degradation assay of synthesized collagen hydrogels

To evaluate the enzymatic degradation of our synthesized materials, we topically applied a solution of collagenase to collagen hydrogels and with multiphoton optical imaging method (a) for ~24 hours continuously imaged *in situ* the degradation of collagen gels; and (b) quantified the percent of materials left after 24 hours of degradation. Figure 4.3 shows a typical *in situ* degradation kinetic profile of collagen hydrogels. Depending on the experiment, these types of kinetic profiles were obtained by following SHG or TPF signals as a function of time. The typical data for 2 g l^{-1} 37 °C materials show the microstructure of a collagen hydrogel immediately after collagenase solution was topically added (Figure 4.3A) and 25 min later (Figure 4.3B). For all non-crosslinked collagen gels, regardless of the hydrogel preparation conditions, the half-time for degradation was approximately fifteen minutes. Tables in Figure 4.3 summarize the observed increase in collagen hydrogels' porosity detected in real time *in situ* during degradation reactions.

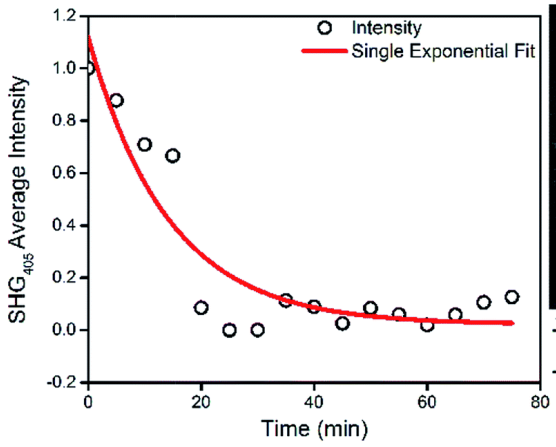

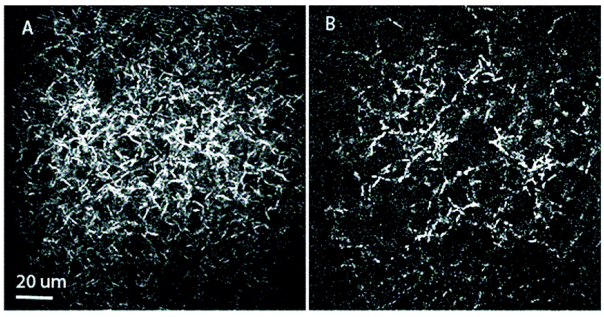

37 °C materials		27 °C materials	
SHG contrast		SHG contrast	
Time (minutes)	Pore Size (μm)	Time (minutes)	Pore Size (μm)
0	*7.7 ± 2.0*	*0*	*20.2 ± 6.1*
18	*17.1 ± 2.2*	*18*	*39.2 ± 9.3*

Genipin materials				EDC+NHS materials		EDC materials	
TPF (470-550) contrast		TPF (570-610) contrast		SHG contrast		SHG contrast	
Time (hours)	Pore Size (μm)	Time (hours)	Pore Size (μm)	Time (hours)	Pore Size (μm)	Time (hours)	Pore Size (μm)
2	*11.0 ± 3.1*	*2*	*13.0 ± 2.4*	*2*	*8.7 ± 1.6*	*0*	*10.2 ± 2.2*
16	*24.1 ± 3.5*	*16*	*23.4 ± 3.9*	*16*	*42.1 ± 3.9*	*16*	*15.7 ± 3.3*

Figure 4.3 The effect of collagen hydrogels' digestion by a topically applied collagenase solution. Typical *Insitu* degradation kinetics plot for 2 g l^{-1} 37 °C polymerized non-crosslinked hydrogel (left). Second Harmonic Generation (SHG) images collected with 20× Olympus objective show the microstructure of a collagen hydrogel immediately after collagenase solution was added (A) and 25 min later (B). Tables (bottom) summarize the porosity of collagen hydrogels detected in real time during degradation with collagenase.

All non-crosslinked collagen hydrogels completely degraded after 24 hours while cross-linked hydrogels showed enhanced stability. For the genipin-crosslinked materials, after 20 h of degradation, hardly any material was removed by collagenase. Thus for the conditions we sampled, no time constants could be determined. The situation was similar for the EDC + NHS crosslinked collagen hydrogels and EDC-crosslinked collagen hydrogels at the spots where we collected kinetic data.

The percent of each material left after 24 hours of degradation with collagenase is shown in Figure 4.S2 Genipin stabilized hydrogels are nearly 94% intact after 24 hours of

degradation. EDC cross-linked hydrogels show great spatial variability of degradation and there is ~30% to 80% of material that remains intact depending on the location sampled. EDC/NHS cross-linked hydrogels exhibit medium degradability with 75% of the material remaining intact at 24 hours of degradation with collagenase.

Rheology analysis of synthesized hydrogel

The linear regime in which collagen gels exhibit equilibrium storage modulus is 8% for 27 °C self-assembled gels and 40% for 37 °C self-assembled gels (data not shown) with the latter exhibiting a strain-stiffening response.[14] For unmodified hydrogels, the viscosity, storage modulus G' and loss modulus G'' all increased with increasing collagen solid content from 2 g l^{-1} to 4 g l^{-1} for hydrogels prepared at both 37 °C and 27 °C incubation temperatures (Figure 4.4). The data shown are for 0.1 Hz frequency. Figure 4.S3. shows the dynamic mechanical properties for 2 g l^{-1} and 4 g l^{-1} collagen gels prepared at 27 °C and 37 °C. For all the materials, the average storage modulus G' is always higher than the loss modulus indicating that the hydrogels have polymerized into solid materials prior to measurements. The measured dynamic mechanical properties (viscosity, G', G'') reach higher values for hydrogels prepared at 27 °C compared to the materials prepared at 37 °C. Nevertheless, the variability in the measured mechanical parameters for 27 °C self-assembled samples is also greater. Therefore, no significant difference in the mechanical properties for hydrogels self-assembled at 27 °C *versus* 37 °C could be reliably measured for either 2 g l^{-1} or 4 g l^{-1} gels. The values of loss tangent ($\tan \delta = G''/G'$) are 0.24 to 0.35 with the highest value of 0.35 for 2 g l^{-1} 27 °C hydrogels.

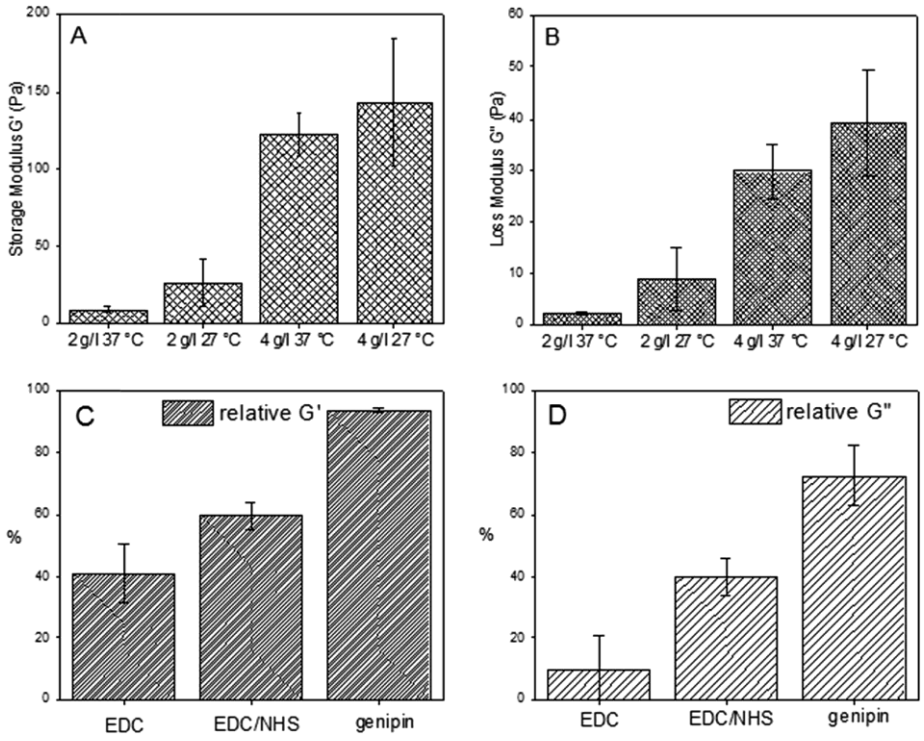

Figure 4.4 Storage moduli *G′* for collagen hydrogels prepared at different collagen solid contents and self-assembly temperatures (A); loss moduli *G″* for collagen hydrogels prepared at different collagen solid contents and polymerization temperatures (B); relative storage moduli *G′* for collagen hydrogels cross-linked with EDC, EDC/NHS and genipin reagents (C); relative loss moduli *G″* for collagen hydrogels cross-linked with EDC, EDC/NHS and genipin reagents (D). For non-crosslinked gels, the data plotted are for 0.1 Hz frequency and error bars reflect the standard deviations from the mean measured values. For cross-linked gels, the data plotted are an average for 0.1–1 Hz frequencies and the error bars are the standard deviations from the mean of the averaged values.

As seen in Figure 4.4, the storage modulus (*G′*) is 40%, 60% and 90% higher in EDC, EDC/NHS and genipin cross-linked materials respectively compared to non-crosslinked controls. The loss modulus (*G″*) is 40% and 70% higher in EDC/NHS and genipin cross-linked materials compared to non-crosslinked controls. The variability in the measured*G″* values for EDC-cross linked materials is high and therefore, no significant difference in these values compared to non-crosslinked controls is reliably detected. The value of loss tangent (tan $\delta = G''/G'$) is the lowest for genipin-stabilized hydrogels. The loss tangent calculated (0.17) is lower by nearly 45% compared to non-crosslinked controls. This

indicated that a *G″* viscose component decreased concomitantly with an increase in the *G′* elastic modulus.

Discussion

Optical properties and microstructure of synthesized collagen hydrogels**:** To date, an understanding of how physicochemical self-assembly conditions, cross-linking and degradation processes of scaffolds affect collagen formulations is limited. In hindsight, low reproducibility and predictability of the fate and behavior of cells interacting with soft materials[15] could be due to their incomplete characterizations as a result of a short supply of noninvasive methods. We employ spectroscopic characterization to further follow the processes taking place during modification of collagen within hydrogels with a genipin reagent and resulting optical properties of synthesized materials. We also quantify collagen fiber and effective pore structure within hydrogels prior to and during cell culture.

An increase in the density of collagen triple helices aligned in a parallel way within fibrils[16] and/or an increase in the number of fibrils' interfaces within the collagen fibers[6] are responsible for second harmonic generation (SHG) signals from collagen structures. The intra- and intermolecular cross-linking of collagen molecules by genipin is expected to extend to all levels of collagen organization, including triple helices, their alignment within fibrils and interfaces of collagen fibrils within fibers. The attenuation of SHG signals in the genipin crosslinked collagen hydrogels is a result of this strong modifying effect. Genipin was shown to form polymeric structures of 40 to 44 monomers long upon its reaction with methylamine.[17] The newly formed genipin oligomeric structures is what

possibly additionally bridges the collagen molecules between the adjacent fibrils[18] within hydrogels. The carbodiimide which connects the carbonyl containing residues of *aspartic* and *glutamic acids* and amino groups cannot bridge these groups when they are located on the adjacent collagen microfibrils, which are too far apart (1.3 μm to 1.7 μm).[18]

Enzymatic degradation assay of synthesized collagen hydrogels: Conventional degradation assays employ *in vitro* methods that determine fractional mass loss during degradation of a polymeric biomaterial such as collagen hydrogel. The methods rely on measuring the dry sample weight of degraded samples and comparing it with the initial dry weight. This process of evaluating the degradation of materials removes materials from further experimentations, can lack accuracy due to a need to precisely weigh increasingly small amounts of sample and is not applicable to *in vivo* examinations of degrading scaffolds. Histological and immunohistochemical methods that are also conventionally employed are invasive as well. They carry little information regarding the structural or functional status of scaffolds. Furthermore, *in vivo*, many enzymes that degrade biomaterials including hydrogels would exert predominantly a surface effect during degradation,[19] necessitating development of non-invasive imaging techniques including fluorescent tagging[20] that have potential to track surface modifications by enzymes. Our work outlines a non-destructive imaging method utilizing SHG and TPF contrasts, to follow degradations of collagen hydrogels *in situ*. It can obtain a more comprehensive level of detail regarding hydrogels' degradation patterns/kinetics, and to

quantify collagen fiber and effective pore structure within them during degradation. The method can be applied to other soft materials with only minor modifications.

Rheology analysis of synthesized hydrogels: Collagen hydrogels exhibit viscoelastic properties that are related to their composition and multiscale organization of collagen protein. The solid phase within the hydrogel further interacts with the liquid phase of the final preparations. To assess the characteristic properties and behavior of all prepared hydrogels, we carried out dynamic mechanical analysis. We determined the storage modulus – a measure of the elastic energy stored (G') and the loss modulus – a measure of the energy lost through the flow (G''). The ratio of G''/G' is used to evaluate viscoelasticity, since in a purely elastic material, $G'' = 0$ and in a Newtonian viscous material $G' = 0$.

The hydrogels prepared in this study are stable over the low frequency range as indicated by G' and G'' running nearly parallel. In the low frequency range, for both 2 g $l^{-1}$and 4 g l^{-1} 37 °C hydrogels, the elastic modulus G' is significantly greater than the viscous modulus G''. On the other hand, for 2 g l^{-1} 27 °C hydrogels, G' and G'' overlap and can be considered indistinguishable within the standard deviation of the measurement, indicating that it is not a very solid gel network. In shear rheology measurements we performed, the collagen fiber network and solution phases deformed together. Therefore, the rheology measurements on 27 °C gels could be affected by the liquid phase of collagen gel's effective pores. For example, the effective pores tend to be much greater in 2 g l^{-1} 27 °C assembled materials (50 μm ± 11 μm) than in 2 g l^{-1} 37 °C assembled materials (5 μm ± 1 μm). Alternatively, the greater variability in the viscosity, G', G'' for

hydrogels prepared at 27 °C could be due to 3D heterogeneity intrinsic to these materials.[6]

The increase in the moduli for the 2 g l^{-1} 37 °C cross-linked hydrogels correlated with the degree of cross-linking: the greater the degree of cross-linking the higher were the moduli. Genipin was the only reagent, however, that led to a sizable increase in the elastic modulus G' of collagen hydrogels. All cross-linkers, however, reduced the viscous part G'' of the modulus, implying that cross-linked materials are more solid-like, rigid and non-flowing compared to non-crosslinked counterparts. The reductions in the viscous modulus were observed in the studies that examined cross-linking of collagen hydrogels with a reducing sugar glucose-6-phopshate.[21]

Conclusion

Multiphoton microscopy (MPM) imaging that combines two-photon fluorescence (TPF) and second harmonic generation (SHG) contrasts helped to identify microstructural and optical properties of crosslinked/non-crosslinked collagen hydrogel. All cross-linkers increased the rigidity of the synthesized collagen gels by reducing the viscous component G'' of the complex shear modulus. Genipin can result in the increasing of TPF signal and decreasing of SHG signal of collagen hydrogel.

Acknowledgements

The work was funded in part by the National Science Foundation (BRIGE EEC-0927297 and CAREER CBET-0847070, J.G.L.), UC Faculty Regents Fellowship, (J.G.L.), UC Riverside startup research funds (J.G.L.). Grant No. P41-RR01192. UC BSAS Grant (J.G.L.) is acknowledged as well.

References

1. B. E. Reubinoff, M. F. Para, C. Y. Fong, A. Trounson, A. Bongso, Embryonic stem cell lines from human blastocysts: somatic differentiation in vitro. *Nat. Biotechnol.* **2000,** *18,* 399-404.

2. (a) D. Sengupta, S. C. Heilshorn, Protein-engineered biomaterials: highly tunable tissue engineering scaffolds. *Tissue Eng., Part B* **2010,** *16,* 285-294; (b) M. M. Stevens, J. H. Grorge, Exploring and engineering the cell surface interface. *Science* **2005,** *310,* 1135-1138.

3. (a) A. J. Engler, S. Sen, H. L. Sweeney, D. E. Discher, Matrix elasticity directs stem cell lineage specification. *Cell* **2006,** *126,* 677-689; (b) G. C. Reilly, A. J. E., Intrinsic extracellular matrix properties regulate stem cell differentiation. *Journal of Biomechanics* **2010,** *43,* 55-62.

4. V. L. Cross, Y. Zheng, C. N. Won, S. S. Verbridge, B. A. Sutermaster, L. J. Bonassar, C. Fischbach, A. D. Stroock, Dense type I collagen matrices that support cellular remodeling and microfabrication for studies of tumor angiogenesis and vasculogenesis in vitro. *Biomaterials* **2010,** *31,* 8596-8607.

5. X. Lang, J. G. Lybovitsky, Structural dependency of collagen fibers on ion types revealed by in situ second harmonic generation (SHG) imaging method. *Anal. Methods* **2015,** *7,* 1680-1690.

6. Y. Hwang, J. G. Lyubovitsky, Collagen hydrogel characterization: multi-scale and multi-modality approach. *Anal. Methods* **2011,** *3,* 529-536.

7. R. J. J. Pelham, Y. Wang, Cell locomotion and focal adhesions are regulated by substrate flexibility. *Proc. Natl. Acad. Sci. U. S. A.* **1997,** *94,* 13661-13665.

8. (a) A. Pathak, S. Kumar, Biophysical regulation of tumor cell invasion: moving beyond matrix stiffness. *Integr. Biol.* **2011,** *3,* 267-278; (b) G. P. Raeber, M. P. Lutolf., J. A. Hubbell, Molecularly engineered PEG hydrogels: A novel model system for proteolytically mediated cell migration. *Biophys. J.* **2005,** *89,* 1374-1388.

9. (a) A. Meshkinpour, P. Ghasri, K. Pope, J. G. Lyubovitsky, J. Risteli, T. B. Krasieva, K. M. Kelly, Treatment of hypertrophic scars and keloids with a radiofrequency device: A study of collagen effects. *Lasers Surg. Med.* **2005,** *37,* 543-549; (b) J. G. Lyubovitsky, T. B. Krasieva, J. A. Spencer, B. Andersen, B. J. Tromberg, Imaging corneal pathology in a transgenic mouse model using nonlinear microscopy. *J. Biomed. Opt.* **2006,** *11,* 014013; (c) J. G. Lyubovitsky, X. Xu, T. B. Krasieva, B. Andersen, B. J. Tromberg, In situ multiphoton optical tomography of hair follicles in mice. *J. Biomed. Opt.* **2007,** *12,* 044003; (d) J. G. Lyubovitsky, X. Xu, C. Sun, B.

Andersen, T. B. Krasieva, B. J. Tromberg, Characterization of dermal structural assembly in normal and pathological connective tissues by intrinsic signal multiphoton optical microscopy. *Proc. SPIE* **2008,** *6859*, 1-9; (e) B. R. Msters, P. So, *Handbook of Biomedical Nonlinear Optical Microscopy, Oxford University Press, New York* **2008**; (f) Y. Hwang, J. Granelli, M. Tirumalasetty, J. G. Lyubovitsky, Microscopic imaging of glyceraldehyde-induced tissue glycation with intrinsic second harmonic generation and two-photon fluorescence contrasts. *Proc. SPIE* **2013,** *8587*, 858725.

10. (a) C. B. Raub, V. Suresh, T. B. Krasieva, J. G. Lyubovitsky, J. D. Mih, A. J. Putnam, B. J. Tromberg, S. C. George, Noninvasive assessment of collagen gel microstructure and mechanics using multiphoton microscopy. *Biophys. J.* **2007,** *92*, 2212-2222; (b) N. I. Zur Nieden, C. C. Turgman, X. Lang, J. M. Larsen, J. Granelli, Y. Hwang, J. G. Lyubovitsky, Fluorescent hydrogels for embryoid body formation and osteogenic differentiation of embryonic stem cells. *ACS Appl. Mater. Interfaces* **2015,** *7*, 10599-10605; (c) X. Lang, M. Spousta, J. G. Lyubovitsky, Detecting the collagen-based hydrogels degradationby Multiphoton Microscopy (MPM). *Proc. SPIE* **2015,** *9329*, 93293V; (d) Y. Hwang, J. Granelli, J. G. Lyubovitsky, Effects of zero-length and non-zero-length cross-linking reagents on the optical spectral properties and structures of collagen hydrogels. *ACS Appl. Mater. Interfaces* **2011,** *4*, 261-267; (e) Y. Hwang, J. Granelli, J. G. Lyubovitsky, Multiphoton opticali mage guided spectroscopy method for characterization of collagen-based materials modified by glycation. *Anal. Chem.* **2011,** *83*, 200-206; (f) Y. Hwang, J. Larsen., T. Krasieva, J. G. Lyubovitsky, Effect of genipin crosslinking on the optical spectral properties and structures of collagen hydrogels. *ACS Appl. Mater. Interfaces* **2011,** *3*, 2579-2584; (g) Y. Hwang, N. Kolettis, M. Yang, E. Sanchez, C. Sun, E. R. Gillard, B. J. Tromberg, T. B. Krasieva, J. G. Lyubovitsky, Multiphoton imaging of actin filament formation and mitochondrial energetics of human ACBT gliomas. *Photochem. Photobiol.* **2011,** *87*, 408-417.

11. (a) M. L. Petreaca, S. Dhall, A. Serafino, D. Do, D. McLelland, J. G. Lyubovitsky, N. Schiller, M. M. Martins-Green, Deletion of a tumor necrosis superfamily gene in mice leads to impaired healing that mimics chronic wounds in humans. *Wound Repair Regen.* **2012,** *20*, 353-367; (b) M. Martins-Green, M. Frankso, N. Adhami, M. Valdez, B. Goodwin, J. Lyubovitsky, S. Dhall, M. Garcia, I. Egiebor, B. Martinez, P. Jacob III, C. Havel, L. Yu, M. Curras-Collazo, Cigarette smoke toxins deposited on surfaces: implications for human health. *PLoS One* **2014,** *9*, e8639; (c) S. Dhall, D. C. Do, M. Garcia, J. Kim, S. Mirebrahim, J. Lyubovitsky, S. Lonardi, E. A. Nothnagel, N. L. Schiller, M. Martins-Green, Generating and reversing chronic wounds in diabetic mice by manipulating wound redox parameters. *J. Diabetes Res.* **2014,** *2014*, 562625; (d) S. Dhall, D. C. Do, M. Garcia, D. S. Wijesinghe, A. P. Brandon, J. Kim, A. Sanchez, J. Lyubovitsky, S. Gallagher, E. A. Nothnagel, C. E. Chalfant, R. P. Patel, N. Schiller, M. Martins-Green, A novel model of chronic wounds: importance of redox imbalance and biofilm-forming bacteria for establishment of chronicity. *PLoS One* **2014,** *9*, e109848.

12. S. Fujikawa, Y. Fukui, K. Koga, J. Kumada, Brilliant skyblue pigment formation from gardenia fruits. *J. Ferment. Technol.* **1987,** *65*, 419-424.

13. Y. Hwang, J. G. Lyubovitsky, The structural analysis of three-dimensional fibrous collagen hydrogels by raman microspectroscopy. *Biopolymers* **2013,** *99*, 349-356.

14. S. Motte, L. J. Kaufman, Strain stiffening in collagen I networks. *Biopolymers* **2012,** *99*, 35.

15. A. M. Schaap-Oziemlak, P. T. Kuhn, T. G. van Kooten, P. van Rijn, Biomaterial–stem cell interactions and their impact on stem cell response. *RSC Adv.* **2014,** *4*, 53307-53320.

16. S. Bancelin, C. Aime, I. Gusachenko, L. Kowalczuk, G. Latour, T. Coradin, M.-C. Schanne-Klein, Determination of collagen fibril size via absolute measurements of second-harmonic generation signals. *Nat. Commun.* **2014,** *5*, 4920.

17. R. Touyama, Y. T., K. Inoue, I. Kawamura, M. Yatsuzuka, T. Ikumoto, T. Shingu, T. Yokoi, H. Inouye, Studies on the Blue Pigments Produced from Genipin and Methylamine. I. Structures of the Brownish-Red Pigments, Intermediates Leading to the Blue Pigments. *Chem. Pharm. Bull.* **1994,** *42*, 668-673.

18. H. Sung, W. Chang, C. Ma, M. Lee, Crosslinking of biological tissues using genipin and/or carbodiimide. *J. Biomed. Mater. Res., Part A* **2003,** *64*, 427-438.

19. B. D. Ratner, A. S. Hoffman, F. J. Schoen, J. E. Lemons, *Biomaterials Science, Third Edition: An Introduction to Materials in Medicine* **2013**.

20. N. Artzi, N. Oliva, C. Puron, S. Shitreet, S. Artzi, A. Bon Ramos, A. Groothuis, G. Sahagian, E. R. Edelman, In vivo and in vitro tracking of erosion in biodegradable materials using non-invasive fluorescence imaging. *Nat. Mater.* **2011,** *10*, 704-709.

21. M. E. Francis-Sedlak, S. Uriel, J. C. Larson, H. P. Greisler, D. C. Venerus, E. M. Brey, Characterization of type I collagen gels modified by glycation. *Biomaterials* **2009,** *30*, 1851-1856.

Supplementary materials

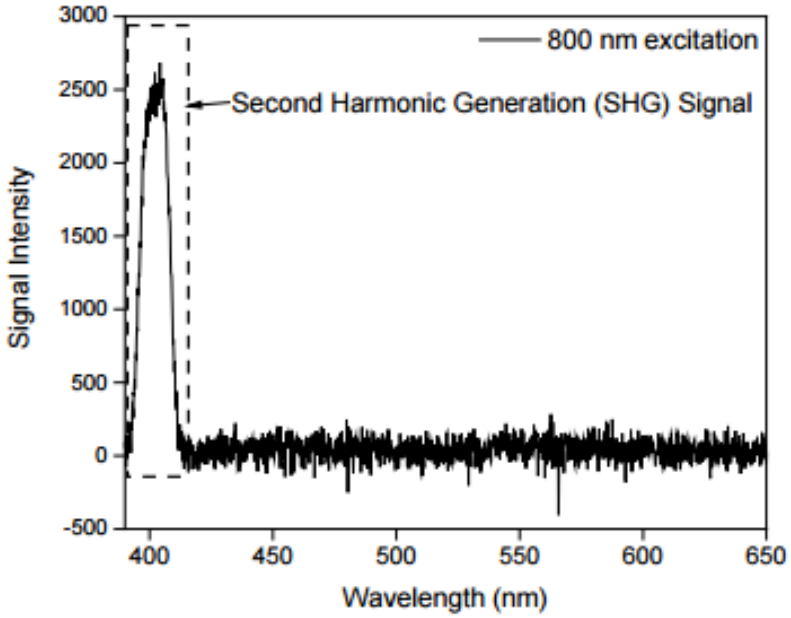

Figure 4.S1 Typical two-photon spectrum of a non-cross-linked collagen hydrogel. Only second harmonic generation (SHG) signal at 400 nm is readily observed.

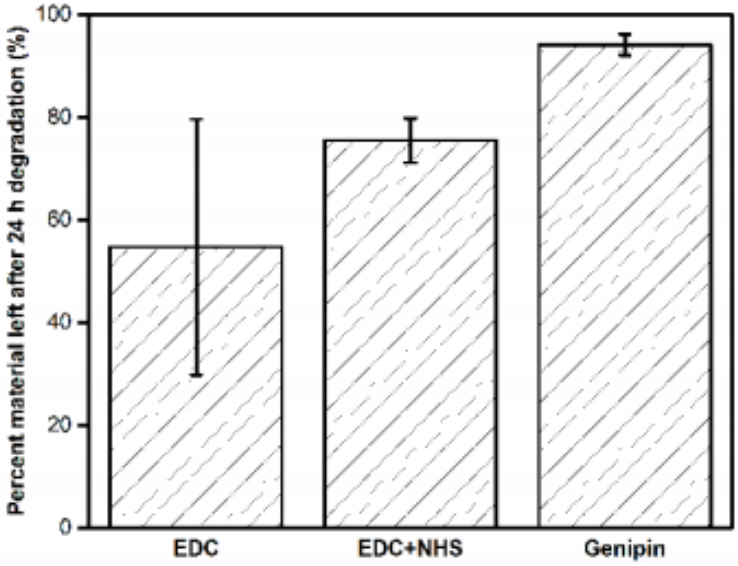

Figure 4.S2 The percent of the cross-linked materials that remained present after 24-hrcollagenase degradation. The non-cross-linked materials were all fully degraded after 24 hrs of exposure to collagenase. The collagen hydrogels were prepared at 0.3 M sodium chloride, pH 7.4, 30 mM phosphate, 37 °C polymerization temperature, 2 g/l collagen solid content. They were separately cross-linked with carbodiimide (EDC), carbodiimide (EDC)/N hydroxysuccinimide (NHS) or genipin.

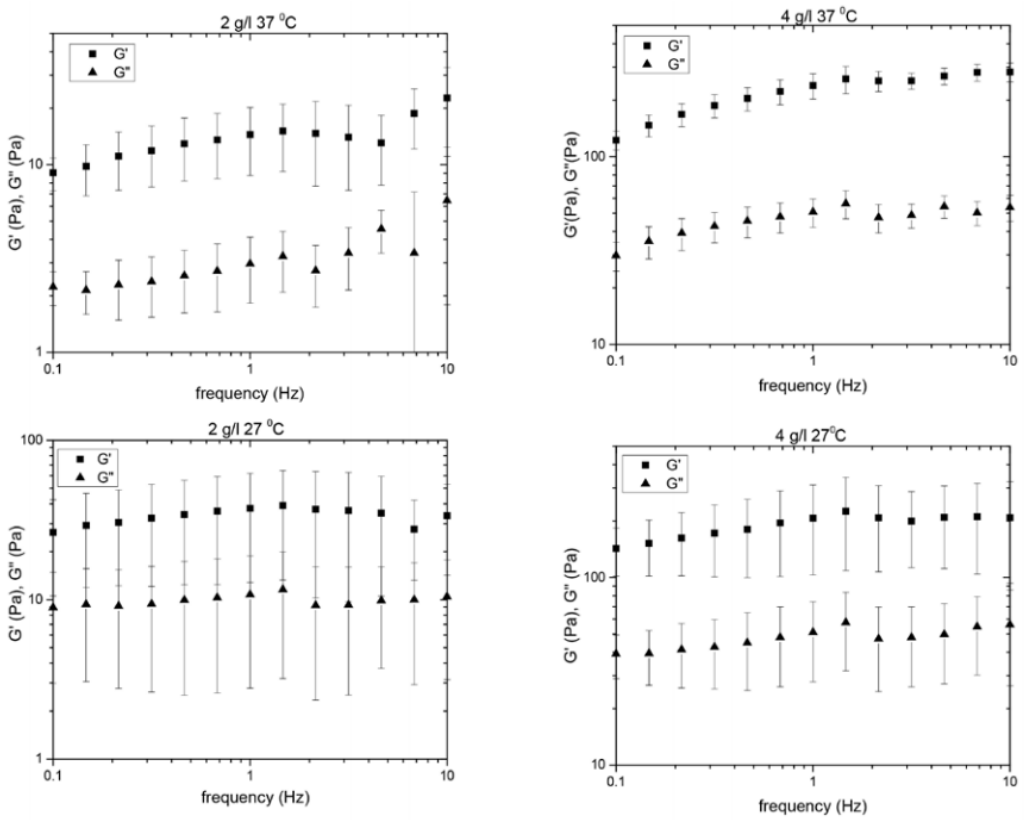

Figure 4.S3 The dynamic mechanical properties of 2 g/l and 4 g/l collagen gels prepared at 27 °C and 37 °C.

Chapter 5: The study of the optical, mechanical and microstructural properties of Genipin Crosslinked Collagen hydrogel (GCC) and the 3T3 fibroblast cells response to GCC

Abstract

Genipin, a kind of natural and non-cytotoxic crosslinker is widely used in tissue engineering field to strengthen biopolymer materials. Based on our research results, the crosslinking with pre-incubated genipin solution altered the two-photon excited emission peaks intensity ratio of GCC compared to crosslinking with fresh genipin solution. The results showed that pre-incubated-genipin-solution-crosslinked collagen hydrogel's (pGCC) blue-green emission (λ_{ex} = 400 nm) peak was greatly enhanced. On the contrary, the pGCC's red emission peak (λ_{ex} = 590 nm) disappeared. The locations of the peaks in the two-photon- excited-emission-spectra of genipin crosslinked collagen hydrogel (GCC) were the same as in the one-photon-excited-emission spectra. However, the ratio of blue emission peak and red emission peak was completely different. Crosslinking with pre-incubated genipin solution decreased the fibers' length, storage modulus (G'), loss modulus (G'') and crosslinking degree of GCC compared to crosslinking with fresh genipin solution. There was no correlation between G' or G'' and microstructural properties of GCC. The embryonic BALB/3T3 (clone A31) fibroblasts cultured on pGCC were rounder compared to the cells cultured on un-crosslinked collagen hydrogel or fresh genipin solution crosslinked collagen hydrogel. Cellular extension had some correlation with fibers' thickness of collagen hydrogels, and no correlation with mechanical properties of materials.

Introduction

Genipin is an extract from the fruit of *Gardenia jasminoides Elli*[1], a kind of Chinese herbal medicine[2], It also can be used as food dye (gardenia blue) via the reaction between genipin and primary amine in presence of oxygen.[3] Recently, the genipin is more and more popular as a chemical crosslinker in tissue engineering field because of its biocompatibility,[4] low toxicity[5] and anti-inflammatory properties.[6]

Genipin-protein reaction molecular mechanisms have been described in literature: (a) the amino group nucleophilic attack on the C-3 atom of genipin molecule, subsequently the tertiary nitrogen takes the place of oxygen;[3, 7] (b) the amino group can nucleophilic substitute the ester group of Genipin.[3] Besides that, under alkaline environments,[8] the genipin monomer can form the genipin polymer via polymerization reaction. It has been reported by Mu et al. that the ring-opening polymerization of genipin can happen under alkaline environment by aldol condensation.[8] The genipin polymers has the potential to induce the long-range modification into amino-group containing materials.

Based on the analysis of the product of reaction genipin-polymer chitosan, it was shown that short genipin polymers (about 4 genipin monomers units, MW (genipin) = 226.3 g/mol) exist at acidic and neutral pH, long chains of cross-linked genipin molecules (7 to 88 genipin monomers units) are formed at strongly basic pH, the short and long genipin polymers exist at the same time at the pH values in-between.[8b] Other studies[9] also described genipin monomer instability in aqueous solutions. Furthermore, some studies focused on effect of temperature and pH on the genipin polymers formation.[9a] There are also some studies focused on the effect of phosphate ions[9b] on genipin polymer

formation. Besides those, based on the study of kinetics of the reaction between β-lactoglobulin and genipin,[10] it was shown that the cross-linking reaction is approximately pseudo-first-order with respect to genipin. All the above findings indicated that the genipin monomer polymerization process and the modification process by genipin of materials strongly depend on the reaction system conditions.

Collagen hydrogel has been widely used in tissue engineering field as a 3D scaffold because of the biocompatibility, biodegradability and relatively low cost of collagen. The microstructure of collagen hydrogels can be affected by concentration and type of ions,[11] collagen concentration[12] and temperature.[12-13] The mechanical properties of collagen hydrogels are poor and cannot easily support cell behavior within them. Then collagen hydrogel needs to be crosslinked by chemical crosslinkers[14] to improve its mechanical properties. After the crosslinking by chemical crosslinkers, the properties of collagen hydrogel are altered (microstructural properties, mechanical properties and optical properties). Thus properties of different crosslinker crosslinked collagen hydrogels need to be studied before applying these materials in the tissue engineering field.

The cell behaviors within 3D scaffold can be affected by the physical interactions between cells and scaffolds, chemical components in the scaffolds and the charge state of the scaffolds. It has been reported that properties of the scaffolds (dimensionality, surface topography, chemistry and mechanics) can result in different cell migration rate[15], cell proliferation[16], gene expression[17] and cell morphology[18]. Chemical crosslinker modifications of collagen can improve the mechanical properties of the materials, but at the same time, they also alter materials' other properties, such as morphology and

electrostatics[19], which in turn can change the interactions between scaffolds and integrin cell receptors.[20] The interaction between cells and the crosslinked collagen hydrogel is very complicated, and the minor differences in the material preparation protocol can result in the different cell behavior. It is necessary to study the effect of crosslinker preparation method (such as genipin) on the properties of collagen hydrogel ahead of the study of the cell response to materials.

In situ second harmonic generation (SHG)[21] and two-photon excited fluorescence (TPF)[22] contrasts have been used to detect different structural components within the thick tissues,[14d, 23] ,engineered tissue systems[2, 11-13, 14b, 14d, 24] and 3D biomaterials system due to the noninvasive and nondestructive property, longer tissue penetration property and labels free peopertiy.[25] SHG signal is generated when two NIR photons interact with fibrillar collagen and then are combined to generate new double frequency photons. The near-infrared wavelength laser source allows deeper tissue penetration distance within the biological tissues and tissue engineered matrices compared to visible sources because of the less scattering.[26] MPM technology provides a method to study the 3D materials *in-situ*, in real time and non-destructively.

In the study, we characterized the properties of different "aged" genipin solution crosslinked collagen hydrogel: (1) One photon and two photon optical properties, (2) collagen fiber thickness and pore diameter prior to cell culture, (3) cross-linking degree of crosslinked collagen hydrogel, (4) rheological properties (G' and G''), (5) fibroblast viability and spreading during cell culture. During the collagen hydrogel preparation process, we changed (1) collagen polymerization time and (2) the "age" of genipin

solution. **(Table 5.1)** The "age" of genipin solution had significant influences on the properties of collagen hydrogel, which in turn changed the cell behavior. Thus this study provides a very important guideline, which can be used to conduct the genipin cross-linker applications in the tissue engineering field.

Table 5.1 Summary of the fabrication parameters employed to prepare 3D collagen hydrogels

Genipin Age Polymerization Time	0 Days (fresh)	2 Days	8 Days	15 Days
2 Hours	2H GCC 0d	2H GCC 2d	2H GCC 8d	2H GCC 15d
24 Hours	24H GCC 0d	24H GCC 2d	24H GCC 8d	24H GCC 15d

Materials and Methods

Preparation of collagen hydrogels: High concentration (9.46 g/l) rat-tail collagen type I stock was bought from BD Bioscience and it was kept at 4 °C. The 2g/l collagen hydrogel was prepared according to Lang's methods. [11] mixing 2X PBS buffer (pH 7.4±0.1), 0.02N acetic acid, 1N NaOH and collagen stock. The collagen hydrogel final pH was 7.4±0.1. All preparation process was carried out on ice. Then the samples were incubated under 37 °C. The component of 2X PBS buffer was 36 mM K_2HPO_4, 23 mM KH_2PO_4 and 0.6 M NaCl and it was filtered by 0.22 μm filter.

Preparation of genipin solutions: The genipin was dissolved in the 1X PBS, the concentration of genipin solution was 1mM. The pH of genipin solution was adjust to 7.4 ± 0.1 by NaOH and filtered by 0.22 μm filter. The genipin solution was incubated at 37 °C for further experiments.

Genipin solution absorption spectra: The absorption spectrum of 1 mM genipin solution was collected from 190 nm to 900 nm by Carry 50. The cuvette was 1 cm quartz cuvette. The age of the genipin solution was 0, 1, 2, 3, 4, 5, 7, 9, 12, 13, 14, 15 days.

Genipin-solution-modified collagen hydrogel absorption spectra: One photon emission spectra: The collagen hydrogel was prepared according to the above description. 110 µl of final mix for collagen hydrogel were added to 96-well pre-chilled clear Falcon plate. After 2 hours of incubations at 37 °C, 110 µl of 1 mM genipin solution were added on the top of polymerized collagen hydrogel. The emission spectrum was collected by FlexStation II fluorescence microplate reader in a backscattering mode (Molecular Devices) after 24 hours of incubating collagen hydrogel with genipin solutions at 37 °C. The "ageing" of genipin solutions was for 0 days, 2 days, 4 days, 8 days or 13 days.

Genipin-solution-modified collagen hydrogel emission spectra: The collagen hydrogel was prepared according to the description above. 110 µl collagen hydrogel was added in 96 well falcon clear plate, which was pre-chilled on the ice. After 2 hours incubations at 37 °C, 110 µl 1 mM genipin solution was added on the top of collagen hydrogel. The emission spectrum was collected by flex station after 24 hours incubation at 37 °C. The age of genipin solution was 0 day, 2 days, 4 days, 8 days and 13 days.

The absorption spectrum of genipin-amino acid reaction product and the genipin-amino acid reaction product separation: The genipin-amino acid reaction system condition is same as the genipin-collagen hydrogel reaction system conditions (1x PBS buffer). The phosphate concentration is 30 mM and NaCl concentration is 0.3 M. The reaction temperature is 37 °C and pH is 7.4. In the genipin-amnio acid reaction system,

the genipin concentration is 1 mM and the amino acid concentration is 10 mM. The absorption spectra of genpin-amino acid reaction product was collected after 24 hours reaction at 37 °C by UV-Vis spectrophotometer form 190 nm to 900 nm. Bio-Gel P2, 100-1800 MW working range, was employed to separate the components of the genipin-amino acid reaction product. The volume of 1x PBS buffer, which was used to hydrate the gel, was 2 times as the expected packed final bed volume. The volume of every gram of dry Bio-Gel P2 was 3 ml after hydration. The diameter of the column is 2.5 cm. The final height of the packed column bed was 19 cm. The flow rate was 5 ml/min established using gravity. The separated genipin-amino acid product was collected into the 2 ml centrifuge tubes. The absorption spectrum of each centrifuge tube was collected by UV-Vis spectrophotometer from 190 nm to 900 nm.

Rheology measurements of genipin modified collagen hydrogels: 2 g/l collagen hydrogel was prepared according to the description above. 2 ml collagen hydrogel was added in the cell culture plate (diameter is 35 mm) which was pre-chilled on ice. 2 ml genipin solution was added on the top of collagen hydrogel after 2 hours incubation at 37 °C. The rheology data was measured by Haake rheostress rheometer after 24 hours crosslinking at 37 °C. The age of genipin solution was 0 days, 4 days, 8 days and 15 days. The diameter of the plate is 35mm, the gap between two plates was 1 mm and the strain was 0.05.

Multiphoton microscopy (MPM) imaging and spectroscopy of genipin modified collagen hydrogels: Collagen hydrogel was prepared based on protocol of preparation section. 350 µl 2 g/l collagen hydrogel was added into the pre-chilled 8-well cell culture

chamber. 350 µl genipin solution was added on top of collagen hydrogel after 2 hours incubation at 37 °C. The MPM images were collected after 24 hours crosslinking at 37 °C. The upright Thorlabs multiphoton microscope was employed to image the genipin crosslinked collagen hydrogel or uncrosslinked collagen hydrogel. The laser source was femtosecond titanium:sapphire laser excitation source. In this study, we used 100 mW horizontally polarized 810 nm laser excitation wavelength to excite the genipin crosslinked collagen hydrogel and Zeiss 63× (water, N.A. 1.0) to collect the images. Two fluorescence signal filters (470-550 nm and 570-610 nm) were employed to collect fluorescence signals, narrow filter (400-410 nm) was employed to collect SHG signal. Every image was 2048 × 2048 pixels which corresponded to 200 µm × 200 µm. The pixel average intensity was evaluated with Matlab.

The multi-photon spectra were acquired with Acton SP2300 spectrograph equipped with a 68 mm × 68 mm, 300 grooves/mm ruled grating blazed at 500 nm and a Pixis1024B CCD camera (Princeton Instruments, Trenton, New Jersey).[14b] Briefly, the spectrograph and camera settings were PC-controlled through WinSpec/32 v.2.5K software and the CCD temperature was maintained at −75 °C in all the experiments. A typical spectral acquisition time was 16 s and the collection of spectra was repeated at least three times on at least two independently prepared samples, averaged and corrected for dark noise background. 10×, 2.6 mm working distance, N.A. 0.3, N-Acroplan, water immersion objective from Zeiss (420947-9900-000) was used to obtain spectra in the epi-collected configuration. The spectra were filtered from the laser excitation with a long pass 705 nm single-edge dichroic beamsplitter (Semrock, FF705-Di01-34×46) and additionally filtered

through a 720 nm short pass filter (Semrock, FF01-720/SP-25) introduced at the exit port of the modified Zeiss Axioexaminer.Z1.

The distribution of genipin crosslinked collagen hydrogel fiber's diameters: The areas selected for measurements were 70 μm × 70 μm in the central part of the 200 μm × 200 μm MPM images. Then at least 60 fibers' diameters in these fields were measured using Image J. [11] After measuring the fibers, we grouped them into different size ranges and calculated fractions of fibers in a defined specific range. We repeated this procedure separately for fibers emitting in 470 nm – 550 nm and 570 nm – 610 nm spectral regions and for two different "ages" of genipin solutions.

Crosslinking degree of genipin modified collagen hydrogel: In order to detect the degree of genipin modification of collagen hydrogels, we assayed the percentage of free amines after crosslinking with genipin using ninhydrin colorimetric method.[24b] 2 g/l collagen hydrogel was prepared based on the description above. 100 μl sample was added into the 1.5 ml pre-cold centrifuge tube. After 2 hours of polymerization, different age 1 mM genipin solution was added on the top of collagen hydrogel for 24 hours crosslinking at 37 °C. Collagen hydrogel was rinsed by deionized water three times (20 min per time) at room temperature after crosslinking process. After rinsing, the material was digested by activated collagenase in the water system at 37 °C for 72 hours. The digested product was mixed with 0.7% ninhydrin solution (in ethanol) and boiled for 2 min. The absorption spectrum was collected in the 900-190 nm spectral range. The calibration curve was obtained with glycine and added identical amounts of collagenase used to

digest materials. The relative crosslinking degree was calculated based on the formula below:

Crosslinking degree (%) = [1 – Crosslinked absorbance 570/non-Crosslinked absorbance 570]*100%

Fibroblast Cell Culture on Collagen Hydrogels: The embryonic BALB/3T3 (clone A31) fibroblasts were purchased form ATCC. It is stored in liquid nitrogen and sub-cultured in Advanced DMEM (Dulbecco's Modifed Eagle Medium, 12491) media according to standard procedures.

The 2g/l collagen hydrogel was prepared in the 8-well chambered coverglass (MP Biomedicals) as described above (250 µl/well). After 2 hours or 24 hours of polymerization at 37 °C, 1 mM fresh or 1 mM 15 dyas old genipin solution were employed to crosslink the polymerized collagen hydrogel for 24 hours at 37 °C. After crosslinking, the GCC material was washed by the same volume of 1X PBS three times (20 min/per wash) at room temperature. 3×10^4 fibroblast cells were seeded on the surface of the gel and cultured at 37 °C. 42,800 fibroblast cells/cm^2 were seeded per gel surface. Then cells were cultured in 37 °C, 10% CO_2 incubator. The cell culture medium was changed every 3 days.

In order to test the cell survival rate, the cell culture medium, which existed on the top of collagen hydrogel, was carefully removed, then 50 µl 0.4% toluidine blue solution was added on the top of collagen hydrogel to stain cells for 20 minutes at room temperature. After that, the cells were imaged with a phase contrast microscope. To identify the round cells in the phase contrast images, phase contrast images were visually divided into four

equivalent sections. Then Image J was used to measure pixel number of each individual cell length and width, only when the numbers were within 1.5 pixels, the cell was defined as a round cell. We counted the total number of cells in the entire image and subtracted the number of round cells obtained to obtain the count of the extended cells.

766 nm center wavelength of the excitation laser and 470 nm to 550 nm emission filters were employed to collect the MPM images of fibroblast cells cultured on collagen hydrogel. The images were used to determine how spherical (round) the cellular components are by calculating their aspect ratios. The aspect ratio was estimated as a percent of sphericity by calculating the width to length ratio. Twenty to thirty independent measurements were performed to establish sphericity estimates. The aspect ratio of 100% indicates a perfectly round cell while small numbers indicate extended, slender objects. The errors reported are the standard deviations of the mean.

Results

Genipin cross-linker solution

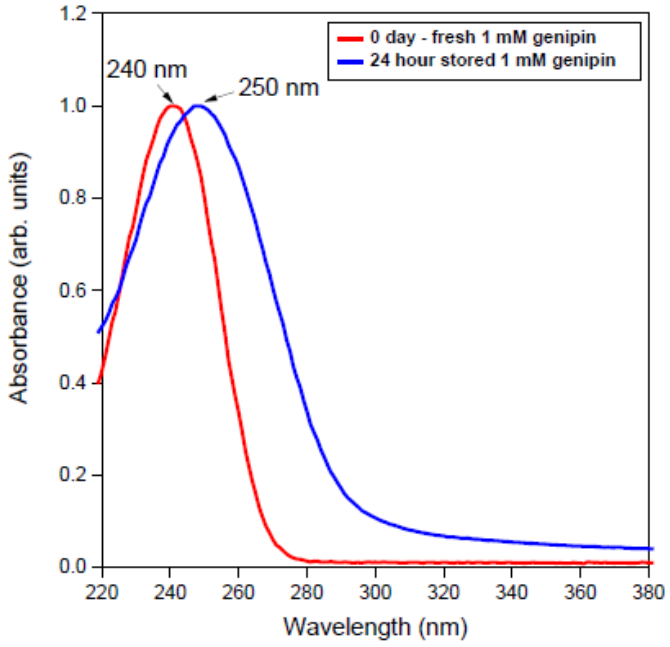

Figure 5.1 The absorbance spectra of freshly prepared and 24 hr stored 1 mM genipin solutions.

Based on our experience, the fresh prepared pH 7.4 1 mM solution genipin prepared in 30 mM phosphate buffer is clear and colorless. It will change color to yellow after long term storage at 4 °C, the color becomes darker along with prolonging the storage time. Higher temperature (37 °C) can shorten the time of the color change process and the yellow color of genipin solution can be obviously observed after 1 day incubation at 37 °C. We believe that color change of genipin solution is due to the formation of genipin polymers because it has been reported that genipin monomer has the potential to form polymeric molecules in basic conditions.[8a] Currently, there is little published data about the color change process of genipin solutions. In order to understand this process/polymeric genipin formation, we collected absorbance spectra of genipin solutions on different days. The genipin monomer ~240 nm [8b] absorbance shifts to ~250 nm (**Figure 5.1**) after

24 hours of storing solutions at 37 °C. The shifting of the ~240 peak is because of the ring-opened genipin polymer formation.[8a]

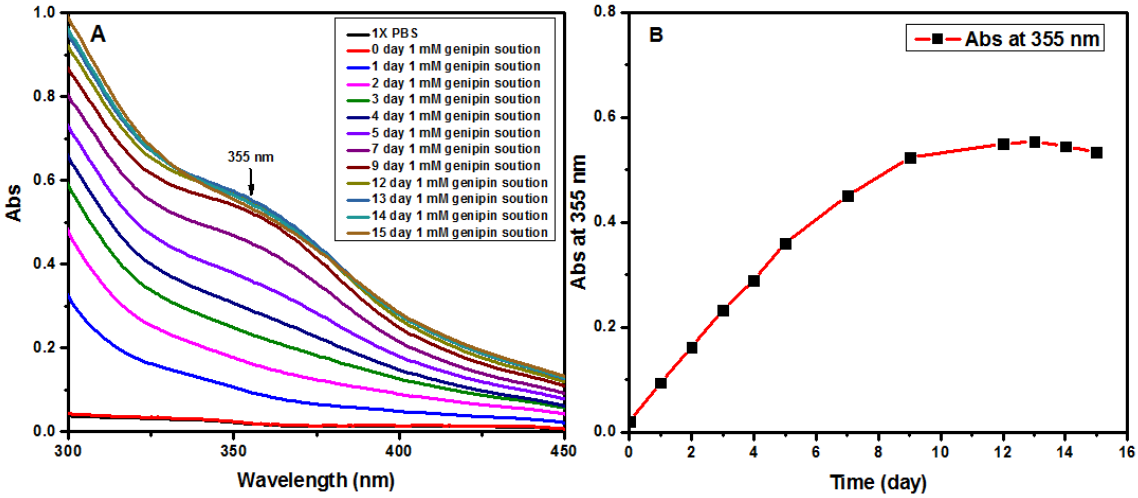

Figure 5.2 The absorbance spectra of freshly prepared and stored 1 mM genipin solutions. (A)250-550 nm spectral range; (B) the increase in absorbance at ~355 nm.

We observed the development of genipin solution absorbance peak at ~355 nm (**Figure 5.2A**) when genipin solution was incubated at 37 °C. Genipin solution ~355 nm absorption peak got highest absorption value after 8 day incubation at 37 °C (**Figure 5.2B**). 37 °C kinetics data can be fitted by single exponential, the ~ 355 nm peaks increasing rate is about 0.18±0.02 (per day) at 37 °C. We believe that that ~355 nm absorption peak is the characteristic peak for the formation of genipin polymers. Arrenius equation can be employed to model the colorful genipin polymer formation at different temperature. It shown that higher incubation temperature can accelerate the genipin polymer formation process, the modeling result also corresponds to our genipin solution storage experience.

Mu et al.[8a] reported the characteristic absorbance peak of genipin polymer is about 300 nm and 355 nm shoulder peak can be also recognized if pH was increased. For our reaction system, we did not change the pH of solutions, but higher genipin concentration (1 mM) was employed to prepare genipin polymer. It is also reported that ~265 nm absorbance peak corresponds to the genipin polymer.[8b] So far, there isn't clearly absorption for the genipin polymers based on the literature and our experiment result. This is maybe because the absorption peak of genipin polymer/genipin polymer formation is very sensitive to the reaction system.

Polymerization of collagen into hydrogels

After the collagen self-assembly process, the samples change from transparent liquid state to opaque hydrogel state. The 24 hours self-assembled collagen hydrogel's second harmonic generation (SHG) intensity is almost two times as that for the 2 hours self-assembled materials. And the microstructure of 24 hours self-assembled and 2 hours self-assembled collagen hydrogels are also different. The 2 hours self-assembled collagen hydrogel's and 24 hours self-assembled collagen hydrogel's SHG contrasted fiber length is around 15.2 μm and 4.8 μm respectively. But the SHG contrasted pore diameter is similar for both materials. (**Figure 5.3**)

A

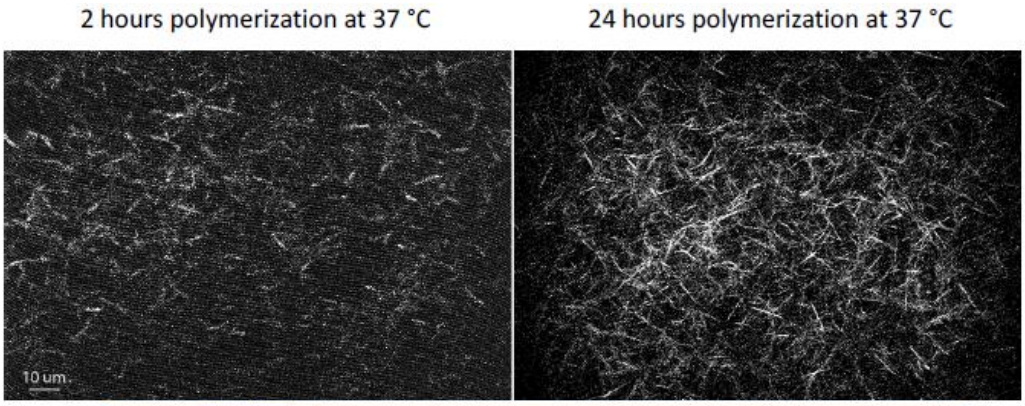

B

Material Parameters / Polymerization time	Fiber Length (μm)	Pore Diameter (μm)	SHG Intensity
2 hours polymerization materials	15.19 ± 2.09	7.85 ± 2.02	1090
24 hours polymerization materials	4.75 ± 1.14	5.17 ± 1.00	1823

Figure 5.3 2 g/l collagen hydrogels self-assembled for 2 hours versus 24 hours. (A) Second harmonic generation (SHG) images. λ_{ex} is 810 nm. (B) Material parameters obtained. Errors reported are the standard deviations from the mean. SHG intensity is measured as the peak in the maximum scattering intensity minus the background.

There is no relationship between the self-assembly time of collagen hydrogel and the color of genipin crosslinked collagen hydrogel (GCC). The color of fresh genipin crosslinked collagen hydrogel is gray-blue. The color of "aged" genipin crosslinked collagen hydrogel is yellow- brown.

One photon optical properties of GCC hydrogels

To study the optical properties of different "aged" genipin crosslinked collagen hydrogel, we collected the absorbance and one photon excited emission spectra of different "aged" genipin crosslinked collagen hydrogel (**Figure 5.4**). It has reported that the characteristic peak ~590 nm is from the reaction of free amines and C3 of fresh genipin (genipin monomer). If the older genipin solution was employed to crosslink collagen hydrogel, the ~590 nm characteristic peak is less and less obvious (**Figure 5.4A**). On the contrary,

~410 nm peak becomes more and more clearly defined in the absorbance spectra of the older genipin crosslinked collagen hydrogel. This band slightly blue-shifts as the storage time of genipin solutions used to modify hydrogels increases from 0 to 4 days. We believe the disappearance of the ~590 nm peak and the appearance of the ~410 nm peak is due to the accumulation of the genipin polymers and the less concentrated genipin monomer.

When the excitation wavelength is 395 nm, the fluorescence emission peak is at ~470 nm (**Figure 5.4B**) and there is also a small emission peak around 620 nm. The 470 nm band intensity increases if "aged" genipin solutions are employed to crosslink collagen hydrogel. When the genipin solutions age is 4 days, the 470 nm band intensity gets the highest value. The 620 nm peak undergoes a blue shift to 610 nm and it completely disappeared if genipin solution age is older than 4 days. (**Figure 5.4B**) This result correspond to the changing of the 410 nm peak which located on the absorption spectra of "aged" genipin crosslinked collagen hydrogel (**Figure 5.4A**).

when excitation wavelength is 590 nm, the emission peak of GCC is at ~625 nm (**Figure 5.4C**). This emission peak has maximum intensity when 2 days old genipin solution was employed to crosslink collagen hydrogels. 625 nm emission peak almost disappeared if the age of genipin solution was older than 4 days. This disappearance of the 625 nm peak in the emission spectra is due to a significant reduction in 590 nm absorbance peak of old genipin crosslinked collagen hydrogel (**Figure 5.4A**).

Our result show that the different storage time can result in different optical properties of GCC. This also indicates that the preparation protocol is very significant for the final

properties of materials. If different “aged” genipin solution was employed to crosslink collagen hydrogel, we can get different characteristic peaks. 590 nm peak for fresh genipin and 410 nm peak for old genipin. We thought this is because of genipin monomer/genipin polymer different modification preference on the amino acid residues of collagen. Lee et al.[27] reported that different product of genipin-amino acid have different absorbance peaks. Genipin-lysine product shows high absorption peak at 590 nm, genipin-proline product only shows a shoulder-like absorbance peak at ~ 420 nm. Park’s study[28] additionally reported a very weak absorbance at 590 nm for genipin polymer-methylamine product. The absorption peaks of the product between single amino acids and genipin also can help us to explain the disappearance of 590 nm peak and the 410 nm appearance.

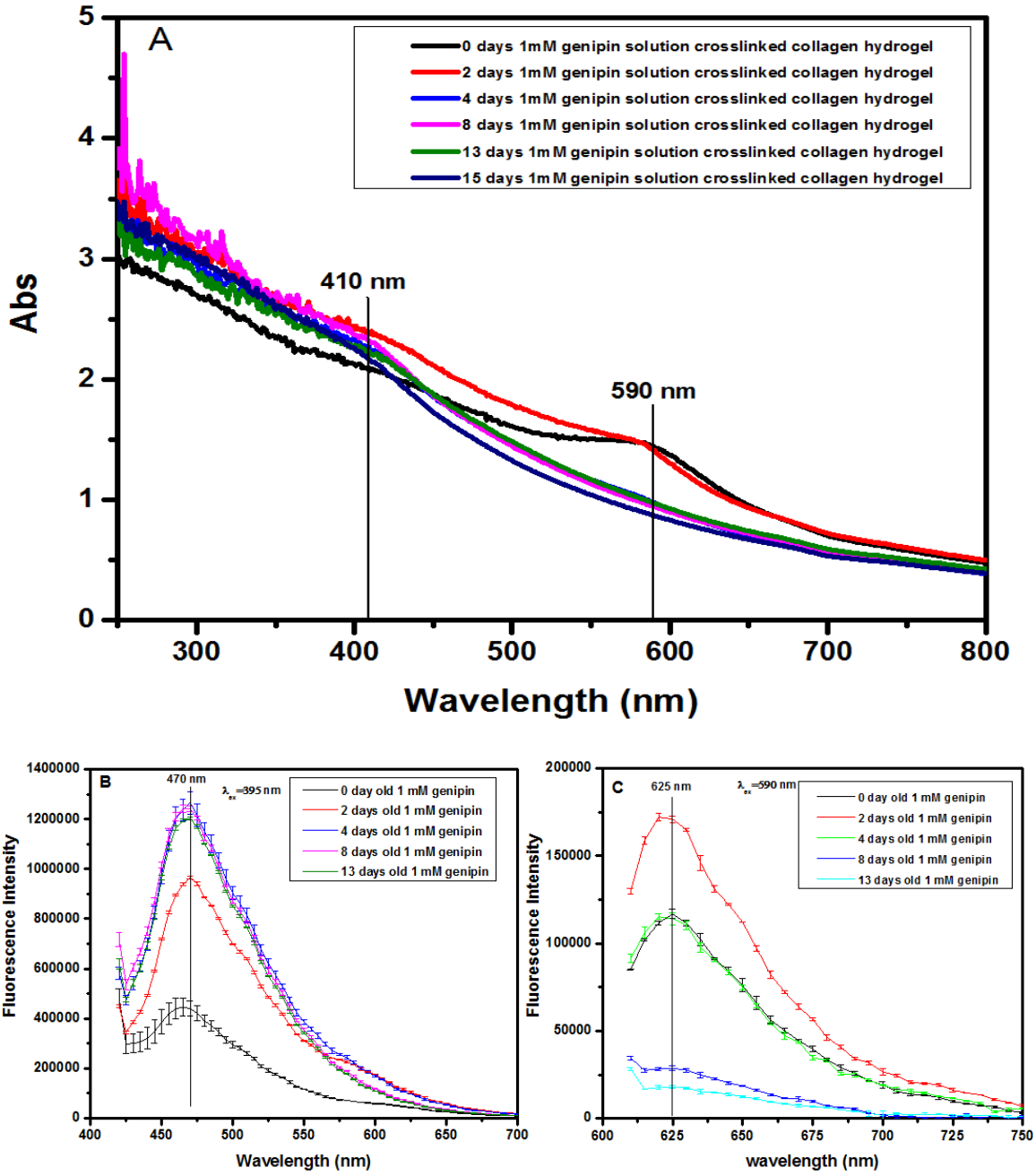

Figure 5.4 The absorption and emission spectra of different "aged" genipin crosslinked collagen hydrogel (A) The absorbance spectra of reaction products between a 2 g/l collagen hydrogel and 1 mM genipin solutions of different ages. (B) Emission spectrum of GCC gel excited with 395 nm wavelength. (B) Emission spectrum of GCC gel excited with 590 nm wavelength. The cross-linking reaction was carried out for 24 hours.

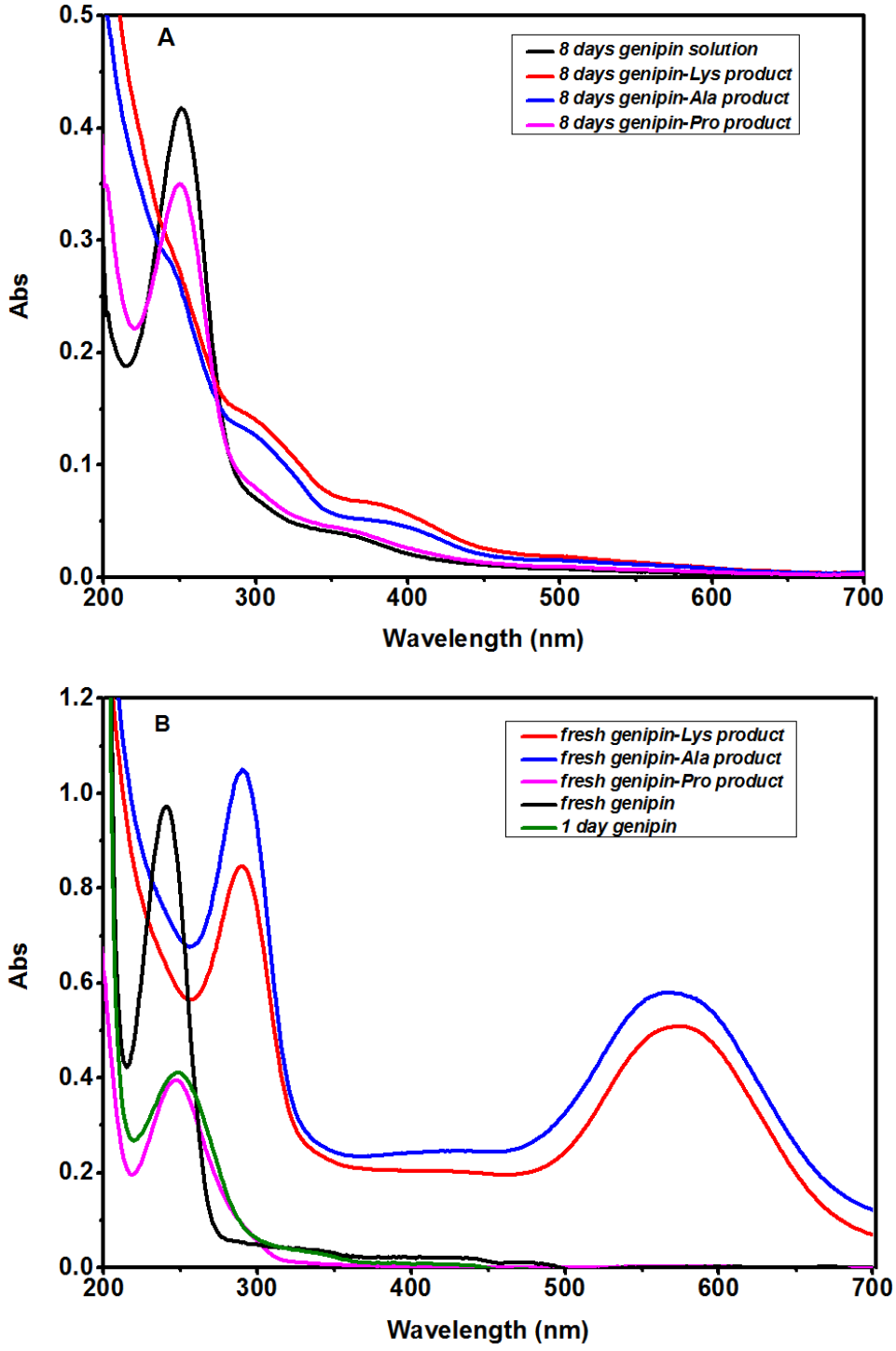

Figure 5.5 The absorption spectrum of genipin-amino acid product. (A) The absorption spectrum of 8 days genipin-amino acid product.(B) The absorption spectrum of fresh genipin-amino acid product. The reaction system is 1X PBS (30 mM phosphate, 0.3 M NaCl, pH is 7.4). Temperature is 37 ℃.

To investigate the differences of the different “aged” genipin crosslinked collagen hydrogel absorption spectrum, the fresh genipin solution and 8 days genipin solution was employed to react directly with selected amino acids, the absorption spectra of different “aged” genipin-amino acid reaction products were collected. For the 8 days genipin solution **(Figure 5.5A black)**, there are two main peaks, one peak is around 250 nm and another peak is around 355 nm. The appearance of the two peaks (250 nm and 355 nm) is because of the genipin polymer formation. For the 8 days genipin solution – proline reaction system **(Figure 5.5A pink)**, the absorption spectrum of 8 days genipin-Pro is similar as 8 days genipin solution absorption spectrum, it can illustrate that there is no reaction between 8 days genipin solution and proline. For the fresh genipin-Pro reaction system **(Figure 5.5B pink),** there was just single absorption peak around 250 nm, the appearance of 250 nm peak is because of the ring-opened genipin polymer formation during the reaction time, the appearance of 250 nm peak is not due to the genipin monomer -Pro reaction. Then we can get the conclusion that there is no reaction between genipin (genipin monomer and genipin polymer) and proline. This is maybe because the proline closed ring structure affect the reaction rate of genipin and proline.

For the 8 days genipin-Lys and 8 days genipin-Ala reaction system, there were two main peaks, one peak is around 305 nm and another peak is around 395 nm. But 590 nm and 250 nm peaks were not obvious any more. **(Figure 5.5A)** This indicated the reaction between 8 days genipin and lysine or alanine can result in the appearance of the 395 nm absorption peak. Possibly, this 395 nm absorption peak is the same as the 410 nm absorption peak observed for the “aged” genipin crosslinked collagen hydrogel. The

wavelength of the two peaks is not exactly same and the peak shift maybe because of the difference in the local environments of reacting amino acids within collagen hydrogel and/or some scattering of the hydrogel.

For the fresh genipin-Lys and fresh genipin-Ala reaction system, there were two main absorption peaks, one peak is around 290 nm and another one is around 575 nm. There was no absorption peak around 250 nm for the fresh genipin-Lys or fresh genipin-Ala reaction system, **(Figure 5.5B)** this is because genipin monomer reacted with the amino acid immediately and there was no ring-opened genipin polymer formation during the reaction period. The 570 nm absorption peak of fresh genipin-Lys or Ala reaction system is likely the same absorption peak observed at 590 nm for fresh genipin crosslinked collagen hydrogel. The peak shift (570 nm to 590 nm) maybe because of the difference in the local environments of reacting amino acids within collagen hydrogel and/or some scattering of the hydrogel. The 290 nm absorption peak has been reported by Park et al. [28] to correspond to the intermediate of the genipin-amino acid product.

According to our experiment results, different "aged" genipin solution can result in different absorption spectra of genipin-amino acid product when it reacted with the same amino acid.

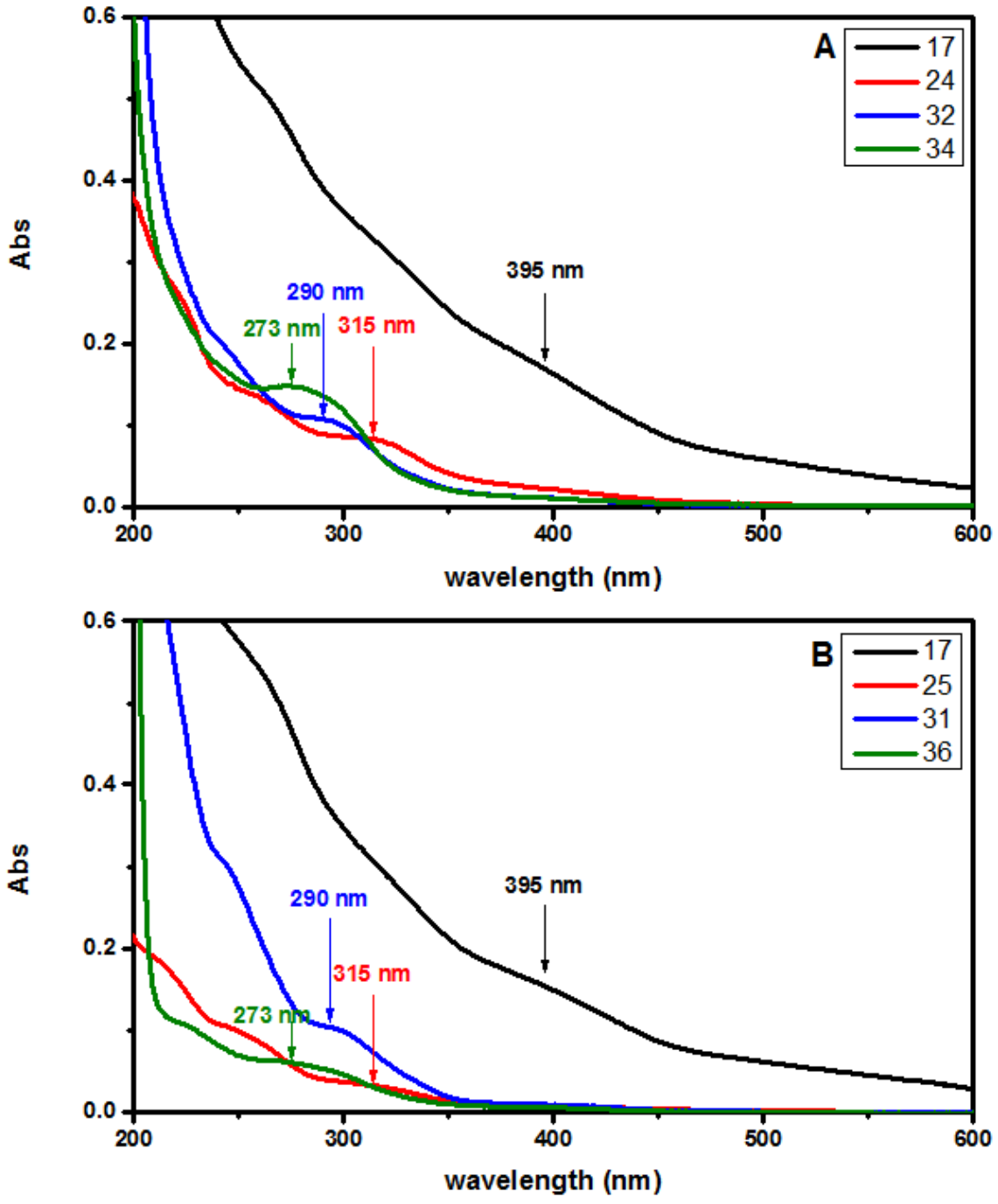

Figure 5.6 The absorption spectra of different fractions separated with Bio-Gel P2 size exclusion chromatography resin. (A) Genipin-Lys reaction product fractions' absorption spectra formed using genipin solutions stored for 8 days. (B) Genipin-Ala reaction product fractions' absorption spectra formed using genipin solutions stored for 8 days. The diameter of column is 2.5 cm. The height of the resin bed is 19 cm. Flow rate is 5 ml/min.

To investigate the reaction products of stored 8 days genipin-collagen hydrogel reaction, we incubated the genipin solution stored for 8 days with different amino acid solutions. After reaction at 37 °C, the stored 8 days genipin-amino acid reaction products were passed though the Bio-rad size exclusion chromatography column eluted with water. **(Figure 5.6)** For 8 days genipin-lysine reaction products and 8 days alanine reaction products, the components are similar. There are at least four components exist in the system after reaction because there are at least 4 separated peaks in the absorption spectra. They are 395 nm peak, 315 nm peak, 290 nm peak and 273 nm peak. **(Figure 5.6)** The 395 nm peak should correspond to the product of genipin polymer-amino acid and the wavelength of the peak (395 nm) is very similar to the main peak (410 nm) of the absorption spectra of 8-days-old-genipin-crosslinked collagen hydrogel. Besides this, this peak (395 nm) is the first elution peak, which means this component has the highest molecular weight, which also can prove that this component (395 nm peak) is the product of genipin polymer-amino acid. For the 290 nm peak component, is has been reported that it is the genipin monomer-amino acid intermediate. The 273 nm peak maybe the ring opened genipin monomer. However, it is needed to conduct further experiments to understand the exact components of the four peaks.

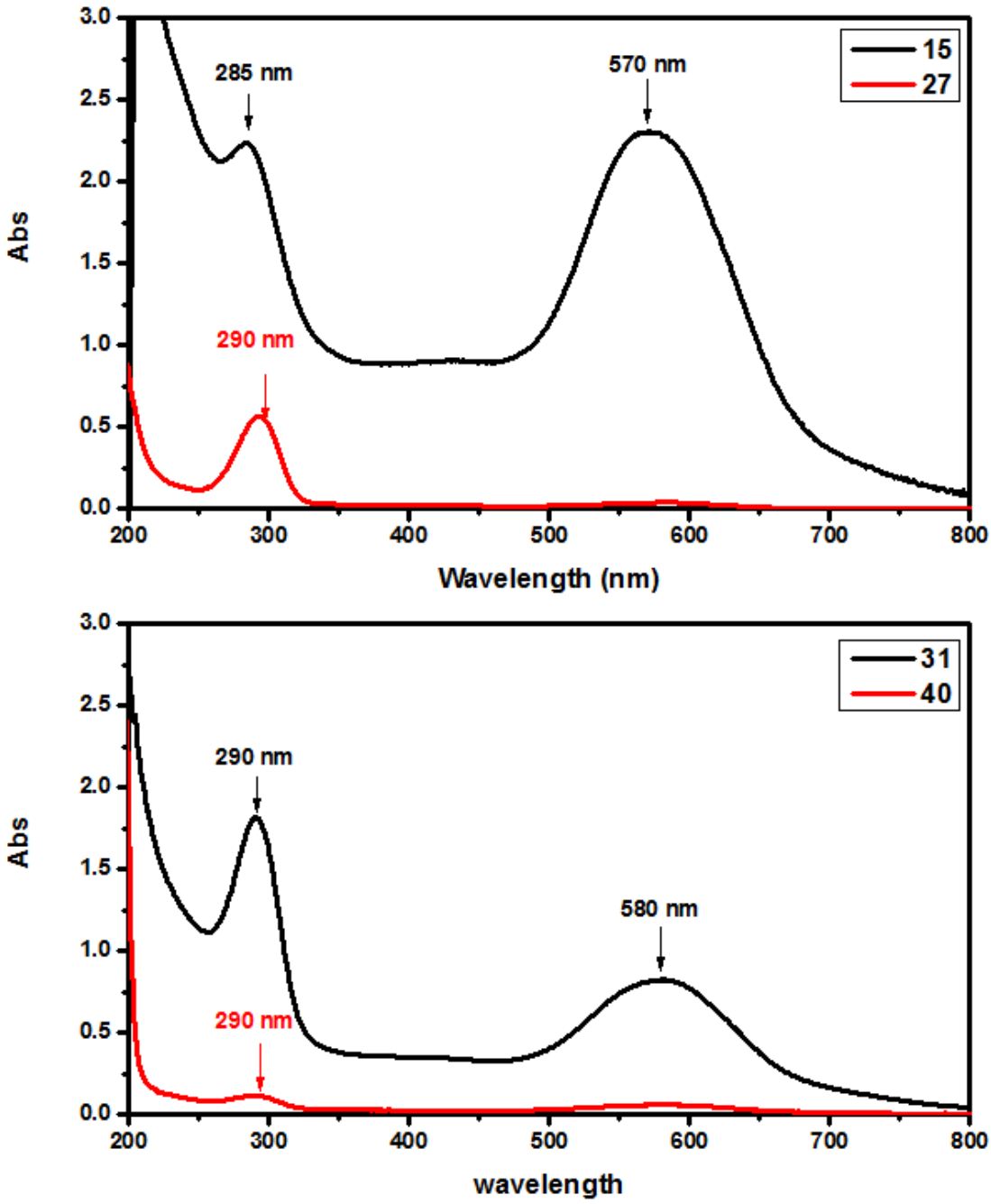

Figure 5.7 The absorption spectra of different fractions separated with Bio-Gel P2 size exclusion chromatography resin (A) fresh genipin-Lys reaction product fractions' absorption spectra. (B) fresh genipin-Ala reaction product fractions' absorption spectra. The diameter of column is 2.5 cm. The height of the bed is 19 cm. Flow rate is 5 ml/min. The reaction carried out 24 hours.

To investigate the products of the reaction between genipin monomer (fresh genipin) and collagen hydrogel, we incubated the fresh genipin solution with different amino acid solutions at 37 °C. There are just two obvious absorption peaks in the absorption spectra, 570 nm peak (or 580 nm) and 290 nm peak. **(Figure 5.7)** The 580 nm (or 570 nm) peak is the absorption peak of the product of genipin monomer-amino acid. 290 nm absorption peak is the absorption peak of genipin monomer-amino acid intermediate. The molecular weight of the two products must be very close, making it harder to separate the two components. According to our experiment results, the fresh genipin-Lys reaction products came out much earlier than genipin-Ala reaction products. The molecular weight of fresh genipin-Lys reaction products and the molecular weight of fresh genipin-Ala reaction products are very close. Therefore, we attribute the later elution of the genipin-Ala reaction products compared to fresh genipin-Lys reaction products to inconsistency in manually packing the resin inside the column

Nonlinear optical and micro-structural properties

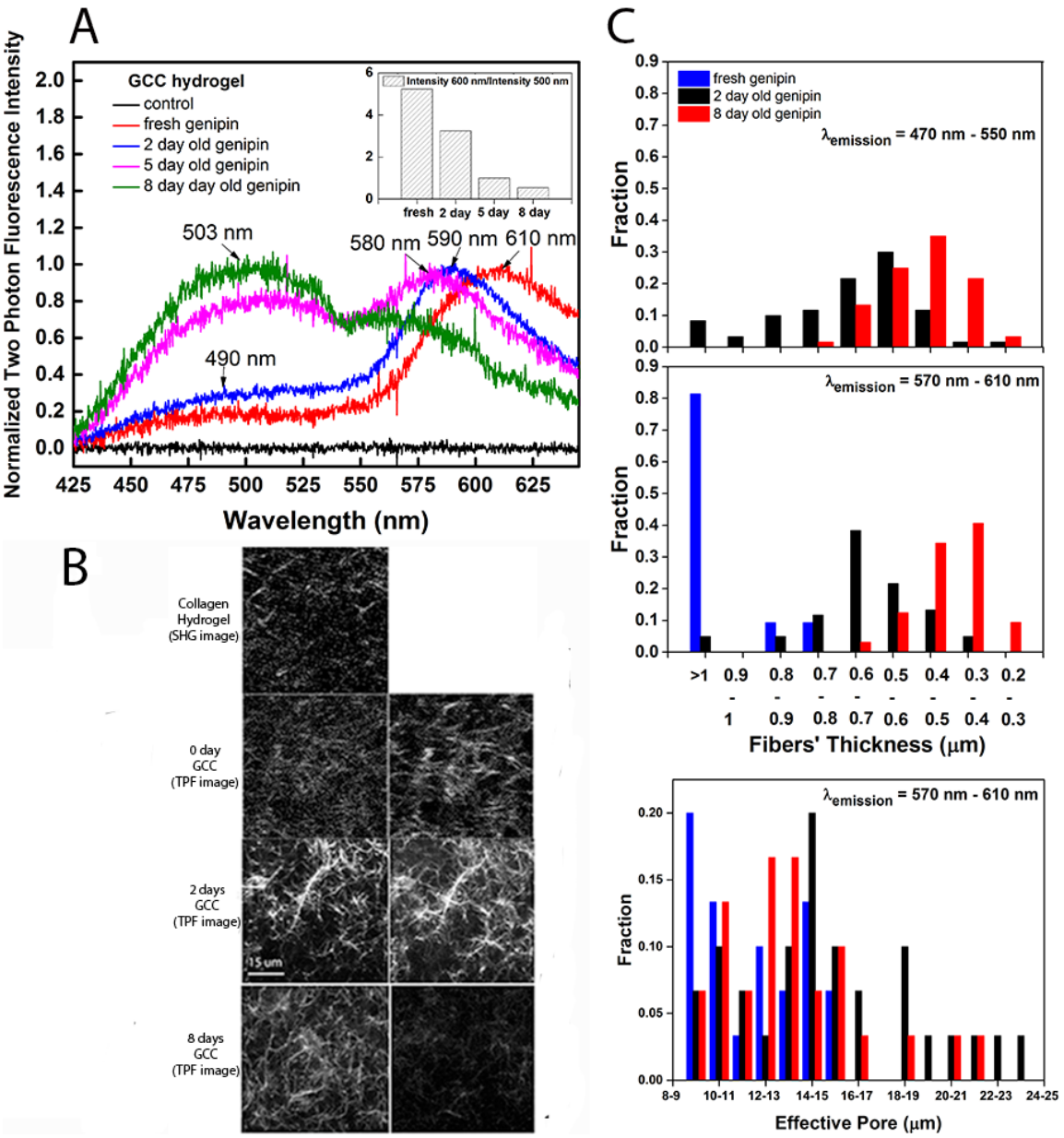

Figure 5.8 The emission spectra and microstructure of different "aged" genipin crosslinked collagen hydrogel (A) Multiphoton emission spectra of GCC gel and ratio of the intensities (insert) for red (intensity at 600 nm) and blue-green (intensity at 500 nm) emitting species induced as a result of modifying collagen gel with genipin solutions stored ("aged") for different times. The intensities were measured from spectra in (A). λex is 810 nm; (B) Multi-photon microscopy (MPM) images. λex is 810 nm. For the GCC (0 day GCC, 2 days GCC and 8 days GCC), only TPF images are shown while SHG images are omitted due to the intensity of SHG signals being significantly reduced upon modification. Images correspond to 470 – 550 nm (left) and 570 – 610 nm (right) spectral ranges. For the collagen hydrogel, the SHG image was shown; (C) average fiber thickness in GCC gels for fibers emitting in 470 – 550 nm and 570 – 610 nm spectral ranges and effective pore sizes. Data shown is for 2 g/l collagen hydrogels cross-linked with 2 days and 8 days stored genipin solutions.

In order to understand two-photon excited emission spectra and the microstructure of GCC, multiphoton spectra (**Figure 5.8A)** and images (**Figure 5.8B**) were collected. When excitation wavelength is 810 nm, there are two main emission peaks in the spectra of fresh genipin crosslinked collagen hydrogel: one peak is at ~490 nm and another one at 610 nm. The location of the two main peaks on the spectra of fresh genipin crosslinked collagen hydrogel (**Figure 5.8B**) is similar to the main peaks location of one photon excited fluorescence spectrum of fresh genipin crosslinked collagen hydrogel (**Figure 5.4B**), but relative ratios of the two main emission peaks are totally different. For the fresh genipin crosslinked collagen hydrogel, the red channel emission signal is much stronger than the green-blue channel. But if the "aged" genipin solution was employed to crosslinked collagen hydrogel, the red channel peak intensity decrease along with the increasing of the genipin age and the green-blue channel peak intensity increase along with the age increasing of genipin solution. On one hand, the red emission band is more than five times as intense as 490 nm band when fresh genipin solution is used to crosslink collagen hydrogel. On the other hand, the intensity of the red emission band significantly decreases compared to emission intensity at ~ 490 nm when 8 days old genipin solution is used to crosslink collagen hydrogels. The changing of relative intensities of the two peaks is also shown in the figure (**Figure 5.8A, insert**), and the two peaks location shift to each other if "aged" genipin was employed to crosslink collagen hydrogel.

Before genipin modification, SHG signal (400 nm-410 nm) is the main signal and there is no TPF signal in the blue-green channel (470-550 nm) and red channel (570-610 nm) (**Figure 5.8A**). After modification, SHG signal (not shown) becomes weaker than before

modification and TPF signal is the main signal which covers both blue-green channel and red channels. The crosslinking by genipin can reconstruct the microstructure of collagen hydrogel, and the reconstructed microstructure is also different if the age of genipin is different (**Figure 5.8B**). The older genipin solution can result in thinner fibers, for example, when a genipin age was 8 days, the induced fibers were thinner (0.3 – 0.5 μm) compared to fluorescent fibers induced with 2 days old genipin (0.5 – 0.7 μm) and fresh (~1.4 μm) genipin solutions (**Figure 5.8C**). Fibers formed are ~ 1.8 μm thick in the materials where collagen was polymerized for 24 hours before subsequent cross-linking with genipin and no variation in the fibers' width was seen (**Figure 5.9**).

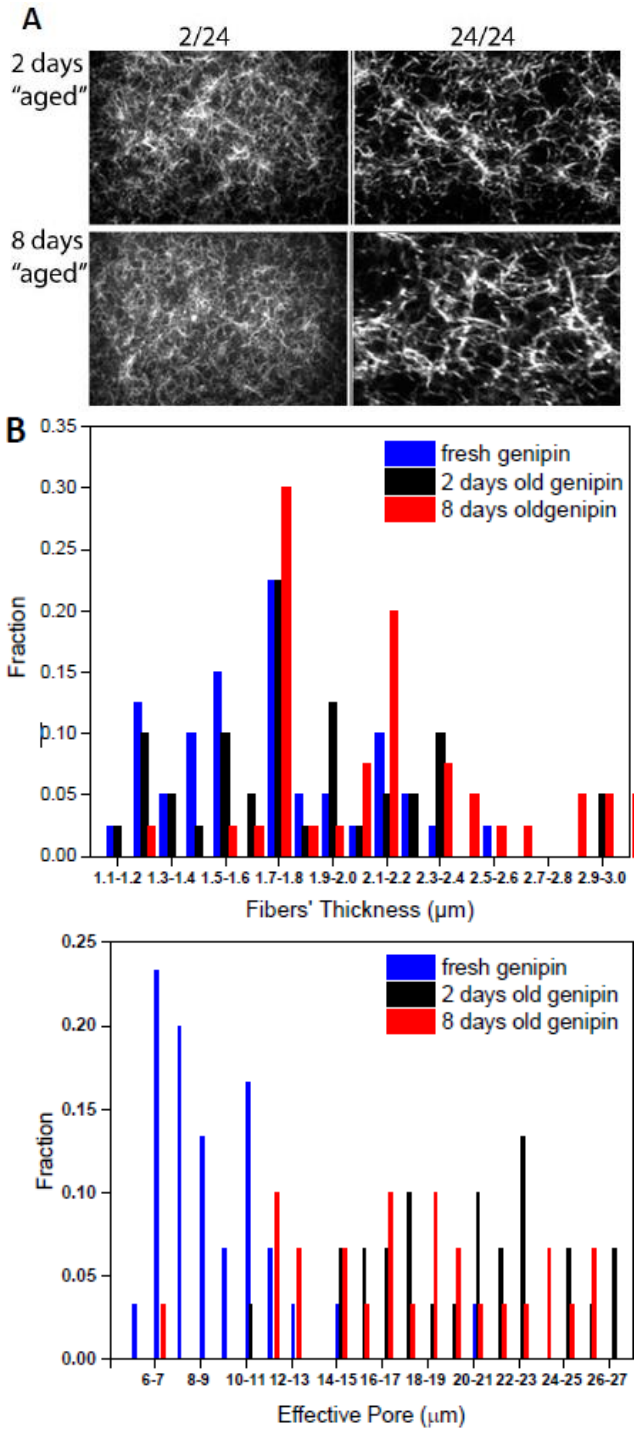

Figure 5.9 The fiber length distribution (A) Multi-photon microscopy (MPM) images. λex is 810 nm. Only TPF images are shown while SHG images are omitted due to the intensity of SHG signals being significantly reduced upon modification. Images correspond to 570 – 610 nm (right) spectral ranges and data shown is for 2 g/l collagen hydrogels self-assembled for 2 hours (2/24) and cross-linked for 24 hours with 2 days and 8 days stored genipin solutions vs. hydrogels self-assembled for 24 hours (24/24) and prepared under the same conditions. (B) average fiber thickness in GCC gels for fibers emitting in 570 – 610 nm spectral ranges and effective pore sizes for 24/24 hydrogels.

Rheological properties and cross-linking degree of GCC hydrogels

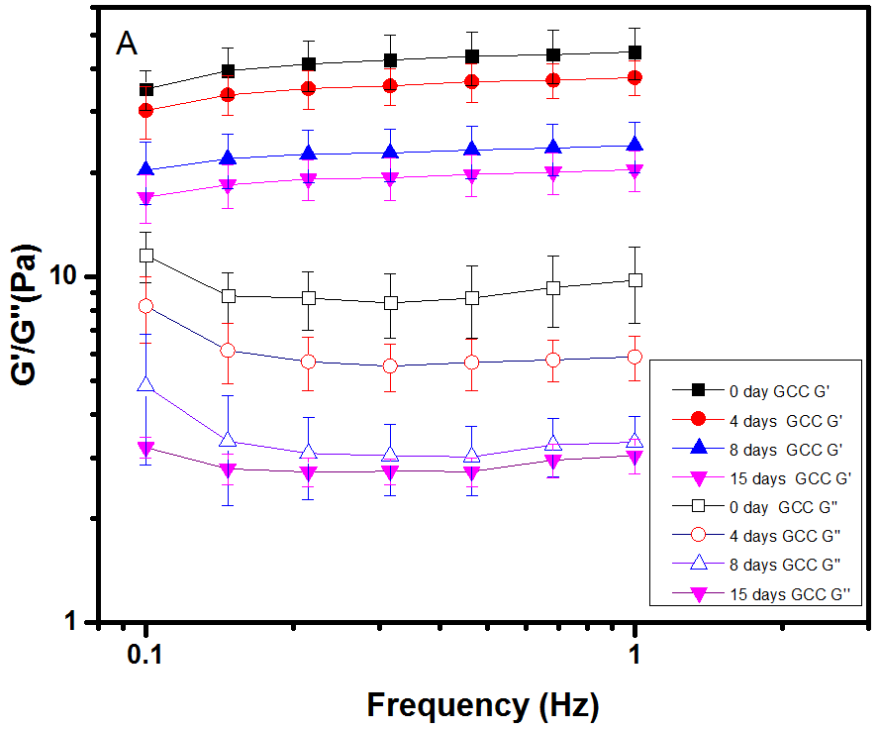

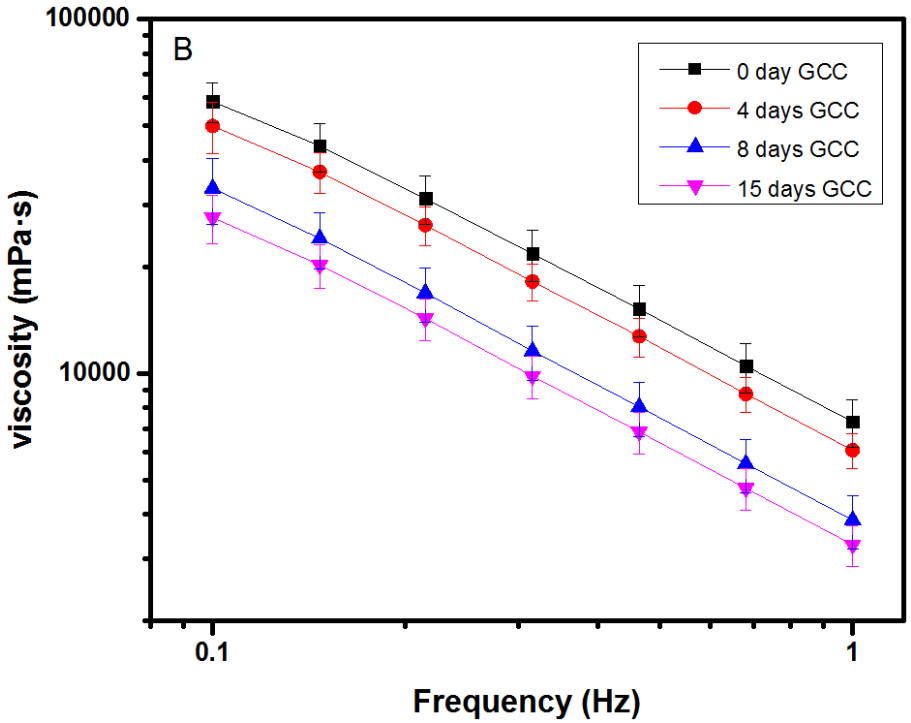

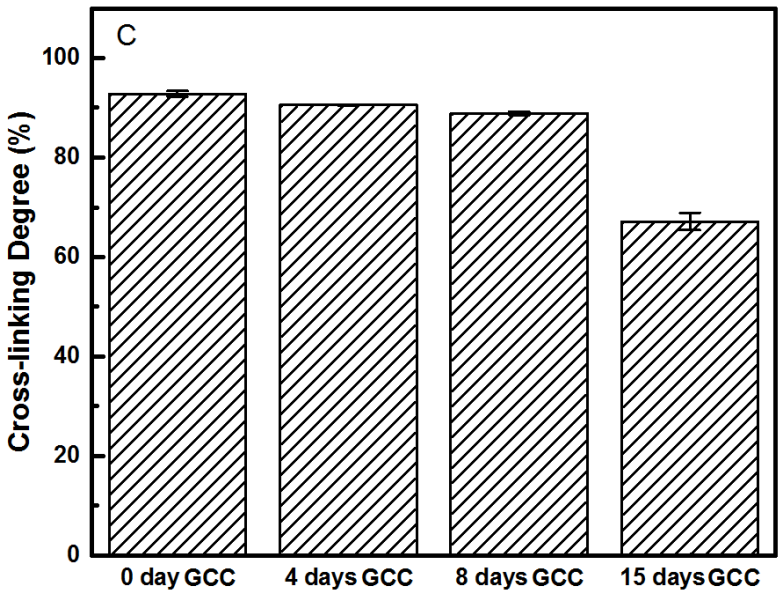

Figure 5.10 The G', G'', viscosity and crosslinking degree of different "aged" genipin crosslinked collagen hydrogel (A) The dynamic mechanical properties of GCC gels prepared with genipin solutions stored for different times as indicated and standard deviations from the mean; (B) The viscosity of GCC gels prepared with genipin solutions stored for different times as indicated and standard deviations from the mean; (C) The cross-linking degree of GCC gels prepared with genipin solutions stored for different times and standard deviations from the mean.

In order to study the effect of the genipin age on the mechanics of the genipin crosslinked collagen hydrogel, we obtained the dynamic modulus of GCC by rheometer (**Figure 5.10A**). When the age of genipin solutions is less than 4 days, storage modulus (G') and loss modulus (G'') of GCC are very similar. G' and G'' has obvious decreased when the genipin age is 8 days. And G' and G'' do not have obvious differences if the genipin age is beyond that of 8 days, such as, 8 day and 15 days genipin crosslinked collagen hydrogel. The "aged" genipin solution also led to a lower viscosity of GCC compared with fresh genipin solution. (**Figure 5.10B**).

The correlation between the mechanical properties and microstructure parameter is also attempted in **Figure 5.11**, it shows that G' of 2 hours self-assembly, different "aged" collagen hydrogel some correlation (R2 = 0.99) with the fiber thickness measured from

TPF images (570 – 610 nm spectral range). And there is no obvious correlation between mechanical properties and microstructure parameters for 24 hours self-assembly, genipin crosslinked collagen hydrogel.

The mechanical behavior of the collagen gels arises from entropic factors due to the movement of the liquid phase through the effective pores and fibers' reorganizations.[29] Since the solid fraction present in the form of fibers within collagen hydrogels is low, the fiber strength usually is not a significant factor in determining bulk mechanical properties of these materials. Cross-linking reduces materials' entropy, constrains fibers capacity to rearrange and affects the bulk elastic properties of the materials.

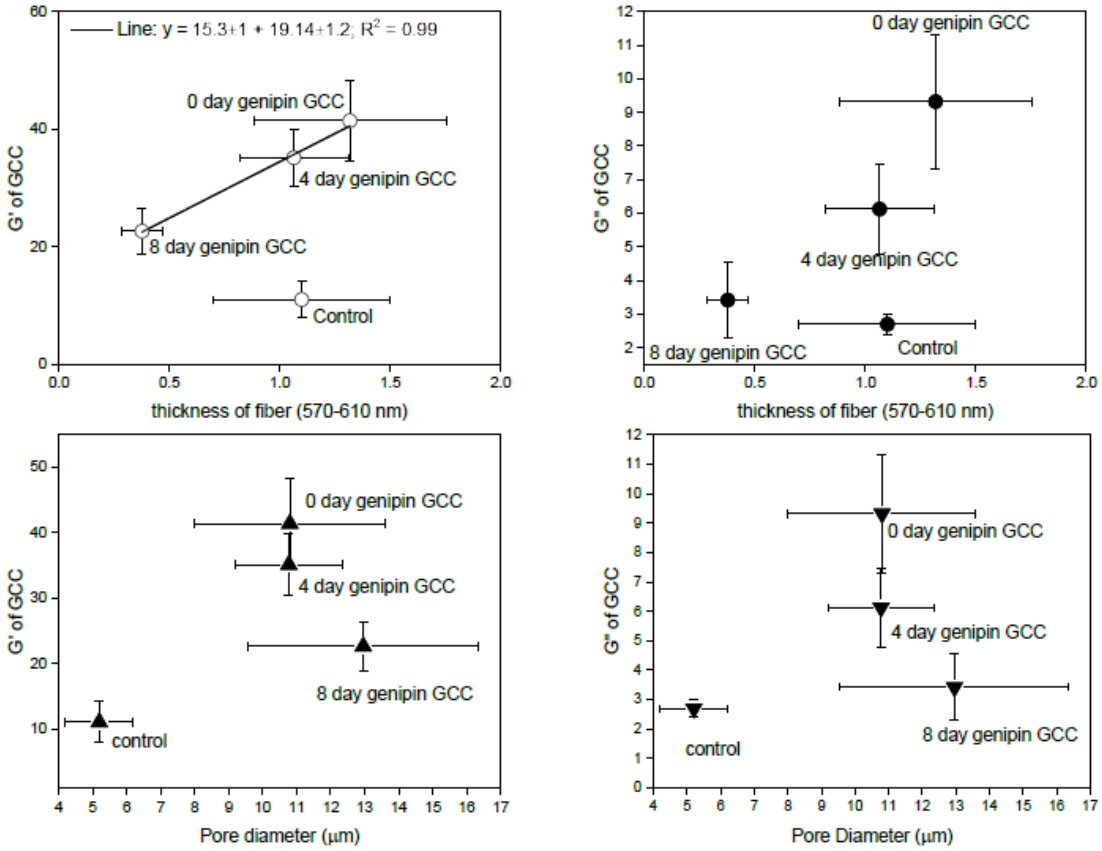

Figure 5.11 Exploration of the correlation of storage (G') modulus and loss (G") modulus with scaffold properties such as fiber thickness and effective pore diameter. The errors are standard deviations of the mean.

According to the ninhydrin reagent measurement, the crosslinking degree of GCC obviously dropped if the genipin age was older than 8 days (**Figure 5.10C**). The decreasing of the crosslinking degree of GCC maybe is the reason which causes the decreasing of G' and G''. The formation of the genipin polymers decrease the amount of the genipin molecules (genipin monomer and/or genipin polymers), it also decreases the crosslinking reaction between genipin and collagen and the crosslinking degree.

After incubation at 37 °C, genipin monomer molecules can form genipin polymers. The molecules length is different for genipin monomer and genipin polymer. The genipin molecules with different length may have different modification pattern, such as, long

range modification by genipin polymers[8a]. The different cross-linking pattern may result in different mechanical properties.

Fibroblasts' interaction with GCC gels

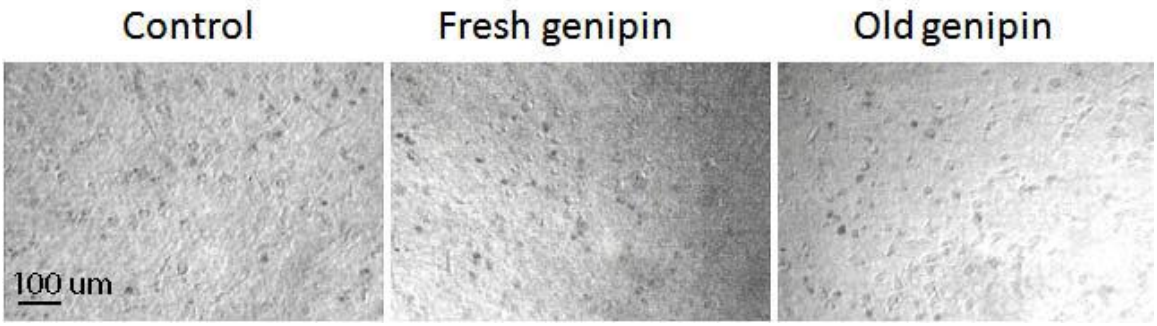

Figure 5.12 Verification of viability of fibroblast cells on the prepared hydrogels with a trypan blue exclusion method . Phase contrast images.

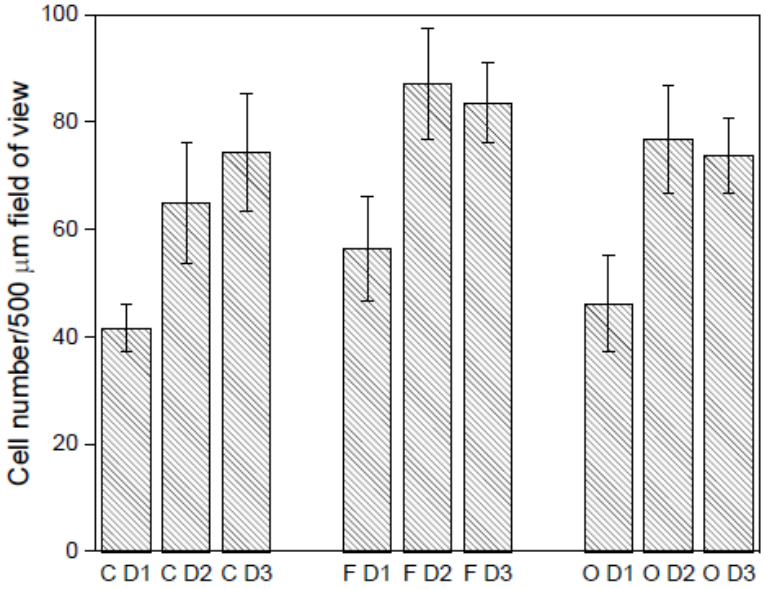

Figure 5.13 Verification of fibroblast cell proliferation on the prepared hydrogels. C = control, uncross-linked gel; F = fresh genipin cross-linked gels; O = 15 day old genipin-cross-linked gels. D1, D2, D3 = day 1, day 2 and day 3 respectively. Error is the standard deviation of the mean.

To understand the interaction between cell and GCC, we cultured BALB/3T3 (clone A31) embryonic fibroblasts on the top of control collagen (uncrosslinked collagen hydrogel) and different "aged" genipin crosslinked collagen hydrogel.

In order to study the survive rate of fibroblast on different "aged" genipin crosslinked collagen hydrogel in the beginning of cell culture, 0.4 % trypan blue exclusion was employed to stain the cell directly.[30] For the dead cells, cell membrane was damaged and the trypan blue stained cells dark blue color that can be observed with an optical microscope. In the beginning of the cell culture (day 2), fibroblasts, which were cultured on the uncrosslinked collagen hydrogels, fresh genipin crosslinked collagen hydrogels and 15 days old genipin crosslinked collagen hydrogels, were alive and the death rate is similar (**Figure 5.12**). For the three materials, the fibroblast cell's proliferation rate is also similar for the first three days of cell culture. (**Figure 5.13**)

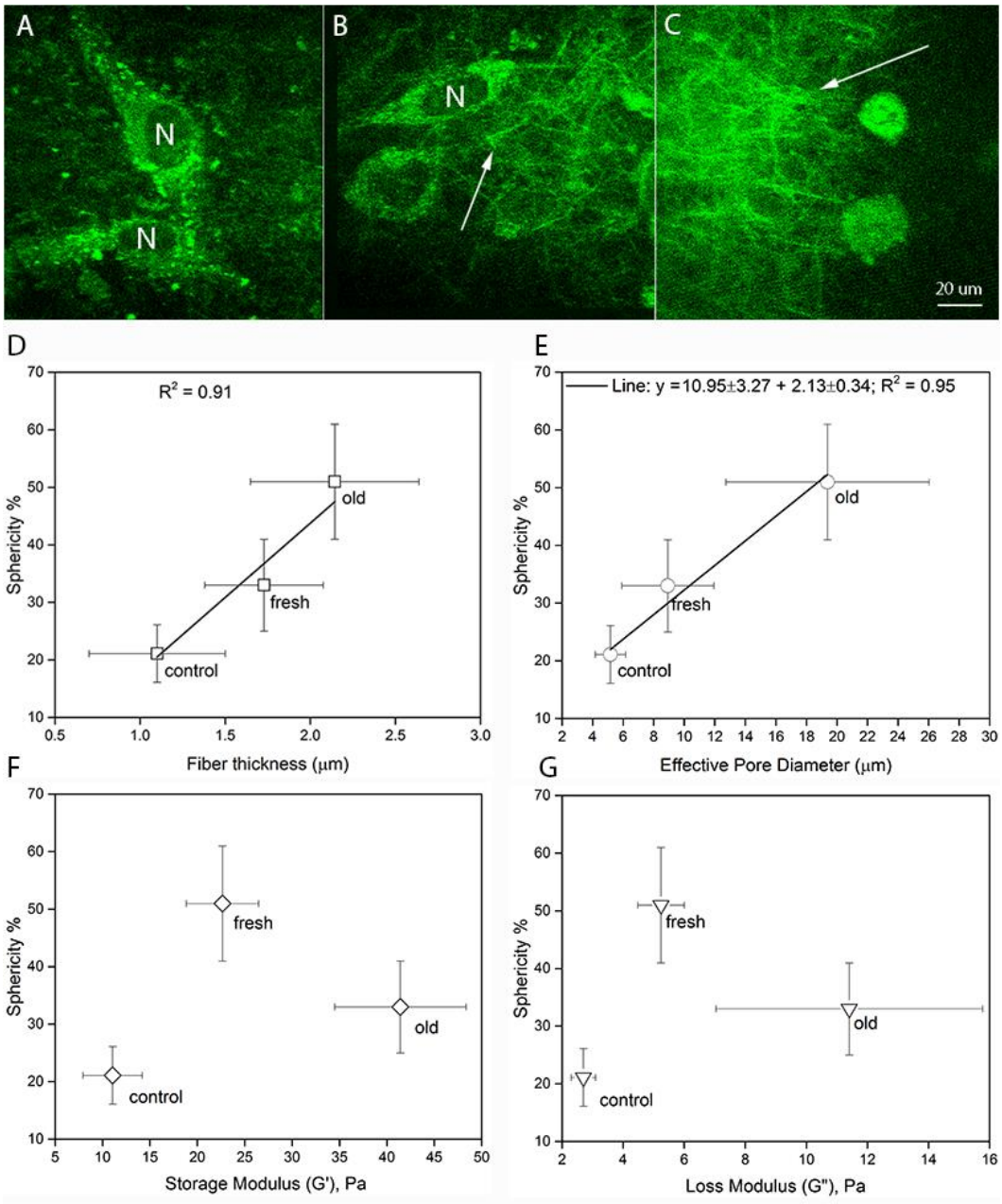

Figure 5.14 Effect of cross-linking collagen hydrogels on BALB/3T3 (clone A31) embryonic fibroblast cells response during cell culture**.** Two-photon fluorescence images of BALB/3T3 (clone A31) embryonic fibroblast cells cultured on (A) control (not cross-linked) collagen hydrogels; (B) fresh-genipin cross-linked collagen hydrogels, white arrow points to newly induced as a result of cross-linking fluorescent collagen fibers of the scaffolds; (C) 15 day-old-genipin cross-linked collagen hydrogel. White arrow points to newly induced as a result of cross-linking fluorescent collagen fibers of the scaffolds; Exploration of the correlation of cellular spread expressed as % sphericity and scaffold properties such as (D) fiber thickness, (E) effective pore diameter, (F) storage and (G) loss modulus. The errors are standard deviations of the mean.

To study the fibroblast morphology and microstructure of GCC after cell culture, MPM was employed to collect the SHG contrasted and TPF contrasted cellular and fiber images. The fibroblasts' morphology was different on the three materials. For the fibroblasts which were cultured on the uncrosslinked collagen hydrogel, the fibroblasts extended very long (> 100 μm). (**Figure 5.14A**) And the percentage of extended cell on uncrosslinked collagen hydrogel is also very high at day 2, ~85 % (**Figure 5.15**). The fibroblasts which were cultured on old genipin crosslinked collagen hydrogels were disproportionately more round compared to cells cultured on uncrosslinked collagen hydrogels and fresh genipin crosslinked collagen hydrogels (**Figure 5.14 A-C**). The sphericity of extended fibroblasts were ~20%, ~40% and ~60% for uncrosslinked collagen hydrogel, fresh genipin crosslinked collagen hydrogel and old genipin crosslinked collagen hydrogel, respectively. This means the cells' shape is different on the three materials. And we can get some correlation between cell sphericity and the microstructure parameters of GCC (fiber width, $R^2 = 0.91$; effective pore diameter, $R^2 = 0.95$) (**Figure 5.14 D-E**). There is no correlation between cell morphology and mechanical properties of the GCC (**Figure 5.14 F-G**). After 9 days cell culture, the extended fibroblast morphology appeared similar on all three materials (**Figure 5.16**).

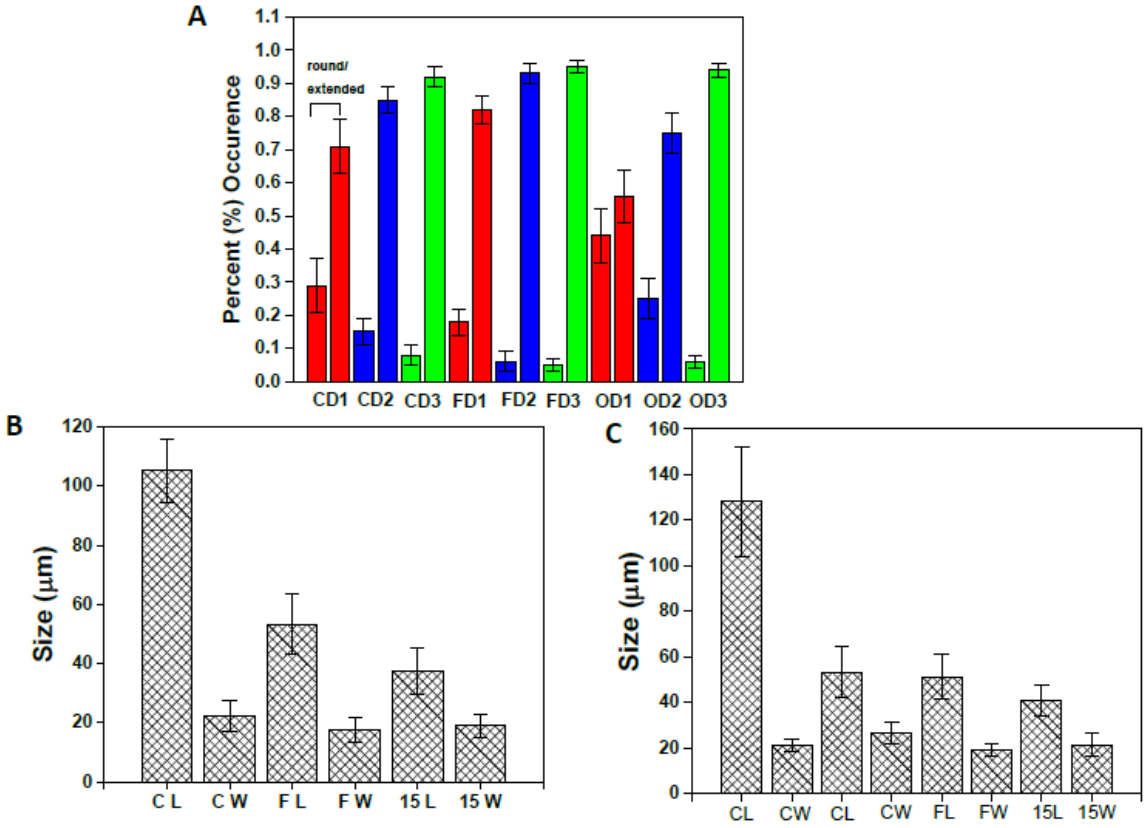

Figure 5.15 Verification of fibroblast cell morphology during cell culture on on the prepared hydrogels. (A) % occurrence of round versus extended cells. Error is the standard deviation of the mean. Bigger (L) and smaller (W) directions as well as sphericity (insert) of cultured BALB/3T3 (clone A31) embryonic fibroblast cells on day 2 (B) and day 9 (C) of cell culture. C = control, uncross-linked gel; F = fresh genipin cross-linked gels; O = 15 day old genipin-cross-linked gels. D1, D2, D3 = day 1, day 2 and day 3 respectively. sh = short cells.

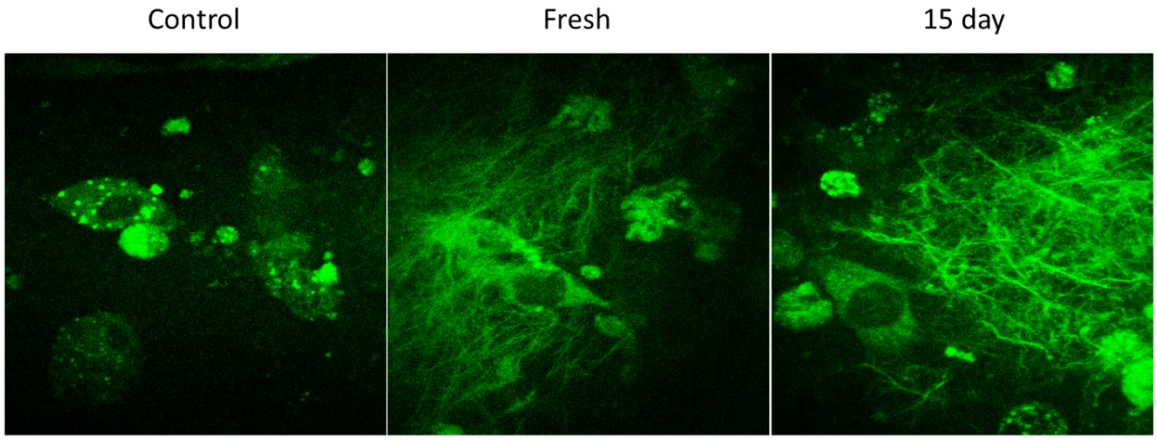

Figure 5.16 Effect of cross-linking collagen hydrogels on BALB/3T3 (clone A31) embryonic fibroblast cells response during cell culture after 9 days cell culture. Two-photon fluorescence images of BALB/3T3 (clone A31) embryonic fibroblast cells cultured on (A) control (not cross-linked) collagen hydrogels; (B) fresh-genipin cross-linked collagen hydrogels; (C) 15 day-old-genipin cross-linked collagen hydrogel.

To investigate the attachment between collagen hydrogel and the fibroblast, we employed grid to simulate the surface of the collagen hydrogel. Initially, for different collagen hydrogels (crosslinked/uncrosslinked, old/fresh genipin crosslinked), the pore diameters are different. The diameter of the pore structure is shown by the diagonal of the square. **(Figure 5.17)** The uncrosslinked collagen hydrogel has smallest pore diameter (5 μm) compared with fresh genipin crosslinked collagen hydrogel (FGCC) (9 μm) and old genipin crosslinked collagen hydrogel (OGCC) (20 μm). Then in the beginning of the cell culture, cells can make more contact with fibers on the unmodified collagen fibers. More attachments would make it easier for the fibroblasts to extent. The fibroblast cultured on the OGCC has less attachment with the fibers due to a larger pore diameter. It is harder for them to extent in the beginning of cell culture. This model can explain the difference of cell morphology in the beginning of the cell culture and the correlation between fibroblast

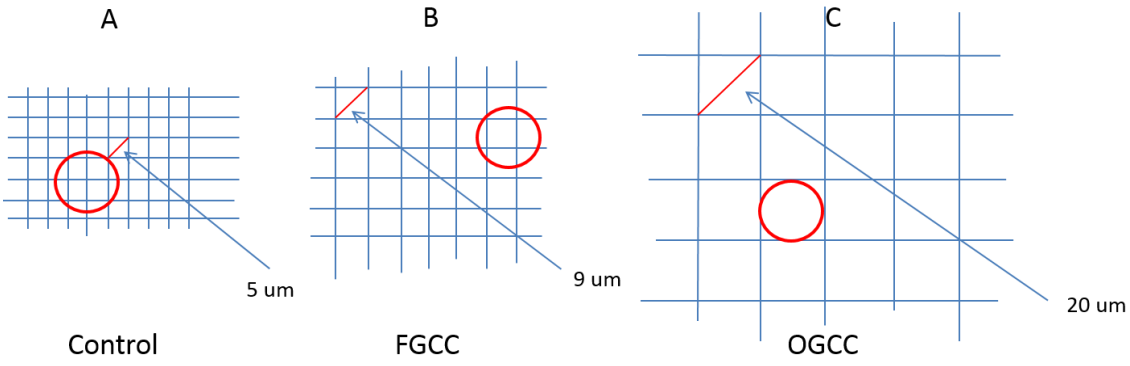

Figure 5.17 A model of the attachment between scaffold and fibroblast. (A) The model of the attachment between control collagen hydrogel and fibroblast. (B) A model of the attachment between fresh genipin crosslinked collagen hydrogel (FGCC) and fibroblast. (C) A model of the attachment between old genipin crosslinked collagen hydrogel (OGCC) and fibroblast.

Conclusions

There is nearly three-fold enhancement in emission intensity at 470 nm when “aged” genipin are employed to cross-link collagen hydrogels. On the contrary, the 620 nm emission band disappears when “aged” genipin was employed to crosslink collagen hydrogel. The location of the emission peaks in two photon excited spectrum is similar as one photon excited emission spectrum, but the relative ratios of the two peaks are very different. Furthermore, the band positions shift towards each other as “aged” genipin is used to prepare GCC gels.

In general, a modification of collagen hydrogels with genipin solutions results in the reconstruction of the original scaffold microstructure. The increasing of the genipin age can lead to the thinner fibers of GCC. The increasing of genipin age also can cause the decreasing of the G’ and G’’ of GCC

In the beginning of the cell culture, fibroblasts are more round on old genipin crosslinked collagen hydrogel compared to uncrosslinked collagen hydrogel and fresh genipin crosslinked collagen hydrogel, and we can obtain some correlation between cell morphology and the materials’ microstructure parameters. After 9 days cell culture on materials, the morphology of fibroblast cultured on the three materials are similar.

Acknowledgements

This work was supported in part with UC Riverside startup research funds (J.G.L.), NSF BRIGE Award EEC-0927297 (J.G.L), NSF CAREER Award CBET-0847070 (J.G.L), UC BSAS Grant (J.G.L) and HSI Undergraduate Research Award (A.V). The authors

thank Prof. Jiayu Liao for access to the FlexStation fluorescence microplate reader (Molecular Devices) at UC Riverside.

References

1. Y. Hwang, J. Larsen, T. Krasieva, J. G. Lyubovitsky, Effect of Genipin Crosslinking on the Optical Spectral Properties and Structures of Collagen Hydrogels. *ACS Appl. Mater. Interfaces* **2011,** *3*, 2579-2584.

2. Y. S. Kwon, E. S. Lim, H. M. Kim, Y. C. Hwang, K. W. Lee, K. S. Min, Genipin, a Cross-linking Agent, Promotes Odontogenic Differentiation of Human Dental Pulp Cells. *J. Endod.* **2015,** *41*, 501–507

3. M. F. Butler, Y. Ng, P. D. A. Pudney, Mechanism and Kinetics of the Crosslinking Reaction between Biopolymers Containing Primary Amine Groups and Genipin. *J. Polym. Sci., Part A: Poly. Chem.* **2003,** *41*, 3941-3953.

4. (a) H. W. Sung, W. H. Chang, C. Y. Ma, M. H. Lee, Crosslinking of biological tissues using genipin and/or carbodiimide. *J. Biomed. Mater. Res., Part A* **2003,** *64A*, 427-438; (b) W. F. Daamen, H. T. B. Moerkerk, T. Hafmans, L. Buttafoco, A. A. Poot, J. H. Veerkamp, T. H. Kuppevelt, Preparation and Evaluation of Molecularly-defined Collagen–elastin–glycosaminoglycan Scaffolds for Tissue Engineering. *Biomaterials* **2003,** *24*, 4001–4009.

5. (a) C. Nishi, N. Nakajima, Y. Ikada, In vitro evaluation of cytotoxicity of diepoxy compounds used for biomaterials modification. *J. Biomed. Mater. Res., Part A* **1995,** *29*, 829-834; (b) F. L. Mi, Y. C. Tan, H. C. Liang, R. N. Huang, H. W. Sung, In vitro evaluation of a chitosan membrane crosslinked with genipin. *J. Biomater. Sci. Polym. Ed.* **2001,** *12*, 835-850.

6. H. J. Koo, K. H. Lim, H. J. Jung, E. H. Park; , Anti-inflammatory Evaluation of Gardenia Extract, Geniposide and Genipin. *J. Ethnopharmacol.* **2001,** *103*, 496-500.

7. F. L. Mi, H. W. Sung, S. S. Shyu, Synthesis and characterization of a novel chitosan-based network prepared using naturally occurring crosslinker. *J. Polym. Sci., Part A: Polym. Chem.* **2000,** *38*, 2804–2814

8. (a) C. Mu, K. Zhang, W. Lin, D. Li, Ring-opening polymerization of genipin and its long-rangecrosslinking effect on collagen hydrogel. *J. Biomed. Mater. Res., Part A* **2013,** *101A*, 385-393; (b) F. L. Mi, S. S. Shyu, C. K. Peng, Characterization of ring-opening polymerization of genipin and pH-dependent cross-linking reactions between chitosan and genipin. *J. Polym. Sci., Part A: Polym. Chem.* **2005,** *43*, 1985–2000.

9. (a) H. Sung, Y. Chang, W. Chang, Y. Chen, Fixation of biological tissues with a naturally occurring crosslinking agent: Fixation rate and effects of pH, temperature, and initial fixative concentration. *J. Biomed. Mater. Res.* **2000,** *52*, 77–87; (b) P. Slusarewicz,

K. Zhu, T. Hedmana, Kinetic Analysis of Genipin Degradation in Aqueous Solution. *Nat. Prod. Commun.* **2010,** *5*, 1853 - 1858.

10. P. X. Qi, A. Nunez, E. D. Wickham, Reactions between β-Lactoglobulin and Genipin: Kinetics and Characterization of the Products. *J. Agric. Food Chem.* **2012,** *60*, 4327−4335.

11. X. Lang, J. G. Lyubovitsky, Structural Dependency of Collagen Fibers on Ion Types Revealed by *In situ* Second Harmonic Generation (SHG) Imaging Method. *Anal. Methods* **2015,** *7*, 1680 - 1690.

12. Y Hwang, J. G. Lyubovitsky, Collagen Hydrogel Characterization: Multi-scale and Multi-modality Approach. *Anal. Methods* **2011,** *3*, 529-536.

13. C. B. Raub, V. Suresh, T. B. Krasieva, J. G. Lyubovitsky, J. D. Mih, A. J. Putnam, B. J. Tromberg, S. C. George, Non-invasive assessment of collagen hydrogel microstructure and mechanics using multiphoton microscopy. *Biophys. J.* **2007,** *92*, 2212-2222.

14. (a) M. E. Nimni, D. Cheung, B. Strates, M. Kodama, K. Sheikhtt, Chemically modified collagen: A natural biomaterial for tissue replacement. *J. Biomed. Mater. Res., Part A* **1987,** *21*, 741-771; (b) Y. Hwang, J. Granelli, J.G. Lyubovitsky, The Effects of Zero- and Non-zero Length Cross-linking Reagents on the Optical Spectral Properties and Structures of Collagen Hydrogels. *ACS Appl. Mater. Interfaces* **2011,** *4*, 261-267; (c) Y. Hwang, J. Granelli, J.G. Lyubovitsky, Multiphoton Optical Image Guided Spectroscopy Method for Characterization of Collagen-Based Materials Modified by Glycation. *Anal. Chem.* **2011,** *83*, 200–206; (d) Y. Hwang, J. Granelli, M. Tirumalasetty, J. G. Lyubovitsky, Microscopic Imaging of Glyceraldehyde-induced Tissue Glycation with Intrinsic Second Harmonic Generation and Two-photon Fluorescence Contrasts. *Proc. SPIE* **2013,** *8587*, 858725 ; (e) Y. Hwang, J. G. Lyubovitsky, The Structural Analysis of Three-dimensional Fibrous Collagen Hydrogels by Raman Microspectroscopy. *Biopolymers* **2013,** *99* 349-356; (f) Y. Hwang, X. Lang, J. Granelli, C. C. Turgman, J. Gigante, J. G. Lyubovitsky, Collagen Bioengineered Systems: *In situ* Advanced Optical Spatiotemporal Analysis *Proc. SPIE* **2014,** *9129*, 91291H.

15. B. A. C. Harley, H. D. Kim, M. H. Zaman, I. V. Yannas, D. A. Lauffenburger, L. J. Gibson, Microarchitecture of Three-Dimensional Scaffolds Influences Cell Migration Behavior via Junction Interactions. *Biophysical Journal* **2008,** *95*, 4013–4024.

16. K. L. Mui, Y. H. Bae, L. Gao, S. L. Liu, T. Xu, G. L. Radice, C. S. Chen, R. K. Assoian, N-Cadherin Induction by ECM Stiffness and FAK Overrides the Spreading Requirement for Proliferation of Vascular Smooth Muscle Cells. *Cell Reports* **2015,** *10*, 1477–1486.

17. C. Zhu, J. Li, C. Liu, P. Zhou, H. Yang, Bin Li, Effect of scaffold elasticity on the gene expression of annulus fibrosus-derived stem cells. *Data in Brief* **2015,** *5*, 1007–1014.

18. A. M. Pizzo, K. Kokini, L. C. Vaughn, B. Z. Waisner, S. L. Voytik-Harbin, Extracellular matrix (ECM) microstructural composition regulates local cell-ECM biomechanics and fundamental fibroblast behavior: a multidimensional perspective. *J Appl Physiol* **2005,** *98*, 1909 –1921.

19. M. L. B. Palacio, B. Bhushan, Bioadhesion: a review of concepts and applications. *Phil. Trans. R. Soc. A* **2016,** *370*, 2321–2347.

20. (a) B. G. Keselowsky, D. M. Collard, A. J. Garcıa, Surface Chemistry Modulates Focal Adhesion Composition and Signaling through Changes in Integrin Binding. *Biomaterials* **2004,** *25* 5947-5954; (b) J. Jokinen, E. Dadu., P. Nykvist, J. Kapyla, D. J. White, J. Ivaska, P. Vehvilainen, H. Reunanen, H. Larjava, L. Hakkinen, J. Heino, Integrin-mediated Cell Adhesion to Type I Collagen Fibrils. *J. Biol. Chem.* **2004,** *279*, 31956-31963.

21. X. Chen, O. Nadiarynkh, S. Plotnikov, P. J. Campagnola, Second Harmonic Generation Microscopy for Quantitative Analysis of Collagen Fibrillar Structure. *Nat. Protoc.* **2012,** *7*, 654-669.

22. W. Denk, J. H. Strickler, W. W. Webb, Two-photon laser scanning fluorescence microscopy. *Science* **1990,** *248*, 73-76.

23. (a) A. Meshkinpour, P. Ghasri, K. Pope, J. G. Lyubovitsky, J. Risteli, T. B. Krasieva, K. M. Kelly, Treatment of Hypertrophic Scars and Keloids with a Radiofrequency Device: A Study of Collagen Effects. *Lasers in Surg. Med.* **2005,** *37* 343-349; (b) B. R. Masters, P. So, *Handbook of Biomedical Nonlinear Optical Microscopy*. Oxford University Press: New York, 2008; (c) J. G. Lyubovitsky, T. B. Krasieva, J. A. Spencer, B. Andersen, B. J. Tromberg, Corneal damage revealed by endogenous cellular fluorescence and second harmonic signals from collagen. *Proc. SPIE* **2005,** *5700*, 213-217; (d) J. G. Lyubovitsky, T. B. Krasieva, J. A. Spencer, B. Andersen, B. J. Tromberg, Imaging corneal pathology in a transgenic mouse model using nonlinear microscopy. *J. Biomed. Opt.* **2006,** *11*, 014013; (e) J. G. Lyubovitsky, X. Xu, T. B. Krasieva, B. Andersen, B. J. Tromberg, *In situ* multi-photon optical tomography of hair follicles in mice. *J. Biomed. Opt.* **2007,** *12*, *044003* ; (f) J. G. Lyubovitsky, X. Xu, C. Sun, B. Andersen, T. B. Krasieva, B. J. Tromberg, Characterization of dermal structural assembly in normal and pathological connective tissues by intrinsic signal multiphoton optical microscopy. *Proc. SPIE* **2008,** *6859*, 1-9

24. (a) C. B. Raub, J. Unruh, V. Suresh, T. Krasieva, T. Lindmo, E. Gratton, B. J. Tromberg, S. C. George, Image Correlation Spectroscopy of Multiphoton Images Correlates with Collagen Mechanical Properties. *Biophys. J.* **2008,** *94*, 2361-2373; (b) N.

I. zur Nieden, C. C. Turgman, X. Lang, J. M. Larsen, J. Granelli, Y. Hwang, J. G. Lyubovitsky, Fluorescent Hydrogels for Embryoid Body Formation and Osteogenic Differentiation of Embryonic Stem Cells. *ACS Appl. Mater. Interfaces* **2015,** *7*, 10599-10605; (c) P, Lee. The Impact of Extracellular Matrix Stiffness on Angiogensis. Texas A&M University; (d) X. Lang, M. Spousta, J. G. Lyubovitsky, Detecting the Collagen-based Hydrogels Degradation by Multiphonton Microscopy (MPM). *Proc. SPIE* **2015,** *9329*, doi:10.1117/12.2080559; (e) X. Lang, M. Spousta., Y. Hwang, J. G. Lyubovitsky Noninvasive Imaging of Embryonic Stem Cell Cultures by Multiphoton Microscopy Reveals Significance of Collagen Hydrogel Preparation Parameters. *RSC Anal. Methods* **2015,** *8*, 280-294; (f) Y. Bai, P. F. Lee, H. C. Gibbs, K. J. Bayless, A. T. Yeh, Dynamic Multicomponent Engineered Tissue Reorganization and Matrix Deposition Measured with an Integrated Nonlinear Optical Microscopy-optical Coherence Microscopy System. *J. Biomed. Opt.* **2014,** *19*, 036014; (g) Y. Hwang, N. Kolettis, M. Yang, E. Sanchez, C. Sun, E. R. Gillard, B. J. Tromberg, T. B. Krasieva, J. G. Lyubovitsky, Multi-photon Imaging of Actin Filament Formation and Mitochondrial Energetics of Human ACBT Gliomas. *Photochem. Photobiol.* **2011,** *87*, 408-417

25. J. Hu, J. D. Humphrey, A. T. Yeh, Characterization of Engineered Tissue Development Under Biaxial Stretch Using Nonlinear Optical Microscopy. *Tissue Eng., Part A* **2009,** *15*, 1553-1564.

26. Y. Bai, P. Lee, J. D. Humphrey, A. T. Yeh, Sequential Multimodal Microscopic Imaging and Biaxial Mechanical Testing of Living Multicomponent Tissue Constructs. *Ann. Biomed. Eng.* **2014,** *42*, 1791-1805.

27. S. Lee, J. Lim, S. Bhoo, Y. Paik, T. Hahn, Colorimetric Determination of Amino Acids using Genipin from Gardenia Jasminoides. *Anal. Chim. Acta* **2003,** *480*, 267-274.

28. J. Park, J. Lee, H. Kim, T. Hahn, Y. Paik, Isolation and Characterization of Water-Soluble Intermediates of Blue Pigments Transformed from Geniposide of *Gardenia jasminoides*. *J. Agric. Food Chem.* **2002,** *50*, 6511-6514.

29. J. A. Pedersen, M. A. Swartz, Mechanobiology in the third dimension *Ann. Biomed. Eng.* **2005,** *33*, 1469-1490.

30. M. Kim, A. Takaoka, Q. V. Hoang, S. L. Trokel, D. C. Paik, Pharmacologic Alternatives to Riboflavin Photochemical Corneal Cross-Linking: A Comparison Study of Cell Toxicity Thresholds. *Invest. Ophthalmol. Vis. Sci.* **2014,** *55* 3247–3257.

Chapter 6: Conclusion

My thesis explored the properties of collagen hydrogel prepared at different conditions, with/without crosslinkers linking form optical, mechanical and microstructural aspects. My thesis work provided a framework which can be used to design collagen hydrogel with the properties we desire. The model of 3T3 fibroblast cells' response to different collagen hydrogel materials are also discussed in my thesis. This information can help us to understand the interaction between collagen hydrogel and cells and how to increase their performance.

The main result of my thesis is:

1. The characterization of properties of collagen hydrogel

(1) How ionic strengthen and ionic type influence the microstructure and polymerization process of collagen hydrogel.

(2) How pH has a dramatic influence on the microstructure of collagen hydrogel.

(3) How specific crosslinkers can alter the properties of collagen hydrogel, such as mechanical, optical and microstructural properties.

(4) Different "aged" genipin can result in different properties of collagen hydrogel.

2. The 3T3 fibroblast cells' behavior:

(1) Different "aged" genipin crosslinked collagen hydrogel can result in a different initial response (morphology, survive rate, replication rate)

The main goal of tissue engineering is to use engineered tissue to replace or repair the damaged tissue in our body. The most important step is to regenerate the engineered tissue by culturing the cell in a scaffold. The effect of the scaffold on the cell's behavior

plays a very significant role in this process. The interaction between scaffold materials and cells needs further investigation. For collagen hydrogel materials, it is necessary to continue to improve the design of collagen hydrogel with desired properties and study cell response to different collagen hydrogel materials. On one hand, so far, most research focused on the nanostructure of collagen molecules and/or the stability of collagen molecules in the solution. Less research has focused on the microstructure of 3D collagen hydrogel. On the other hand, the most cellular behavior study focused on the signal pathway transduction and/or the specific gene expression with molecule biological technologies, such as, bio-marker technology or PCR based technology. Definitely, these researches are very helpful for us to understand the properties of collagen molecules and the cellular behavior controlling pattern in molecular level. But it is insufficient for us to develop the engineered tissue. My thesis work focused on two areas, the properties of collagen hydrogel and the cellular response to different collagen hydrogel. It fills the gap by detailed understanding of the collagen hydrogel properties and the fibroblast response to collagen hydrogel.

Besides those, my thesis further elaborated the application of Multiphoton microscopy (MPM) in the biomaterials and cellular behavior research. The microstructure of collagen hydrogel and the morphology of the cell have been elucidated by using Second Harmonic Generation (SHG) and Two Photon excited Fluorescence (TPF) signals. MPM is one kind of nonlinear optical technology. The non-destructive nature of this technique, its label-free properties and deeper tissue penetration make MPM a suitable technology in tissue engineering or cellular research fields.

In my thesis work, the microstructure parameters were obtained by processing MPM images, optical properties were acquired by collecting the absorption and emission spectra. The mechanical properties were obtained by measuring storage and loss moduli with a rheometer. These engineering parameters are very valuable for the design of the fibrous protein scaffold systems in tissue engineering and other fields. MPM was employed to detect the kinetic data during digestion of collagen hydrogel with activated collagenase. This data is very helpful because it can predict the degradation rate of collagen hydrogel in cell-scaffold systems. MPM can image the fibroblast morphology in addition to imaging the fibroblast-collagen interactions and fibroblast-fibroblast interactions. The fibroblast-collagen system also can work as a model that can help us to understand the some disease development and/or wound healing process by monitoring the new collagen fibers formation and cell morphology.